A COMPREHENSIVE PLACEMENT AND DIVERSION MODEL FOR MATRIX ACIDIZING IN VERTICAL WELLS IN HETEROGENEOUS THICK FORMATIONS

A Dissertation

by

MANABU NOZAKI

Submitted to the Office of Graduate Studies of
Texas A&M University
in partial fulfillment of the requirements for the degree of

DOCTOR OF PHILOSOPHY

May 2012

Major Subject: Petroleum Engineering

A Comprehensive Placement and Diversion Model for Matrix Acidizing in Vertical Wells in Heterogeneous Thick Formations

A COMPREHENSIVE PLACEMENT AND DIVERSION MODEL FOR MATRIX ACIDIZING IN VERTICAL WELLS IN HETEROGENEOUS THICK FORMATIONS

A Dissertation

by

MANABU NOZAKI

Submitted to the Office of Graduate Studies of
Texas A&M University
in partial fulfillment of the requirements for the degree of

DOCTOR OF PHILOSOPHY

Approved by:

Chair of Committee,	Alfred Daniel Hill
Committee Members,	Ding Zhu
	Hisham Abou-El-Fath Nasr-El-Din
	Victor M. Ugaz
Head of Department,	Stephen A. Holditch

May 2012

Major Subject: Petroleum Engineering

ABSTRACT

A Comprehensive Placement and Diversion Model for Matrix Acidizing in Vertical Wells in Heterogeneous Thick Formations. (May 2012)
Manabu Nozaki, B.Eng., Waseda University;
M.S., Texas A&M University
Chair of Advisory Committee: Dr. Alfred Daniel Hill

Diversion methods are routinely used in both matrix acidizing and fracturing stimulation treatments. In this study, we focus on one of the classical mechanical diversion methods, ball sealers. Ball sealer diversion is used in cased and perforated wells to divert stimulation fluids by temporarily blocking perforation holes in the casing with rubber-coated balls. This diversion method can be very effective, but there is no general methodology to design ball sealer diversion, or to evaluate its effectiveness from the treating rate and pressure record.

Experimental data from an extensive series of full-scale flow experiments conducted by BP were analyzed. One field treatment was analyzed and compared, and a similar trend in seating efficiency was observed. Then, we developed an empirical correlation on the basis of BP experimental data. The correlation enables us to estimate how many ball sealers seat on the perforations. By incorporating this correlation into an acid placement model, we can estimate wormhole penetrations along the wellbore with time. We developed a computer program and studied one hypothetical case to show the usefulness of the ball sealer diversion model.

DEDICATION

To my wife and parents, for their loving support and encouragement.

ACKNOWLEDGEMENTS

I would like to take this opportunity to express my deepest gratitude to my advisor and committee chair, Dr. Alfred Daniel Hill, for his continuous encouragement, guidance, and support. Also, I would like to give special thanks to Dr. Ding Zhu for her support and motivation during the course of this research. I would also like to thank Dr. Hisham Abou-El-Fath Nasr-El-Din for his advice, guidance, and encouragement.

Appreciation is extended to the other member of my committee, Dr. Victor M. Ugaz, for his help and time to serve on my committee.

Many thanks are due to all my colleagues who helped me during the course of this research.

I also thank BP for providing their experimental data.

Finally, I would like to acknowledge financial support from the Middle East Carbonate Stimulation joint industry project at Texas A&M University. The facilities and resources provided by the Harold Vance Department of Petroleum Engineering of Texas A&M University are gratefully acknowledged.

NOMENCLATURE

a_J	=	coefficient defined in Eq. 2.24
A_{pipe}	=	pipe cross-sectional area, L^2, ft^2
b_J	=	coefficient defined in Eq. 2.25
c_J	=	coefficient defined in Eq. 2.58
C_0	=	injection acid concentration, weight fraction, kg/kg
c_t	=	total compressibility, $m^{-1}L^{-1}t^2$, psi^{-1}
d_{core}	=	core diameter, L, inch
$d_{e,wh}$	=	effective wormhole radius, L, ft
d_J	=	coefficient defined in Eq. 2.59
d_{perf}	=	perforation diameter, L, inch
d_{pipe}	=	pipe diameter, L, inch
e_J	=	coefficient defined in Eq. 2.70
F_D	=	drag force tending to divert ball to perforation, mLt^{-2}, lb_m-ft/sec^2
f_f	=	fanning friction factor, dimensionless
F_I	=	inertial force, mLt^{-2}, lb_m-ft/sec^2
f_{wall}	=	wall factor, dimensionless
g	=	acceleration of gravitation, Lt^{-2}, ft/sec^2
g_c	=	gravitational dimensional constant
h	=	thickness, L, ft
h_{perf}	=	perforation spacing, L, ft
I_{ani}	=	anisotropy ratio, dimensionless
k	=	permeability, L^2, md
K_D	=	drag coefficient, dimensionless
K_d	=	discharge coefficient, dimensionless
k_d	=	damage permeability, L^2, md
k_H	=	horizontal permeability, L^2, md
k_V	=	vertical permeability, L^2, md

L	=	length, L, ft
L_{core}	=	core length, L, inch
l_{perf}	=	perforation length, L, inch
l'_{perf}	=	modified perforation length defined in Eq. 2.54, L, inch
m_{wh}	=	number of dominant wormholes per 2D plane
n_{perf}	=	number of open perforations
N_{Ac}	=	acid capacity number, dimensionless
$n_{perf,after}$	=	number of open perforations after ball sealer blockage
$n_{perf,ball}$	=	number of ball sealers seated on perforations
$n_{perf,before}$	=	number of open perforations before ball sealer blockage
N_{Re}	=	Reynolds number, dimensionless
p	=	pressure, mLt^{-2}, psi
p_D	=	dimensionless pressure, dimensionless
p_i	=	initial reservoir pressure, mLt^{-2}, psi
$PV_{bt,opt}$	=	optimum pore volume to breakthrough, dimensionless
p_w	=	well pressure, mLt^{-2}, psi
q	=	flow rate, L^3t^{-1}, ft^3/min
q_{sR}	=	specific reservoir outflow rate, L^2t^{-1}, bbl/min/ft
q_w	=	flow rate in the wellbore, L^3t^{-1}, bbl/min
r	=	radial coordinate, L, ft
r_d	=	damage radius, L, ft
r_e	=	external reservoir radius, L, ft
r_w	=	wellbore radius, L, ft
r'_w	=	modified wellbore radius defined in Eq. 2.55, L, ft
r_{we}	=	effective wellbore radius, L, ft
r_{wh}	=	wormhole penetration radius, L, ft
s	=	skin factor, dimensionless
s_{da}	=	damage/acidization skin factor, dimensionless
$s_{overall}$	=	overall skin factor, dimensionless

s_{Total}	=	total skin factor, dimensionless
s_{wb}	=	wellbore blockage skin factor, dimensionless
s_{θ}	=	slant skin factor, dimensionless
s_{2D}	=	2D plane skin factor, dimensionless
s_{3D}	=	3D convergence skin factor, dimensionless
t	=	time, t, minute
t_D	=	dimensionless time, dimensionless
v	=	velocity, Lt^{-1}, ft/min
v_{ball}	=	ball velocity, Lt^{-1}, ft/min
v_i	=	interstitial velocity, Lt^{-1}, ft/min
$v_{i,opt}$	=	optimum interstitial velocity, Lt^{-1}, cm/min
$v_{i,tip}$	=	interstitial velocity at the tip of wormholes, Lt^{-1}, cm/min
v_{perf}	=	velocity through a perforation, Lt^{-1}, ft/min
v_{slip}	=	slip velocity, Lt^{-1}, ft/min
$v_{t,\phi}$	=	terminal settling or rising velocity for multi-ball, Lt^{-1}, ft/min
$v_{t,0}$	=	terminal settling or rising velocity for single ball, Lt^{-1}, ft/min
v_{wh}	=	wormhole propagation rate, Lt^{-1}, ft/min
Z	=	elevation, L, ft

Greek

α_z	=	wormhole axial spacing coefficient
γ	=	specific gravity, dimensionless
Δp	=	pressure drop, mLt^{-2}, psi
Δp_{ball}	=	pressure drop due to ball sealer blockage, mLt^{-2}, psi
Δp_F	=	frictional pressure drop, mLt^{-2}, psi
Δp_{KE}	=	kinetic energy pressure drop, mLt^{-2}, psi
Δp_{PE}	=	potential energy pressure drop, mLt^{-2}, psi
Δp_{perf}	=	perforation pressure drop, mLt^{-2}, psi
$\Delta p_{perf,after}$	=	perforation pressure drop after ball sealer blockage, mLt^{-2}, psi

$\Delta p_{perf,before}$	=	perforation pressure drop before ball sealer blockage, mLt^{-2}, psi
Δp_s	=	pressure drop due to skin factor, mLt^{-2}, psi
Δv	=	velocity difference, Lt^{-1}, ft/min
ΔZ	=	elevation difference, L, ft
ε	=	roughness, dimensionless
θ	=	deviation angle, degree [radian]
μ	=	viscosity, $mL^{-1}t^{-1}$, cp
ρ	=	density, mL^{-3}, g/cm^3
ρ_{acid}	=	acid density, mL^{-3}, g/cm^3
ρ_{ball}	=	ball density, mL^{-3}, g/cm^3
ρ_{fluid}	=	fluid density, mL^{-3}, g/cm^3
ρ_{perf}	=	perforation density, shots/ft
ρ_{rock}	=	rock density, mL^{-3}, g/cm^3
ϕ	=	porosity, fraction
ϕ_{ball}	=	volume fraction of ball sealer

TABLE OF CONTENTS

Page

Page

LIST OF FIGURES

Page

Page

LIST OF TABLES

1. INTRODUCTION

1.1 Background

Matrix stimulation is a technique in which a solvent is injected into the formation to dissolve some of the materials present and hence recover from formation damage or increase the permeability in the near-wellbore region (Hill and Schechter 2000). For this type of treatment, the solvent is injected at pressures below the parting pressure of the formation so that fractures are not created (Hill and Schechter 2000).

The most common matrix stimulation treatment is acidizing, in which an acidic solution is injected to dissolve minerals in the formation (Hill and Schechter 2000). In carbonate formations, the most common acids are hydrochloric acid (HCl), used primarily to dissolve carbonate minerals and hence create high conductive channels called wormholes (**Fig. 1.1**). HCl reacts with carbonates to form carbon dioxide (CO_2), water (H_2O), and a calcium or magnesium salt. Typical reactions in carbonates are (Williams et al. 1979):

$$2HCl + CaCO_3 \Leftrightarrow CaCl_2 + CO_2 + H_2O \quad \text{..... (1.1)}$$

and

$$4HCl + CaMg(CO_3)_2 \Leftrightarrow CaCl_2 + MgCl_2 + 2H_2O + 2CO_2 . \quad \text{..... (1.2)}$$

According to the recent assessments of a series of buidup tests after matrix stimulation in carbonates by Furui et al. (2010), 10 to 20 ft stimulation radii were confirmed. These radii are considered to be deep enough to penetrate the damage region if there is no natural fractures which enable deep damage penetration.

A critical factor to the success of matrix acidizing treatments is proper placement of the acid so that all of productive intervals are contacted by sufficient volumes of acid (Economides et al. 1993; Robert and Rossen 2000). If there are significant variations in reservoir permeability and/or severity of damage, the acid will tend to flow primarily

---

This dissertation follows the style of *SPE Journal*.

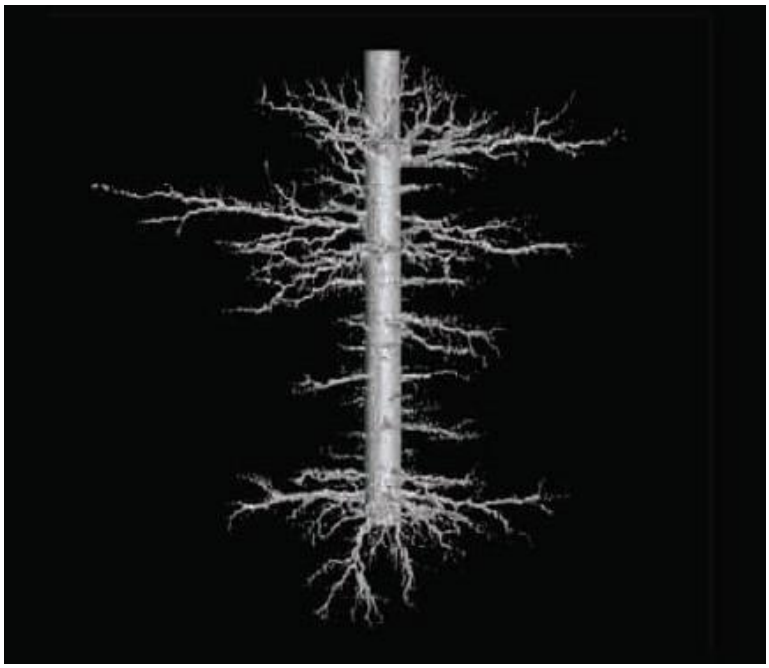

Fig. 1.1—CT-scanned wormhole structures from a radial coreflood experiment (from McDuff et al. 2010).

into the highest-injectivity zones, leaving lower-injectivity zones virtually untreated (Economides et al. 1993). As shown in Fig. 1.1, even in a relatively homogeneous core, wormholes were distributed unevenly.

As a diversion method, ball sealers were introduced to the oil and gas industry in 1956 for cemented, cased and perforated wells (Kastrop 1956; Derrick and Kaltenberger 1956). **Fig. 1.2** graphically demonstrates the principle of the perforation sealing process in simplified form (Neill et al. 1957):

a) the higher-permeability interval is stimulated in the first stage;
b) ball sealers, rubber-coated balls, are pumped in with a flush fluid or the stimulation fluid;
c) the perforations of the higher-permeability interval are sealed by the ball sealers;
d) the lower-permeability interval is stimulated; and
e) the ball sealers fall to the bottom or are collected at the surface when the pressure differential across the perforations is released.

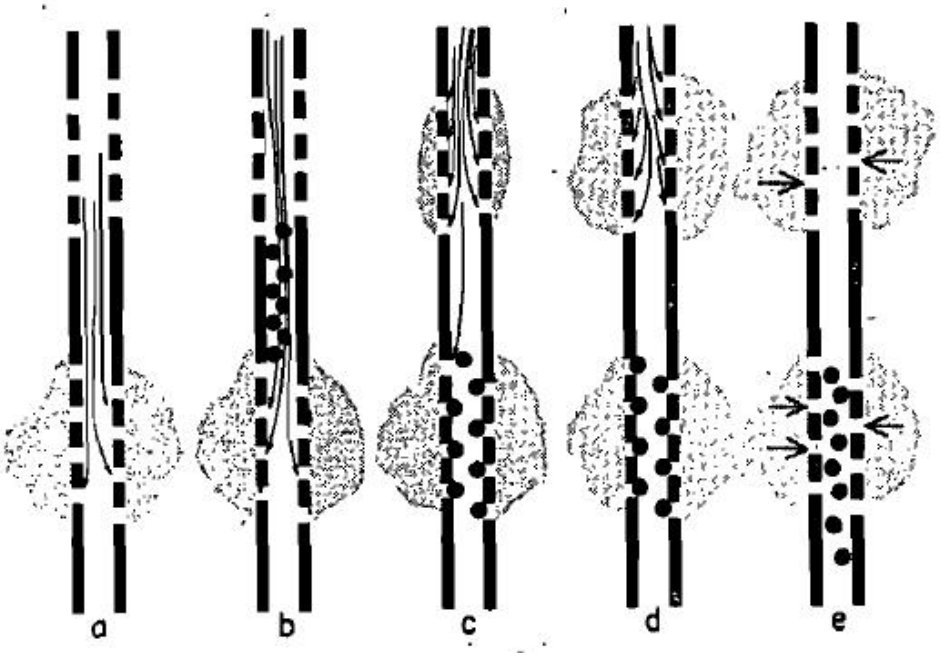

Fig. 1.2—Ball sealer application (from Neill et al. 1957).

The complete treatment is conducted without slowing down the pumps (Neill et al. 1957). Ball sealers have been used successfully since then.

Although some design methodologies, such as the use of buoyant ball sealers to improve the ball sealer efficiency (Erbstoesser 1980), have been suggested, no model has been presented for determining how many balls seat on the perforations and simulating how much stimulation fluids is diverted from a higher-permeability zone to a lower-permeability zone. In this study, we develop a model which enables us to simulate an entire matrix acidizing stimulation treatment in which ball sealers are used as a diversion method.

1.2 Literature Review

1.2.1 Acid Placement Model

Hill and Galloway (1984) simulated an injection fluid distribution along a pay zone in a vertical well with and without diverting agents (oil-soluble resin particles). In their numerical model, a steady-state reservoir outflow equation was used. By assuming that

the injection fluids are incompressible and the pressure gradient in the wellbore is same as in the reservoir, they numerically calculated injection fluids' penetration along the pay zone. They could get a match with their experimental results.

Later, Hill and Rossen (1994) presented a similar fluid placement model to Hill and Galloway (1984). They additionally simulated acid reaction by changing a skin factor. They assumed that the skin factor linearly decreases with the cumulative acid volume.

Jones and Davies (1996) presented and acid placement model for horizontal wells. The model was for barefoot completions in sandstone formations. They combined the pressure drop equation for the formation (pseudo-steady-state reservoir outflow equation) and the pressure gradient equation in the wellbore (hydrostatic, frictional and inertial pressure drops). Radially segmented grids were used to simulate the pressure drop between the wellbore and the reservoir. They emphasized the need to include wellbore phenomena.

Glasbergen and Buijse (2005) developed a fluid placement simulator on the basis of the Jones and Davies model (1996). They showed good pressure and skin factor matches in two field cases.

Mishra et al. (2007) presented an acid placement model for horizontal wells. The model was for carbonate formations. They used a transient reservoir outflow equation with variable injection rate which is commonly used in well testing. To account for the effect of the acid stimulation, they changed the skin factor at each time step by assuming that the pressure drop in the wormhole region is negligible.

In 2007, Mogensen and Hansen presented a similar acid placement model to Mishra et al (2007). They additionally took into consideration the effect of friction reducer by introducing a drag reduction model presented by Virk (1975).

Nozaki and Hill (2010) presented an acid placement model for gas reservoirs in vertically extensive wells. Their model can be applied to the case where the original wellbore fluid is reservoir gas.

Furui et al. (2010) presented an integrated acid placement model. Their model is based on the Mishra et al. model (2007). Their model is applicable for both fully-

completed wells (i.e., radial flow) and selectively-completed perforation cluster wells (i.e., spherical flow) commonly employed in carbonate reservoirs. They used a steady-state pipe network model which was presented by Greyvenstein and Laurie (1994). As a result, they obtained a good and quick convergence in their pressure and flow rate computations.

1.2.2 Ball Sealer Diversion

Ball Sealer Technology

Ball Sealers were introduced to the oil and gas industry in 1956 for a multi-stage fracturing treatment (Kastrop 1956; Derrick and Kaltenberger 1956). Their purpose is to seal off casing perforations opposite the more permeable zones, permitting controlled fracturing of the less permeable layers through casing perforations not sealed by rubber-coated balls (Kastrop 1956). They are used not only in hydraulic fracturing treatments but also in acidizing treatments (Bale 1984; Erbstoesser 1980; Gabriel and Erbstoesser 1984; Gilchrist et al. 1994). They have been extensively used because of the ease of operations and low cost.

Usually, ball sealers are denser than the treating fluid, so that after treatment, the ball sealers will gravitate into the rathole (Economides et al. 1993). However, those non-buoyant ball sealers often fail to provide satisfactory diversion effect (Webster et al. 1964; Stipp and Williford 1968) because of low injection rate (Howard 1962; Bale 1984) and high perforation density (Bale 1984). The number of perforations is limited to 2 shots per foot for successful non-buoyant ball sealer treatments (Bale 1984).

Erbstoesser (1980) conducted laboratory tests with ball sealers having various densities, and found that buoyant ball sealers provided higher seating efficiencies (the ratios of the total number of ball seated on the number of perforations) when compared to non-buoyant ball sealers, especially at low flow rates (**Fig. 1.3**).

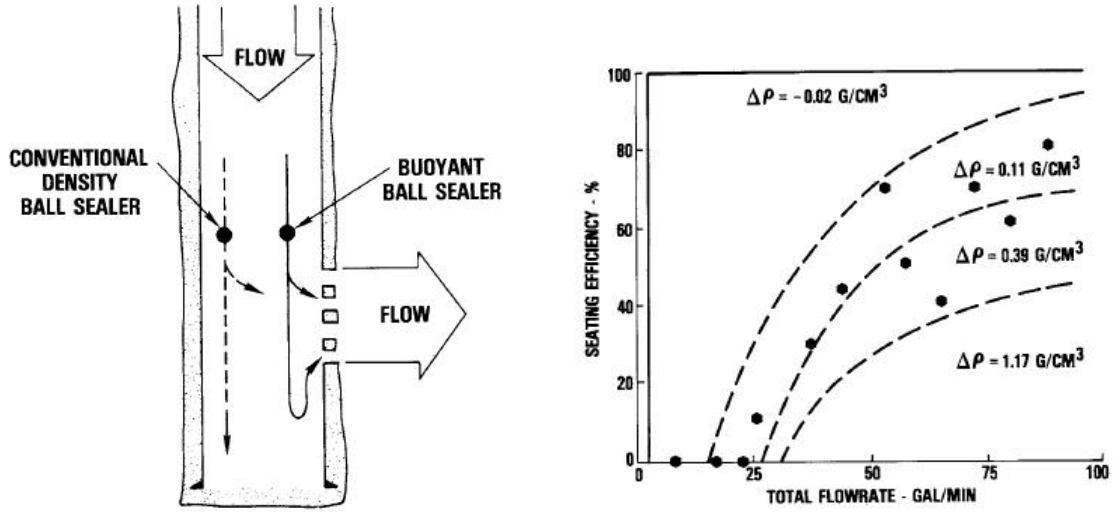

Fig. 1.3—Buoyant ball sealer: (a) schematic representation; (b) seating efficiency (from Erbstoesser 1980).

From the tests, he also identified three other parameters of critical importance to ball sealer seating efficiency:

- flow rate through the perforations,
- flow rate past the perforations, and
- fluid viscosity.

In addition, he presented case studies of buoyant ball sealer applications in acid fracturing treatments and matrix acidizing treatments. Bale (1984) also presented a case study which showed buoyant ball sealers were effective in matrix acidizing treatments in carbonate reservoirs in Saudi Arabia. High injection rate is necessary for buoyant ball sealer treatments to transport the buoyant ball sealers down the wellbore to the perforations.

Design Methodology of Ball Sealer Diversion

A general guideline for ball sealer use is to use twice as many non-buoyant ball sealers as perforations; with buoyant ball sealers, a 50% excess of ball sealers is recommended (Economides et al. 1993). The seating efficiency of ball sealers will increase as injection

rate increases and ball sealers are not recommended for low rate (< 1 bbl/min) treatments (Economides et al. 1993).

In 1959, Brown and Loper proposed design procedure for hydraulic fracturing treatments with ball sealers. They applied the method to 35 treatments and 32 of those treatments were successful.

Later, Brown et al. (1963) studied the factors affecting the performance of a ball sealer:

- inertial force,
- drag force on ball sealers through a perforation,
- force tending to unseat ball sealers, and
- force tending to hold ball sealers.

They figured out that these factors provide useful aid to design and operation of successful ball sealer treatments. By considering these factors, they evaluated nine ball sealer treatments. However, their analysis was qualitative. Still, they could not determine the seating efficiency.

Gabriel and Erbstoesser (1984) proposed a field-tested design methodology to optimize the diversion efficiency of buoyant ball sealers. They presented several methods of controlling ball sealers' movement inside the wellbore during and after the operations, especially for buoyant ball sealer treatments.

Baylocq et al. (1999) presented a design procedure for hydraulic fracturing treatment with non-buoyant ball sealers. Their recommendation was to inject as many ball sealers as the number of perforations that are aligned with the fracture. Although this recommended number is less than the recommended number in the general guideline by Economides et al. (1993), their design procedure was successful in their field treatment.

Post-Evaluation Methodology of Ball Sealer Diversion Treatments

Commonly, the bottomhole pressure record is used to evaluate whether ball sealers seat on perforations or not (e.g., Kastrop 1956). For multi-stage hydraulic fracturing

treatments, if ball sealers hit the perforations, there is an abrupt pressure increase and an immediate subsequent pressure decrease caused by initiation of a new fracture (Howard 1962). This abrupt pressure increase is commonly used to identify how many ball sealers seat on the perforations.

It is possible to identify how many ball sealers seated on the perforations by examining the recovered ball sealers. Ball sealers that had been in contact with the perforations have usually some marks on the surface.

Also, production logging is used to evaluate effectiveness of ball sealer diversion qualitatively. For example, radioactive tracers were injected in acid stages to assist with well evaluation (Gilchrist et al. 1994). By using three different types of tracers, it was able to evaluate the effectiveness of the ball sealer diversion at each acid stage qualitatively. However, with the presented production logging methods in the literature, it is not possible to assess ball sealer treatments in a real-time monitoring manner.

Study on Seating Efficiency

Seating efficiency is usually used as an index to ascertain the success or otherwise of a ball sealer treatment. Intensive studies on seating efficiency have been done using laboratory tests (Neill et al. 1957; Brown and Loper 1959; Erbstoesser 1980; Bern and Lewis 1992a; Bern and Lewis 1992b; Bern 1993) and numerical simulation (Bartko et al. 1996; Li et al. 2005).

No equation or criterion exists which determines seating efficiency on the basis of experimental studies. Basically, they investigated final seating efficiency for several conditions.

Bartko et al. (1996) developed a simulator for vertical wells to evaluate ball sealer seating efficiency and calculate the pressure increases due to placement of the balls. However, they did not describe the equations which they used to determine balls' seating although they showed the input data for the simulation.

Li et al. (2005) simulated seating efficiency. They used a Lagrangian particle tracking methodology with which ball sealers are tracked from the surface until the balls

seat on the perforations. Unfortunately, the details of their calculation method were not supplied although their simulation results were presented graphically. Also, they did not combine their ball sealer model with any well stimulation simulator. Instead their model was coupled with a steady-state reservoir outflow equation. Their model cannot be applied to field well stimulation cases since a transient or pseudo-steady-state reservoir outflow equation is appropriate.

1.3 Objective and Approach

1.3.1 Objectives

The overall objectives of the study are:

1. To develop an acid placement model for oil and gas reservoirs in vertical/deviated wells.
2. To develop a ball sealer diversion model which is coupled with the acid placement model.

1.3.2 Approach

Acid Placement Model

In the same way as Nozaki and Hill (2010) we take the following approach:

- The movement of the interfaces between the two different fluids in the wellbore is tracked.
- The volume of acid solution injected at any location is simultaneously determined with its injectivity.
- Injectivity is a function of location because the injectivity at any location changes due to damage removal.
- The injectivity is predicted by incorporating skin factor equations into a transient reservoir out flow equation with variable flow rates.

Piston-like displacement is assumed at the interface between two different fluids both in the wellbore and in the reservoir.

Ball Sealer Diversion Model

1. To analyze an extensive series of full-scale ball sealer experiments conducted by BP (Bern and Lewis 1992a, Bern and Lewis 1992b).
    - First, BP experiments are compared to Erbstoesser's experiments (1980).
    - The procedure presented by Brown et al. (1963) is used to evaluate the statistical nature of the ball seating behavior in BP experiments.
    - At the end of the analysis, we develop an empirical correlation to determine ball sealer seating efficiency.
2. To incorporate the empirical correlation from the analysis of BP experiments into the acid placement model and a ball tracking model in order to develop a ball sealer diversion model. Using the ball sealer diversion model, we will be able to simulate the wellbore rate and pressure for matrix acidizing treatments. This computer program can be used for both pre- and post-evaluation of field matrix acidizing treatments.
3. To apply the new ball sealer diversion model to a hypothetical case.

1.4 Organization of the Dissertation

In section 2, we present the acid placement model which includes: wellbore flow model, reservoir outflow model, fluid interface tracking model, wormhole propagation model, and skin factor model. In addition, we show how to discretize the domain. Finally, the computer program structure for the acid placement model is presented.

In section 3, we apply the acid placement model to hypothetical cases. We study single layer cases with and without heterogeneity, and multi-layer cases. In this section, we compare two different wormhole propagation models.

In section 4, we analyze BP experimental results and develop an empirical correlation for ball sealer seating efficiency. Additionally, we present a ball sealer tracking model. Also, we present how to deal with the ball sealers' blockage. Then, the computer program structure for the ball sealer diversion model is presented.

In section 5, we apply the acid placement and diversion model to a hypothetical case. We study a multi-layer case.

In section 6, we summarize the entire work and suggest a recommendation for future work.

2. ACID PLACEMENT MODEL

2.1 Introduction

In this section, an acid placement model is presented. In a typical carbonate matrix acidizing treatment, acid is injected into the formation through production tubing, coiled tubing, or drill pipe. The acid flows into the formation and creates several large channels, called wormholes (Fig. 1.1). This enhances the productivity of a well. One of critical factors to the success of a matrix acidizing treatment is proper placement of the acid so that all of the productive intervals are sufficiently treated by the acid. If the reservoir properties such as permeability vary significantly, then the acid will tend to flow primarily into the higher-permeability zones, leaving lower-permeability zones virtually untreated. The longer the target zone is, the more difficult it is to simulate all zones efficiently.

To simulate the matrix acidizing process, an acid placement model needs a wellbore model which handles the pressure drop and material balance in the wellbore; an interface tracking model to predict the movement of interfaces between different fluids in the wellbore; a transient reservoir outflow model with variable flow rates; and skin factor models. The injectivitity at each point changes in response to acid injection. A wormhole propagation model predicts the depth of penetration of wormholes along the wellbore based on the injectivity history at every point.

2.2 Wellbore Flow Model

The wellbore flow model is developed on the basis of wellbore material balance and wellbore pressure drop equations. The injection fluids during the matrix acidizing process are mostly slightly compressible (e.g., water). We make the following assumptions:

1. The flow is steady-state.
2. The system is isothermal.

3. The displacement is piston-like between any two different fluids inside the wellbore.
4. The fluids are incompressible.

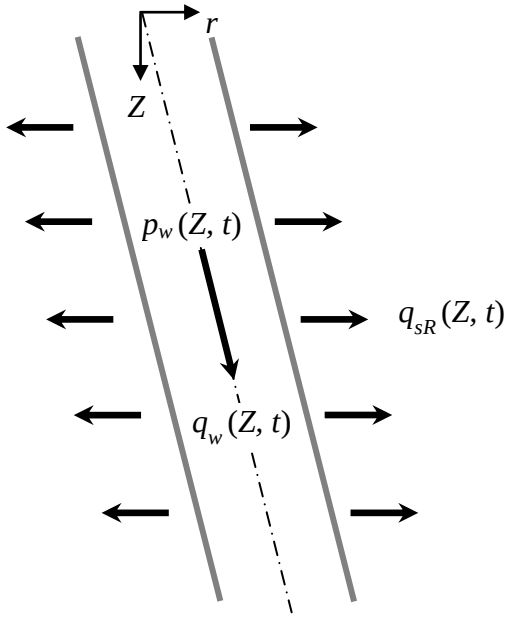

Fig. 2.1—Material balance in the wellbore.

2.2.1 Wellbore Material Balance

An acid placement model begins with a material balance on the acid in the wellbore (**Fig. 2.1**). Single-phase flow through a reservoir in a fully penetrating vertical/deviated well is considered. In Fig. 2.1, p_w is the wellbore pressure at any point in the wellbore, q_w is the volumetric flow rate in the wellbore, and q_{sR} is specific reservoir outflow in the horizontal direction (for vertical wells, the direction is perpendicular to the well). Basically, we assume the well is vertical even for deviated wells and account for the deviation effect by using a slant skin model. If the change of the fluid density is negligible, then the volumetric flow rate change along the wellbore due to the fluid flow into the reservoir can be expressed as:

$$\frac{\partial q_w(Z,t)}{\partial Z} = -q_{sR}(Z,t). \quad \text{.....(2.1)}$$

Eq. 2.1 states that the specific reservoir outflow should be equal to the decrease in the wellbore flow rate.

2.2.2 Wellbore Pressure Drop

The pressure drop of single-phase flow in a pipe over distance L can be obtained by solving the mechanical energy balance equation, which in a differential form is (Economides et al. 1993)

$$\frac{dp}{p}+\frac{vdv}{g_c}+\frac{g}{g_c}dZ+\frac{2f_f v^2 dL}{g_c d_{pipe}}+dW_s=0. \quad \text{.....(2.2)}$$

If the fluid is incompressible (ρ is constant) and there is no shaft work device in the pipeline, this equation can be readily integrated to yield

$$\Delta p=\frac{g}{g_c}\rho\Delta Z+\frac{\rho}{2g_c}\Delta v^2+\frac{2f_f\rho v^2 L}{g_c d_{pipe}}, \quad \text{.....(2.3)}$$

for fluid moving for one position to another. The three terms on the right-hand-side of Eq. 2.3 are potential energy, kinetic energy, and frictional contribution to the overall pressure drop respectively,

$$\Delta p=\Delta p_{PE}+\Delta p_{KE}+\Delta p_F. \quad \text{.....(2.4)}$$

We study the wells in which there is no change in cross-sectional area of the pipe in the reservoir zone. Hence, the pressure drop due to kinetic energy change is zero. Then Eq. 2.3 becomes for the system described in Fig. 2.1

$$\frac{\partial p_w(Z,t)}{\partial Z}=\frac{g}{g_c}\rho-\text{sgn}[q_w(Z,t)]\frac{2f_f\rho q_w^2(Z,t)}{\pi^2 g_c d_{pipe}^5\cos\theta}. \quad \text{.....(2.5)}$$

Here $\partial L = \partial Z/\cos\theta$. Eq. 2.5 can be transformed in the following unit system;

$$\frac{\partial p_w(Z,t)}{\partial z}=6.939\times10^{-3}\rho-\text{sgn}[q_w(Z,t)]\frac{1.525f_f\rho q_w^2(Z,t)}{d_{pipe}^5\cos\theta} \quad \text{.....(2.6)}$$

where p_w is in psi, ρ is in lb_m/ft^3, q_w is in bbl/min, d_{pipe} is in inch, and θ is in degrees. f_f is the Fanning friction factor. This factor is dependent on the flow regime, turbulent or laminar flow. The regime can be determined by evaluating the Reynolds number (N_{Re}):

$$N_{\mathrm{Re}} = \frac{d_{pipe}\left|\bar{v}\right|\rho}{\mu}. \quad \text{.....(2.7)}$$

where μ is the fluid viscosity. Consistent units must be used in the evaluation of the Reynolds number so that N_{Re} is dimensionless. Laminar and turbulent flows are distinguished by $N_{\mathrm{Re}} < 2{,}000$ and $N_{\mathrm{Re}} > 4{,}000$, the flow is the called transitional when $2{,}000 < N_{\mathrm{Re}} < 4{,}000$ and can display characteristics of either laminar or turbulent flow, depending on upstream flow characteristics and pipe roughness. In our simulations, we set the flow as laminar when $N_{\mathrm{Re}} < 2{,}100$ and set the flow as turbulent when $N_{\mathrm{Re}} > 2{,}100$. In laminar flow, the friction factor is a simple function of the Reynolds number:

$$f_f = \frac{16}{N_{\mathrm{Re}}}. \quad \text{.....(2.8)}$$

The frictional pressure drop is obtained from the Fanning equation as shown in Eq. 2.2. The Fanning friction factor, f_f is most commonly obtained from the Moody friction factor chart. An explicit equation for the friction factor with similar accuracy to the Colebrook-White equation (Gregory and Fogarasi 1985) is the Chen equation (Chen 1979):

$$\frac{1}{\sqrt{f_f}} = -4\log_{10}\left\{\frac{\varepsilon}{3.7065} - \frac{5.0452}{N_{\mathrm{Re}}}\left[\frac{\varepsilon^{1.1098}}{2.8257} + \left(\frac{7.149}{N_{\mathrm{Re}}}\right)^{0.8981}\right]\right\}. \quad \text{.....(2.9)}$$

2.3 Reservoir Outflow

2.3.1 Openhole Completion

The differential equation for fluid flow in a porous medium, the diffusivity equation, is a combination of the law of conservation of matter, an equation of state, and Darcy's law (Earlougher 1977). In radial coordinates, the diffusivity equation can be expressed as:

$$\frac{1}{r}\frac{\partial}{\partial r}\left(r\frac{\partial p}{\partial r}\right) = \frac{\phi\mu c_t}{k}\frac{\partial p}{\partial t}. \quad \text{.....(2.10)}$$

By assuming horizontal flow, negligible gravity effects, a homogeneous and isotropic porous medium, a single fluid of small and constant compressibility, and applicability of Darcy's law, and that μ, c_t, k, and ϕ are independent of pressure, Eq. 2.10 is linear and

readily solved (Earlougher 1977). Additionally, by assuming that the well can be represented as a line source, in other words, the wellbore is infinitesimally small ($r_w \rightarrow 0$), and that the effects of the outer boundaries of the reservoir are not seen, the line-source solution of Eq. 2.10 is given by (Dake 1983):

$$p_w(t) = p_i - \frac{q\mu}{4\pi kh}\int_{\frac{\phi\mu c_t r_w^2}{4kt}}^{\infty}\frac{e^{-s}}{s}ds = p_i - \frac{q\mu}{4\pi kh}\mathrm{Ei}\left(\frac{\phi\mu c_t r_w^2}{4kt}\right). \quad \text{.....(2.11)}$$

Now we introduce the following dimensionless pressure and time:

$$p_D = \frac{2\pi kh}{q\mu}[p_i - p_w(t)] \quad \text{.....(2.12)}$$

and

$$t_D = \frac{4kt}{\phi\mu c_t r_w^2}. \quad \text{.....(2.13)}$$

In a common unit system used for matrix acidizing treatments, Eqs. 2.12 and 2.13 become

$$p_D = \frac{kh}{141.2q\mu}[p_i - p_w(t)] \quad \text{.....(2.14)}$$

and

$$t_D = \frac{4.395\times10^{-6}kt}{\phi\mu c_t r_w^2} \quad \text{.....(2.15)}$$

where k is in md, h is in ft, q is in bbl/min, μ is in cp, p is in psi, t is in minutes, c_t is psi^{-1}, and r_w is in ft (Furui et al 2010). Using the same unit system in Eq. 2.11 and combining Eqs. 2.14 and 2.15, we obtain

$$p_D(t_D) = -\frac{1}{2}\mathrm{Ei}\left(-\frac{1}{4t_D}\right). \quad \text{.....(2.16)}$$

Eq. 2.16 can be calculated by using the following approximate equations (Edwardson et al. 1962):

$$p_D(t_D) = \frac{370.529\sqrt{t_D} + 137.582t_D + 5.69549t_D\sqrt{t_D}}{328.834 + 265.488\sqrt{t_D} + 45.2157t_D + t_D\sqrt{t_D}} \quad \text{for } 0.01 < t_D < 500$$

..... (2.17)

and

$$p_D(t_D) = \left(\frac{1}{2}\ln t_D + 0.40454\right)\left(1 + \frac{1}{2t_D}\right) + \frac{1}{4t_D} \quad \text{for } t_D \geq 500. \quad \text{..... (2.18)}$$

To account for an additional pressure drop, the skin concept was originally introduced by van Everdingen and Hurst (1949):

$$\Delta p_s = \frac{q\mu}{2\pi kh}s. \quad \text{..... (2.19)}$$

Using the unit system used in Eq. 2.14 and adding into Eq. 2.12 and solving for $p_w(t)$ gives

$$p_w(t) = p_i - \frac{141.2q\mu}{kh}(p_D + s). \quad \text{..... (2.20)}$$

Eq. 2.20 is valid only for a constant injection or production rate case. The rates are commonly not constant during the matrix acidizing treatments. Using the principle of superposition, the well pressure for *n* flow rates can be expressed as (Earlougher 1977)

$$\begin{aligned} p_w(t^n) &= p_i - \frac{141.2\mu}{kh}\{q^1[p_D(t_D^n) + s^n] + (q^2 - q^1)[p_D(t_D^n - t_D^1) + s^n] \\ &\quad + (q^3 - q^2)[p_D(t_D^n - t_D^2) - s^n)] + \cdots + (q^n - q^{n-1})[p_D(t_D^n - t_D^{n-1}) + s^n]\} \\ &= p_i - \frac{141.2}{kh}\sum_{i=1}^{n}(q^j - q^{j-1})[p_D(t_D^n - t_D^{j-1})] + q^n s^n. \quad \text{..... (2.21)} \end{aligned}$$

If the wellbore is divided into small segments of thickness *h*, then Eq. 2.21 can be applied for each segment. After dividing Eq. 2.21 by *h* and rearranging, we get

$$\begin{aligned} -\frac{kh}{141.2\mu}[p_i - p_w(t^n)] &= \sum_{j=1}^{n-1}(q_{sR}^j - q_{sR}^{j-1})[p_D(t_D^n - t_D^{j-1})] - q_{sR}^{n-1}p_D(t_D^n - t_D^{n-1}) \\ &\quad + q_{sR}^n[p_D(t_D^n - t_D^{n-1}) + s^n]. \quad \text{..... (2.22)} \end{aligned}$$

The term q_{sR} introduced in Eq. 2.1 is the specific reservoir outflow in unit of bbl/min/ft. Solving for q_{sR}^n, we obtain

$$q_{sR}^{n} = -a_J[p_i - p_w(t^n)] - b_J \quad \text{.....(2.23)}$$

where the coefficients, a_J and b_J are defined by Eqs. 2.24 and 2.25 respectively,

$$a_J = \frac{4.918\times10^{-6}k}{\mu[p_D(t_D^n - t_D^{n-1}) + s^n]} \quad \text{.....(2.24)}$$

and

$$b_J = \frac{\sum_{j=1}^{n-1}(q_{sR}^{j} - q_{sR}^{j-1})p_D(t_D^n - t_D^{j-1}) - q_{sR}^{n-1}p_D(t_D^n - t_D^{n-1})}{p_D(t_D^n - t_D^{n-1}) + s^n}. \quad \text{.....(2.25)}$$

2.3.2 Cased and Perforated Completion

Perforating is a commonly practiced method for well completion (Furui 2004). The perforation is the communication tunnel extending beyond the casing or liner into the reservoir formation, through which oil or gas is produced. In most cases, a high penetration is desirable to create effective flow communication to the part of the formation that has not been damaged by the drilling or completion processes (Furui 2004).

The flow for cased and perforated wells is different from the one for openhole completions. In general, a skin factor is used to account for this difference (Karakas and Tariq 1991; Furui et al. 2008). We use Karakas and Tariq's model (1991). We show the model in detail in Sec. 2.6.4.

In addition, we sometimes need to take into consideration the pressure drop through the perforations. This pressure drop is significant when the flow rate is high or the limited-entry technique, in which the perforation shot density is very small, is used (Lagrone and Rasmussen 1963). Therefore, the sandface pressure is significantly different from the wellbore pressure. In general, the perforations are regarded as a sharp-edged orifice to calculate the pressure drop through the perforations. The classical derivation for pressure loss across a sharp-edged orifice is based on solving the mechanical energy balance between points 1 and 2 as shown in **Fig. 2.2** (Bird et al. 1960). In this derivation, velocity profiles at both locations are assumed to be flat,

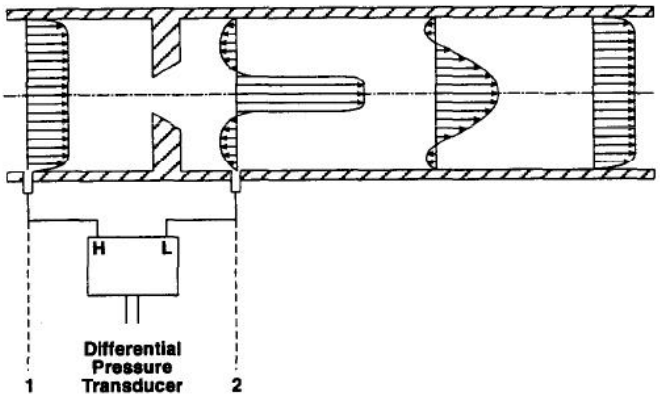

Fig. 2.2—Approximate velocity profiles used to derive the flow equation of a sharp-edged orifice (from Bird et al. 1960).

and the reduced flow area at point 2 is assumed to approximate the condition found at the *vena contracta* (Lord et al. 1994). Additionally, the friction loss is assumed to be zero since the sharp-edged orifice does not have length. To account for errors introduced by these assumptions, the equation derived for flow rate is multiplied by a discharge coefficient, K_d, (Lord et al. 1994). The pressure drop is expressed by the following formula (Furui et al. 2010):

$$\Delta p_{perf} = 1.98244\,(q^2 / n_{perf}^2)\gamma / (K_d d_{perf}^2)^2 \quad \text{.....(2.26)}$$

where n_{perf} is the number of open perforations, and γ is the fluid specific gravity. Hence, for the cased and perforated wells, Eq. 2.23 becomes

$$q_{sR}^n = -a_J\{p_i - p_w(t^n) + 1.98244[q_{sR}^2 h^2 / n_{perf}^2]\gamma / (K_d d_{perf}^2)^2\} - b_J\,. \quad \text{.....(2.27)}$$

2.4 Interface Tracking

A model to track the interfaces created between two different fluids was presented by Jones and Davies (1996) and Eckerfield et al. (2000). The acid placement model uses a discretized solution approach which is integrated with the reservoir outflow. **Fig. 2.3** depicts a part of the wellbore with one interface created between injected acid and original wellbore fluid (completion fluid). Assuming piston-like displacement, the velocity of the interface located at z_{int} is given by

$$\frac{dZ_{int}}{dt} = \left.\frac{q_w}{A_{pipe}}\right|_{Z=Z_{int}} . \quad \text{.....(2.28)}$$

where A_{pipe} is the cross-sectional area of the flow in the pipe. Eq. 2.28 is solved by discretizing the wellbore into small segments and assuming constant q_w over each segment.

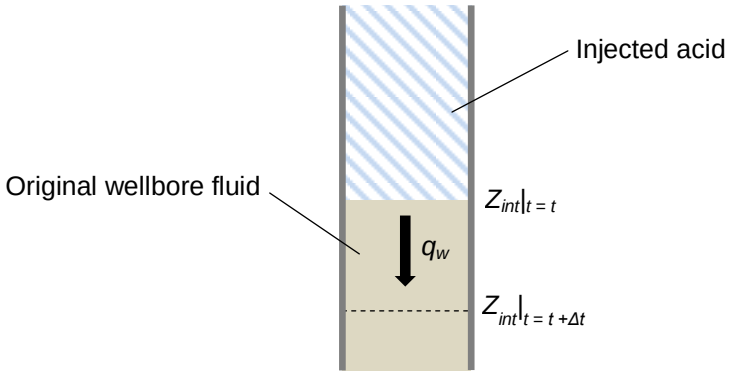

Fig. 2.3—Interface tracking from *t* to *t* + *Δt*.

2.5 Wormhole Propagation

2.5.1 Buijse and Glasbergen Model

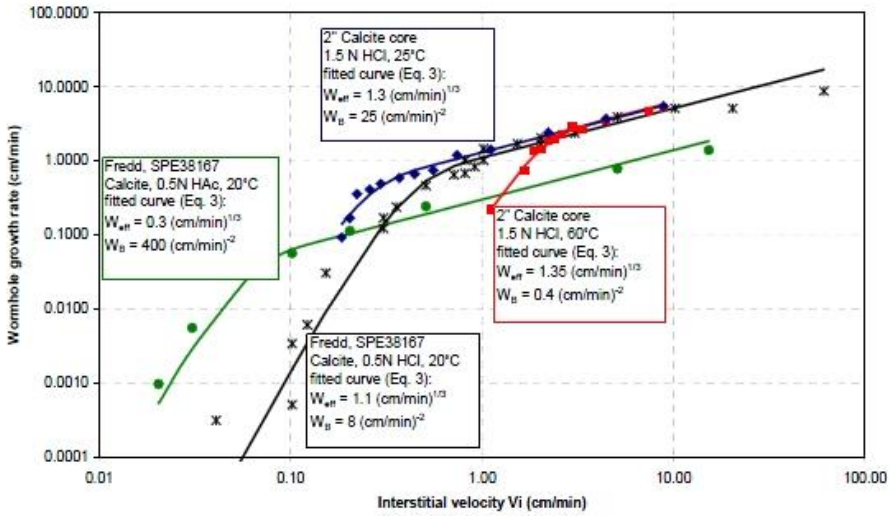

Fig. 2.4—Wormhole growth rate (v_{wh}) vs. interstitial velocity (v_i) (from Buijse and Glasbergen 2005).

Buijse and Glasbergen (2005) recently presented a semi-empirical wormhole growth model. According to their model, the wormhole growth rate, v_{wh}, can be approximated by

$$v_{wh} = \left(\frac{v_i}{PV_{bt,opt}}\right) \times \left(\frac{v_i}{v_{i,opt}}\right)^{-\gamma} \times \left\{1 - \exp\left[-4\left(\frac{v_i}{v_{i,opt}}\right)^2\right]\right\}^2 \quad \text{.....(2.29)}$$

where γ is the coefficient that represents the effect of the fluid loss limited wormholing, $PV_{bt,opt}$ is the optimum pore volumes to breakthrough, $v_{i,opt}$ is the optimum interstitial velocity, and v_i is the interstitial velocity at the front of the wormhole zone. $PV_{bt,opt}$ and $v_{i,opt}$ are obtained by fitting linear coreflooding experimental data. For the linear coreflooding experimental data, γ should be set to 1/3 as Buijse and Glasbergen originally presented. **Fig. 2.4** shows some examples of the fitting results from Buijse and Glasbergen's paper. Their model enables us to translate linear coreflooding experimental results into radial flow conditions which are actual field conditions. Buijse and Glasbergen (2005) suggested the following equation to estimate v_i for openhole completions,

$$v_i = \frac{q}{2\pi h r_{wh}(t)\phi} \quad \text{.....(2.30)}$$

where q is the injection rate at sandface, h is the thickness of the treating zone, r_{wh} is the wormhole penetration radius at time t, and ϕ is the porosity. For cased and perforated completions, they proposed the following equations:

$$v_i = \frac{q}{\pi h \rho_{perf} d_{perf} l_{perf} \phi} \quad \text{for } r_{wh} = r_w + l_{perf}, \quad \text{.....(2.31)}$$

$$v_i = \frac{q}{\pi(2r_{we} - l_{perf} - r_w)h\phi}\left(\frac{r_{wh} - l_{perf} - r_w}{\rho_{perf} d_{perf} l_{perf}} + \frac{2r_{we} - r_{wh}}{2r_{we}}\right)$$

$$\text{for } r_{wh} + l_{perf} < r_{wh} < 2r_{we}, \quad \text{.....(2.32)}$$

and,

$$v_i = \frac{q}{2\pi h r_{wh}(t)\phi} \qquad \text{for } r_{wh} \geq 2r_{we}, \quad \text{.....(2.30)}$$

where r_{we} is the effective wellbore radius defined by Karakas and Tariq (1991). When the well is cased and perforated, then the surface area available to flow is smaller than for openhole completions in the early time. At $t = 0$, when the acid starts invading into the rock ($r_{wh} = r_w + l_{perf}$), the surface area was assumed to be the surface area of the perforations (Eq. 2.31). In their model, for $r_{wh} \geq 2r_{we}$, the flow was assumed to be a radial flow (Eq. 2.30). For $r_{we} < r_{wh} < 2\ r_{we}$, the weighting average of Eq. 2.31 and Eq. 2.30 of $r_{wh} = 2r_{we}$. is used (Eq. 2.32).

2.5.2 Furui et al. Model

Furui et al. (2010) proposed a modified Buijse and Glasbergen model which consists of the following equations:

$$v_{wh} = v_{i,tip} N_{Ac} \left(\frac{v_{i,tip} PV_{bt,opt} N_{Ac}}{v_{i,opt}} \right)^{-\gamma} \left\{ 1 - \exp\left[-4 \left(\frac{v_{i,tip} PV_{bt,opt} N_{Ac} L_{core}}{v_{i,opt} r_{wh}} \right)^2 \right] \right\}^2, \quad \text{.....(2.33)}$$

$$v_{i,tip} = \frac{q}{\phi h \sqrt{\pi n_{wh}}} \left[(1-\alpha_z) \frac{1}{\sqrt{d_{e,wh} r_{wh}}} + \alpha_z \left(\frac{1}{d_{e,wh}} \right) \right], \quad \text{.....(2.34)}$$

$$d_{e,wh} = d_{core} PV_{bt,opt} N_{Ac}, \quad \text{.....(2.35)}$$

and

$$N_{Ac} = \frac{\phi \beta C_0 \rho_{acid}}{(1-\phi)\rho_{rock}} \quad \text{.....(2.36)}$$

where v_{wh} is the wormhole growth rate in cm/min, $v_{i,tip}$ is the interstitial velocity at the wormhole tip in cm/min, N_{Ac} is the acid capacity number (dimensionless), L_{core} is the core length of the liner coreflooding experiments in cm, α_z is the wormhole axial spacing coefficient (dimensionless), $d_{e,wh}$ is the effective wormhole radius in cm, d_{core} is the core diameter of the linear coreflooding experiments in cm, β is the acid dissolving power in kg/kg, C_0 is the injection acid concentration in weight fraction, ρ_{acid} is the acid density in g/cm^3, and ρ_{rock} is the density of the formation rock in g/cm^3.

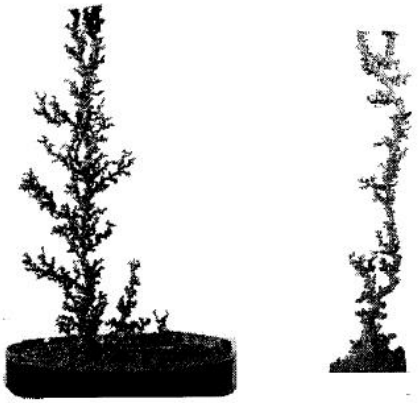

Fig. 2.5—Epoxy castings of wormholes in cores with a diameter 8 cm (left) and 2.5 cm (right) (from Buijse 2000).

First of all, Furui et al. turned their attention to the effect of core diameter. They investigated the effect of the core size on the wormhole propagation efficiency. In 2000, Buijse showed the difference in wormhole shape between two different sizes of cores (**Fig 2.5**). He also showed the impact of the core size on PV_{bt}: 0.5 PV in the 8-cm core, and 1.5 PV in the 2.5-cm core. Furui et al. conducted a series of experiments using outcrop although Buijse conducted two experiments. **Fig. 2.6** shows the Furui et al.

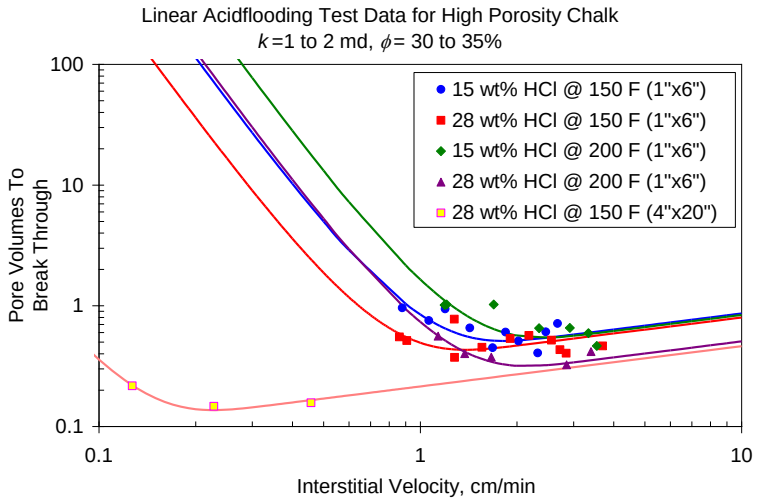

Fig. 2.6—Linear core flooding experiment results for high porosity outcrop chalk samples (from Furui et al. 2010).

experimental results. These results indicate slightly more effective wormholing than those seen in typical calcite core test results (Furui et al. 2010).

Also, Furui et al. incorporate a mechanistic model by Hung et al. (1989) into their model to account for the acid transport inside the wormholes and the fluid loss from wormholes. For deep penetrating wormholes' propagation, this effect is considered to be significant.

Finally, Furui et al. derived a semi-analytical correlation (Eq. 2.34) for estimating interstitial velocities at the tip of the dominant wormholes based on a number of 3D finite element method simulation analyses considering various wormholes patterns. As discussed in the previous section, Buijse and Glasbergen proposed Eqs. 2.30 through 2.32 where the change of cross-sectional area is linear. Furui et al. considered that the flow should be between spherical and radial flow. α_z is the key parameter which controls the weightings although the wormhole penetration radius is also the key factor as in Buijse and Glasbergen's model. They suggested 0.25 to 0.5 for vertical wells, and 0.5 to 0.75 for horizontal wells. α_z should be different in different wells. Hence, α_z should be tuned by history matching.

2.6 Skin Effect

2.6.1 Skin Effect due to Wormhole Propagation

For openhole completions without formation damage, the following equation is used to calculate the skin factor due to wormhole propagation:

$$s_{da} = -\ln \frac{r_{wh}}{r_w}. \quad \text{.....(2.37)}$$

Since $r_{wh} \geq r_w$, the skin factor is always negative once the stimulation starts. For good stimulation treatments, -3 to -4 of skin is generally obtained (Furui et al. 2010). If r_w = 0.328 ft, then the range of r_{wh} is 6.6 to 17.9 ft.

For cased and perforated completions without formation damage, the following equations are used to calculate the skin factor due to wormhole propagation (Furui et al. 2010):

$$s_{da} = \frac{h_{perf}}{2r_{wh}} - \ln\left(\frac{h_{perf}}{2r_w}\right) - 1 \quad \text{for} \quad r_{wh} < \frac{h_{perf}}{2} \quad \text{.....(2.38)}$$

where h_{perf} is the perforation spacing (**Fig. 2.7**). Once r_{wh} reaches to $h_{perf}/2$, wormholes are assumed to grow radially and then the skin factor can be calculated using Eq. 2.37. If standard perforation density is used, for example 4 spf (h_{perf} = 0.25 ft), then it is considered that it takes several seconds before r_{wh} reaches to $h_{perf}/2$. Hence, the effect of the spherical flow in Fig. 2.7 is insignificant. However, when limited-entry technique is used, for instance 0.1 spf (h_{perf} = 10 ft), the effect of the spherical flow is considered to be significant.

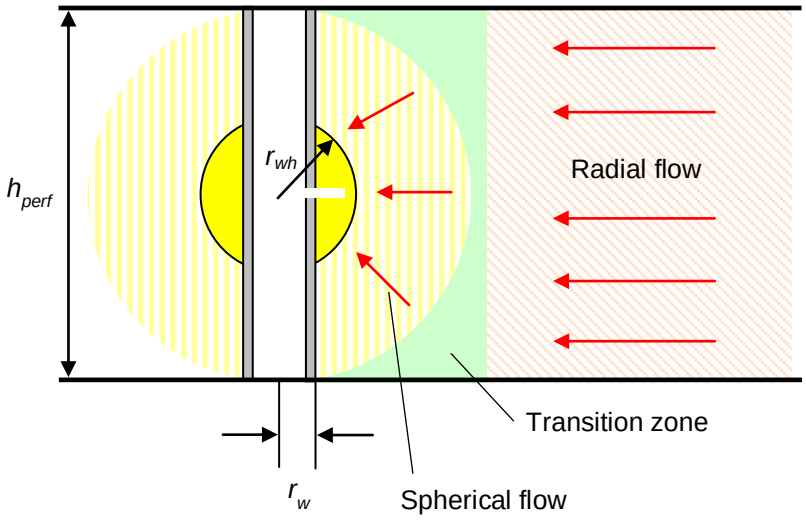

Fig. 2.7—Idealized flow geometry for wormholes extending from a single perforation tunnel (from Furui et al. 2010).

2.6.2 Damage Effect on Skin during Wormhole Propagation

For openhole completions with formation damage, the following equation is used to calculate the skin factor which accounts for the formation damage and wormholes:

$$s_{da} = \frac{k}{k_d}\ln\frac{r_d}{r_{wh}} - \ln\frac{r_d}{r_w} \quad \text{for} \quad r_{wh} < r_d \quad \text{.....(2.39)}$$

where k is the original permeability, k_d is the damage permeability, and r_d is the damage penetration radius. Once wormholes extend beyond the damage region, the effect of the formation damage is assumed to be negligible and then the skin factor can be calculated using Eq. 2.37.

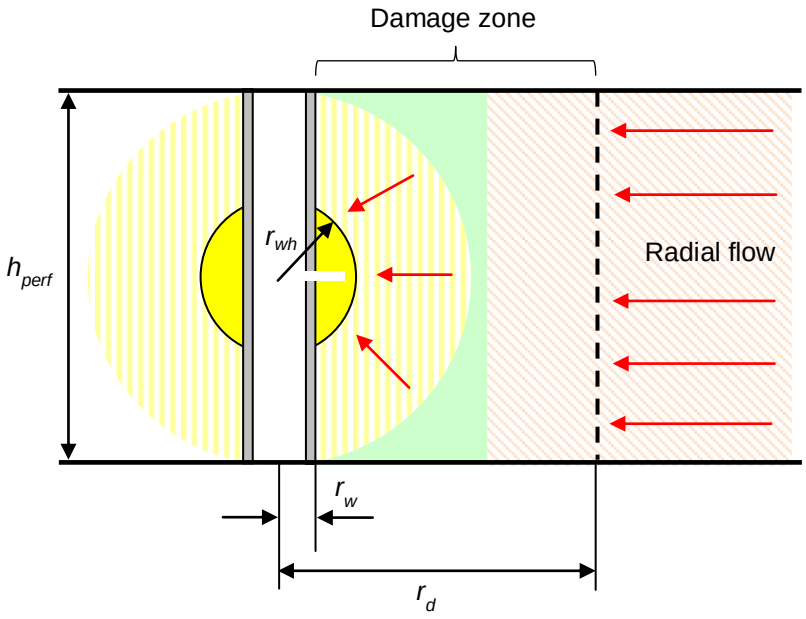

Fig. 2.8—Idealized flow geometry for wormholes extending from a single perforation tunnel with formation damage ($r_d \geq h_{perf}/2$).

For cased and perforated completions with formation damage, the following equations can be used to calculate the skin factor for $r_d \geq h_{perf}/2$ (**Fig. 2.8**):

$$s_{da} = \frac{k}{k_d}\left[\frac{h_{perf}}{2}\left(\frac{1}{r_{wh}} - \frac{2}{h_{perf}}\right) + \ln\left(\frac{2r_d}{h_{perf}}\right)\right] - \ln\frac{r_d}{r_w} \quad \text{for} \quad r_{wh} < \frac{h_{perf}}{2}, \quad \text{.....(2.40)}$$

$$s_{da} = \frac{k}{k_d}\ln\frac{r_d}{r_{wh}} - \ln\frac{r_d}{r_w} \quad \text{for} \quad \frac{h_{perf}}{2} \leq r_{wh} \leq r_d, \quad \text{.....(2.39)}$$

and

$$s_{da} = -\ln\frac{r_{wh}}{r_w} \quad \text{for} \quad r_d < r_{wh}. \quad \text{.....(2.37)}$$

Every equation has been discussed except for $r_{wh} < h_{perf}/2$. For $r_d < h_{perf}/2$ (**Fig. 2.9**),

$$s_{da} = \frac{h_{perf}}{2}\left[\frac{k}{k_d}\left(\frac{1}{r_w}-\frac{1}{r_d}\right)+\left(\frac{1}{r_d}-\frac{2}{h_{perf}}\right)\right]-\ln\frac{h_{perf}}{2r_w} \quad \text{for } r_{wh} < r_d\,, \quad \text{.....} (2.41)$$

$$s_{da} = \frac{h_{perf}}{2r_{wh}}-\ln\frac{h_{perf}}{2r_w}-1 \quad \text{for } \frac{h_{perf}}{2} \le r_{wh} \le r_d\,, \quad \text{.....} (2.38)$$

and

$$s_{da} = -\ln\frac{r_{wh}}{r_w} \quad \text{for } r_d < r_{wh}\,. \quad \text{.....} (2.37)$$

As discussed in the previous section, these equations are significant only for the case where limited-entry technique is used, that is, the perforation density is small. If we use these equations, the time step size needs to be small enough to avoid underestimating the wormhole propagation rate.

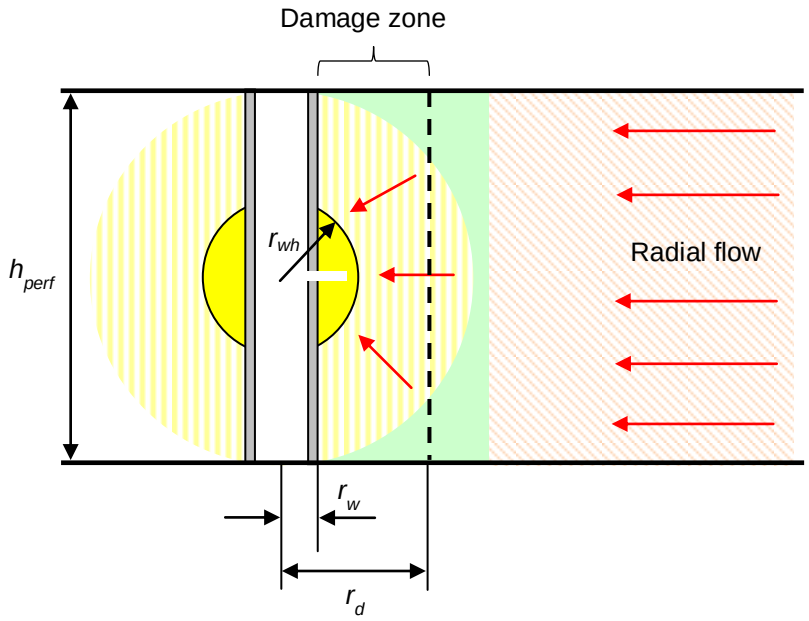

Fig. 2.9—Idealized flow geometry for wormholes extending from a single perforation tunnel with formation damage ($r_d < h_{perf}/2$).

2.6.3 Slant Skin Effect

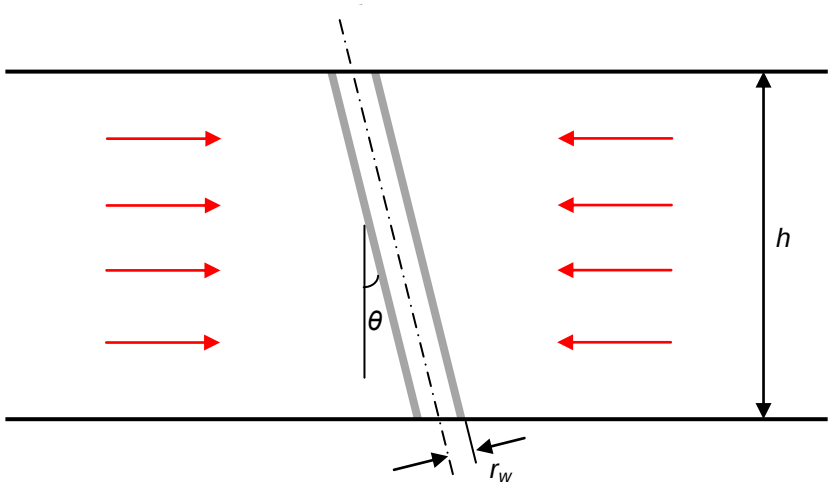

Fig. 2.10—Slanted well.

Besson (1990) studied performance of slanted and horizontal wells. Besson obtained the following correlation of slant skin factor, s_θ:

$$s_\theta = \ln\left(\frac{4r_w\cos\theta}{h\gamma}\sqrt{\frac{k_V}{k_H}}\right)+\frac{\cos\theta}{\gamma}\ln\left(\frac{h}{2r_w(1+\gamma^{-1})}\sqrt{\frac{k_H\gamma}{k_V\cos\theta}}\right) \quad \text{.....(2.42)}$$

where

$$\gamma = \left(\cos^2\theta+\frac{k_V}{k_H}\sin^2\theta\right)^{1/2}. \quad \text{.....(2.43)}$$

θ is the angle from vertical as defined in **Fig. 2.10**, k_H is the horizontal permeability, k_V is the vertical permeability, and γ is the geometric factor of the well.

2.6.4 Skin Effect due to Perforation

Karakas and Tariq (1991) presented a semi-analytical perforation skin factor model on the basis of their 3D finite element method simulator. They divided the perforation skin factor into three components; the 2D plane flow skin factor, s_{2D}; the wellbore blockage skin factor, s_{wb}; and the 3D convergence skin factor s_{3D}. The total perforation skin factor is then given by

$$s_{perf} = s_{2D} + s_{wb} + s_{3D}. \quad \text{.....(2.44)}$$

2D Plane Flow Skin Factor

$$s_{2D} = \ln\left(\frac{r_w}{r_{we}(\theta_{perf})}\right) \quad \text{.....(2.45)}$$

where

$$r_{we}(\theta_{perf}) = \begin{cases} \frac{1}{4} l_{perf} & \text{if } \theta_{perf} = 0^{\circ} \\ \alpha_{\theta}(\theta_{perf})(r_w + l_{perf}) & \text{otherwise.} \end{cases} \quad \text{.....(2.46)}$$

The effective wellbore radius, r_{we}, is dependent on the perforation phasing, θ_{perf}. α_{θ} is shown in **Table 2.1**.

Wellbore Blockage Skin Factor

$$s_{wb} = c_{\theta 1}(\theta_{perf}) \exp\left[c_{\theta 2}(\theta_{perf}) \frac{r_w}{l_{perf} + r_w}\right] \quad \text{.....(2.47)}$$

where $c_{\theta 1}$ and $c_{\theta 2}$ are dependent on the perforation phasing (**Table 2.2**).

3D Convergence Skin Factor

$$s_{3D} = 10^{a}\left[\left(\frac{h_{perf}}{l_{perf}}\right)\sqrt{\frac{k_H}{k_V}}\right]^{b-1}\left[\left(\frac{d_{perf}}{4h_{perf}}\right)\cdot\left(1+\sqrt{\frac{k_V}{k_H}}\right)\right]^{b} \quad \text{.....(2.48)}$$

where

$$a = a_1 \log_{10}\left[\left(\frac{d_{perf}}{4h_{perf}}\right)\cdot\left(1+\sqrt{\frac{k_V}{k_H}}\right)\right] + a_2 \quad \text{.....(2.49)}$$

and

$$b = b_1 \times \left[\left(\frac{d_{perf}}{4h_{perf}}\right)\cdot\left(1+\sqrt{\frac{k_V}{k_H}}\right)\right] + b_2. \quad \text{.....(2.50)}$$

Table 2.3 lists the values of a_1, a_2, b_1, and b_2.

TABLE 2.1—DEPENDENCY OF r_{we} ON PHASING.	
Perforation phasing, degrees	α_θ
0	0.250
180	0.500
120	0.648
90	0.726
60	0.813
45	0.860

TABLE 2.2—VARIABLES $c_{\theta 1}$ and $c_{\theta 2}$ in EQ. 2.47		
Perforation phasing, degrees	$c_{\theta 1}$	$c_{\theta 2}$
0	1.6×10^{-1}	2.675
180	2.6×10^{-2}	4.532
120	6.6×10^{-3}	5.320
90	1.9×10^{-3}	6.155
60	3.0×10^{-4}	7.509
45	4.6×10^{-5}	8.791

TABLE 2.3—3D CONVERGENCE SKIN FACTOR COEFFICIENTS.				
Peroration phasing, degrees	a_1	a_2	b_1	b_2
0	-2.091	0.0453	5.1313	1.8672
180	-2.025	0.0943	3.0373	1.8115
120	-2.018	0.0634	1.6136	1.7770
90	-1.905	0.1038	1.5674	1.6935
60	-1.898	0.1023	1.3654	1.6490
45	-1.788	0.2398	1.1915	1.6392

2.6.5 Total Skin Factor

We have discussed about each skin factor. For Eqs. 2.24 and 2.25, total skin factor is needed. We discuss about the total skin factor before and during the stimulation.

Before the Stimulation

Before the stimulation, the skin effect due to formation damage for openhole completions is given by

$$s_{da} = \left(\frac{k}{k_d} - 1 \right) \ln \frac{r_d}{r_w}. \quad \text{.....(2.51)}$$

For cased and perforated wells, the skin effect due to formation damage and perforation is given by

$$s_{da} = \left(\frac{k}{k_d} - 1 \right) \ln \frac{r_d}{r_w} + \frac{k}{k_d} s_{perf} \quad \text{for } r_w + l_{perf} \le r_d \quad \text{.....(2.52)}$$

and

$$s_{da} = s_{perf}(l_{perf} = l'_{perf}, r_w = r'_w) \quad \text{for } r_w + l_{perf} > r_d \quad \text{.....(2.53)}$$

where

$$l'_{perf} = l_{perf} - \left(1 - \frac{k_d}{k} \right)(r_d - r_w) \quad \text{.....(2.54)}$$

and

$$r'_w = r_w + \left(1 - \frac{k_d}{k} \right)(r_d - r_w). \quad \text{.....(2.55)}$$

The total skin factor, s_{Total}, is calculated by

$$s_{Total} = s_{da} + s_\theta. \quad \text{.....(2.56)}$$

During the stimulation

Also, Eq. 2.56 is used to calculate the total skin factor. s_{da} is calculated using the equations presented in Sec. 2.6.1 or 2.6.2.

2.7 Discretization

From Eq. 2.1, 2.6 and 2.23, the following systems of ODEs are to be solved:

$$\begin{cases} \dfrac{\partial q_w(Z,t)}{\partial Z} = a_J[\,p_i(Z) - p_w(Z,t)] + b_J \\ \dfrac{\partial p_w(Z,t)}{\partial Z} = c_J + d_J q_w(Z,t) \end{cases} \quad \text{.....(2.57)}$$

where

$$a_J = \frac{4.918\times10^{-6}k}{\mu[p_D(t_D^n - t_D^{n-1}) + s^n]}, \quad \text{.....(2.24)}$$

$$b_J = \frac{\sum_{j=1}^{n-1}(q_{sR}^j - q_{sR}^{j-1})p_D(t_D^n - t_D^{j-1}) - q_{sR}^{n-1}p_D(t_D^n - t_D^{n-1})}{p_D(t_D^n - t_D^{n-1}) + s^n}, \quad \text{.....(2.25)}$$

$$c_J = 6.939\times10^{-3}\rho, \quad \text{.....(2.58)}$$

and

$$d_J = -\text{sgn}[q_w(Z,t)]\cdot\frac{1.525 f_f \rho q_w(Z,t)}{d_{pipe}^5\cos\theta}. \quad \text{.....(2.59)}$$

Initial and boundary conditions are required to solve the above systems of ODEs.

$$q_w(Z,0) = 0, \;\; p_w(Z,0) = p_i(Z,0) \quad \text{.....(2.60)}$$

$$q_w(Z = Z_{bottom}, t) = 0 \quad \text{.....(2.61)}$$

$$q_w(Z = Z_{top}, t) = Q_w(t) \quad \text{.....(2.62)}$$

where z_{bottom} is the total vertical depth of the bottom of the reservoir, z_{top} is the total vertical depth of the top of the reservoir, and Q_w is the total injected acid volumetric flow rate. In a discretized form (**Fig. 2.11**), Eq. 2.57 is expressed as

$$\begin{cases} q_{w,i+1} - q_{w,i} = \Delta Z_i[a_{J,i}(p_{i,i} - p_{w,i}) + b_{J,i}] \\ p_{w,i+1} - p_{w,i} = \dfrac{\Delta Z_i + \Delta Z_{i+1}}{2}[c_J + d_J q_{w,i}] \end{cases} \quad \text{.....(2.63)}$$

where i is defined in Fig. 2.11. $p_{i,i}$ represents the initial reservoir pressure for a given segment i.

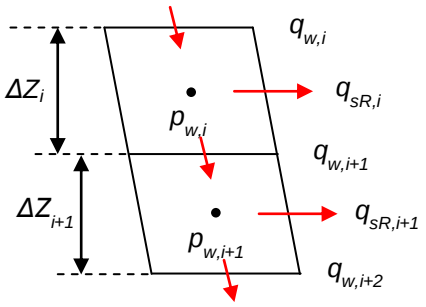

Fig. 2.11—A schematic of segmented wellbore.

In matrix form,

$$\begin{pmatrix} A_{J,1} & 1 & 0 & \cdots & \cdots & \cdots & \cdots & \cdots & \cdots & 0 \\ -1 & D_{J,1} & 1 & 0 & \cdots & \cdots & \cdots & \cdots & \cdots & 0 \\ 0 & -1 & A_{J,2} & 1 & 0 & \cdots & \cdots & \cdots & \cdots & 0 \\ 0 & 0 & -1 & D_{J,2} & 1 & 0 & \cdots & \cdots & \cdots & 0 \\ \vdots & & & \ddots & \ddots & \ddots & & & & \vdots \\ \vdots & & & & \ddots & \ddots & \ddots & & & \vdots \\ \vdots & & & & & \ddots & \ddots & \ddots & & \vdots \\ 0 & \cdots & \cdots & \cdots & \cdots & 0 & -1 & A_{J,n-1} & 1 & 0 \\ 0 & \cdots & \cdots & \cdots & \cdots & \cdots & 0 & -1 & D_{J,n-1} & 1 \\ 0 & \cdots & \cdots & \cdots & \cdots & \cdots & \cdots & 0 & -1 & A_{J,n} \end{pmatrix} \begin{pmatrix} p_{w,1} \\ q_{w,2} \\ p_{w,2} \\ q_{w,3} \\ \vdots \\ \vdots \\ \vdots \\ p_{w,n-1} \\ q_{w,n} \\ p_{w,n} \end{pmatrix} = \begin{pmatrix} A_{J,1}p_{i,1} + B_{J,1} + Q_w \\ C_{J,1} \\ A_{J,2}p_{i,2} + B_{J,2} \\ C_{J,2} \\ \vdots \\ \vdots \\ \vdots \\ A_{J,n-1}p_{i,n-1} + B_{J,n-1} \\ C_{J,n-1} \\ A_{J,n}p_{i,n} + B_{J,n} \end{pmatrix}$$

..... (2.64)

where

$$A_{J,i} = \Delta Z_i a_{J,i}, \quad \text{..... (2.65)}$$

$$B_{J,i} = \Delta Z_i b_{J,i}, \quad \text{..... (2.66)}$$

$$C_{J,i} = \frac{1}{2}(\Delta Z_i + \Delta Z_{i+1}) c_{J,i}, \quad \text{..... (2.67)}$$

and

$$D_{J,i} = \frac{1}{2}(\Delta Z_i + \Delta Z_{i+1}) d_{J,i}. \quad \text{..... (2.68)}$$

For cased and perforated completions, from Eqs. 2.1, 2.6, and 2.27, the corresponding system to Eq. 2.57 is

$$\begin{cases} \dfrac{\partial q_w(Z,t)}{\partial z} = a_J[p_i(Z) - p_w(Z,t) + e_J q_R(Z,t)] - b_J \\ \dfrac{\partial p_w(Z,t)}{\partial z} = c_J + d_J q_w(Z,t) \end{cases} \quad \text{..... (2.69)}$$

where

$$e_J = 1.98244[q_R(Z,t)/n_{perf}^2]\gamma/(K_d d_{perf}^2)^2. \quad \text{..... (2.70)}$$

In a discretized form, Eq. 2.69 becomes

$$\begin{cases} q_{w,i+1} - q_{w,i} = \Delta Z_i \{a_{J,i}[p_{i,i} - p_{w,i} + e_{J,i}(q_{w,i+1} - q_{w,i})] + b_{J,i}\} \\ p_{w,i+1} - p_{w,i} = \dfrac{\Delta Z_i + \Delta Z_{i+1}}{2}(c_{J,i} + d_{J,i} q_{w,i+1}) \end{cases} \quad \text{..... (2.71)}$$

where the index *i* is defined in Fig. 2.11 again. In matrix form,

$$\begin{pmatrix} A_{J,1} & E_{J,1} & 0 & \cdots & \cdots & \cdots & \cdots & \cdots & \cdots & 0 \\ -1 & D_{J,1} & 1 & 0 & \cdots & \cdots & \cdots & \cdots & \cdots & 0 \\ 0 & -E_{J,2} & A_{J,2} & E_{J,2} & 0 & \cdots & \cdots & \cdots & \cdots & 0 \\ 0 & 0 & -1 & D_{J,2} & 1 & 0 & \cdots & \cdots & \cdots & 0 \\ \vdots & & & \ddots & \ddots & \ddots & & & & \vdots \\ \vdots & & & & \ddots & \ddots & \ddots & & & \vdots \\ \vdots & & & & & \ddots & \ddots & \ddots & & \vdots \\ 0 & \cdots & \cdots & \cdots & \cdots & 0 & -E_{J,n-1} & A_{J,n-1} & E_{J,n-1} & 0 \\ 0 & \cdots & \cdots & \cdots & \cdots & \cdots & 0 & -1 & D_{J,n-1} & 1 \\ 0 & \cdots & \cdots & \cdots & \cdots & \cdots & \cdots & 0 & -E_{J,n} & A_{J,n} \end{pmatrix} \begin{pmatrix} p_{w,1} \\ q_{w,2} \\ p_{w,2} \\ q_{w,3} \\ \vdots \\ \vdots \\ \vdots \\ p_{w,n-1} \\ q_{w,n} \\ p_{w,n} \end{pmatrix} = \begin{pmatrix} A_{J,1}p_{i,1} + B_{J,1} + E_{J,1}Q_w \\ C_{J,1} \\ A_{J,2}p_{i,2} + B_{J,2} \\ C_{J,2} \\ \vdots \\ \vdots \\ \vdots \\ A_{J,n-1}p_{i,n-1} + B_{J,n-1} \\ C_{J,n-1} \\ A_{J,n}p_{i,n} + B_{J,n} \end{pmatrix}$$

..... (2.72)

where

$$E_{J,i} = 1 - \Delta Z_i a_{J,i} e_{J,i} \,. \quad \text{..... (2.73)}$$

2.8 Computer Program Structure

The acid placement model has been developed in the FORTRAN programming language. **Fig. 2.12** shows the flow chart for the acid placement model. The wellbore is divided into various segments on the basis of input data in the manner previously defined in Fig. 2.11. Then, the solution matrix, either Eq. 2.64 or 2.72, is constructed and solved at each time step. Then, explicitly the wormhole penetrations are calculated and correspondingly the total skin factors are calculated. Also, the interfaces inside the wellbore are updated. Then, the solution matrix is reconstructed and solved, again. The simulation ends when the time reaches to the end time. The output data give the pressure, reservoir outflow rate, wormhole penetration radius and total skin factor at each segment for each time step. Those data are valuable information for evaluating the performance of matrix acidizing treatment. A history match can be performed for observed data and simulated data by varying the treatment schedule and/or reservoir properties.

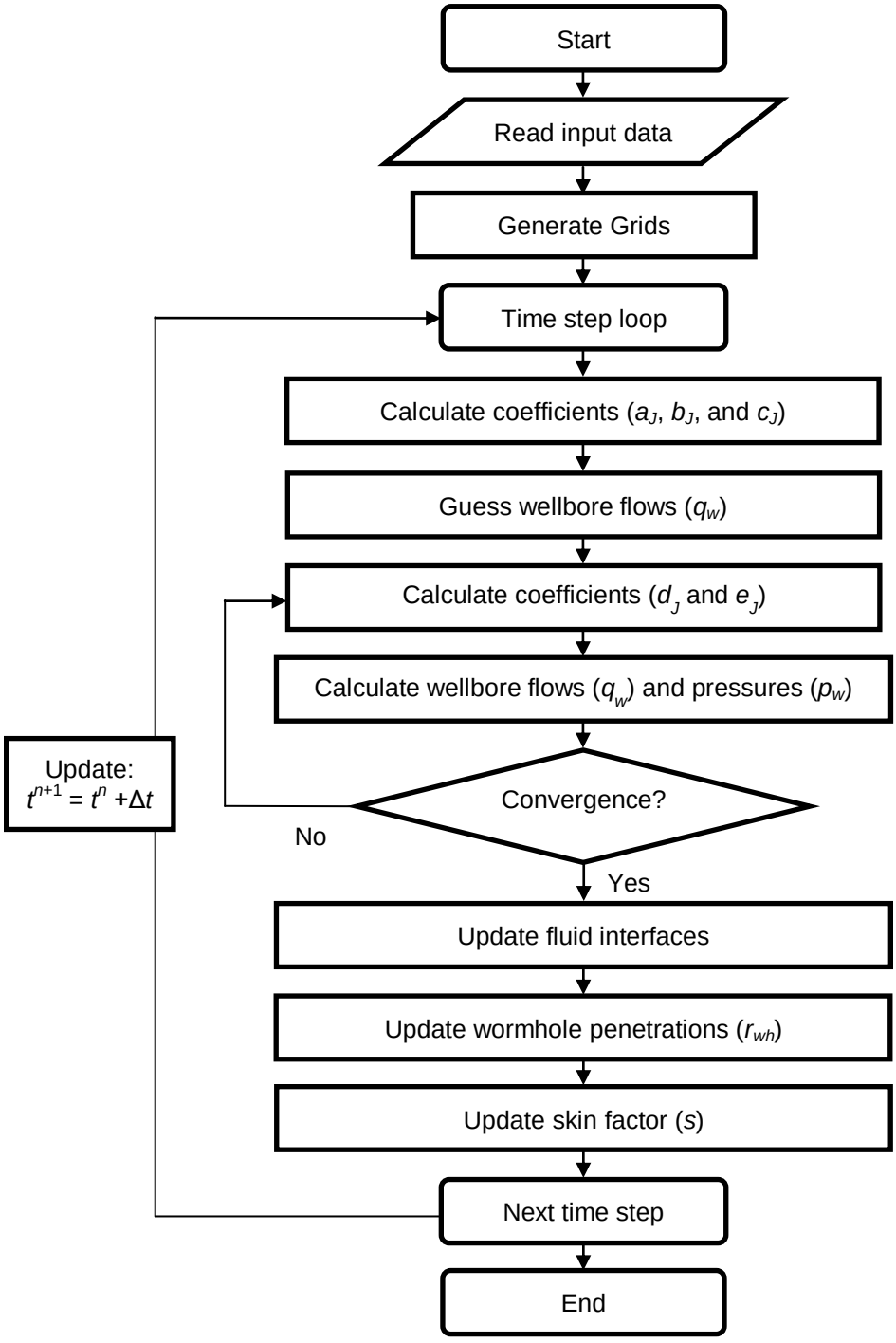

Fig. 2.12—Flow chart for the acid placement model.

2.9 Section Summary

In this section, we presented an acid placement model for openhole completions, and cased and perforated completions. This model includes:

- wellbore flow model,
- reservoir outflow model,
- interface tracking model,
- wormhole propagation model, and
- skin model.

Also, we showed the governing equations in a discretized form, and then presented the computer program structure.

3. HYPOTHETICAL CASE STUDY I

3.1 Introduction

In this section, we show several hypothetical case studies using the acid placement model presented in Sec. 2. In the first two sections, we study a homogenous reservoir with different thicknesses. In those case studies, the objective is to compare the Buijse and Glasbergen model and the Furui et al. model. After that, we study a multi-layer case to see how the overall skin factor and bottomhole pressure change. Finally, we study a heterogeneous thick formation. We use several flow rates and compare the results to see how MAPDIR (Paccaloni 1996) works for the acid distribution.

3.2 Homogenous Thin Single Layer Case

First, we study a matrix acidizing treatment in a homogenous thin single layer. **Tables 3.1 and 3.2** show the input data for this simulation. We use several flow rates (0.5-40 bbl/min) and two different wormhole axial spacing coefficients as shown in Table 3.2. The data ($PV_{bt,opt}$ and $v_{i,opt}$) in Table 3.1 were obtained by fitting Bazin's experimental data (four different HCl concentrations) as shown in **Fig. 3.1** using the following equation:

$$PV_{bt} = PV_{bt,opt} \times \left(\frac{v_i}{v_{i,opt}} \right)^{1/3} \times \left\{ 1 - \exp\left[-4 \left(\frac{v_i}{v_{i,opt}} \right)^2 \right] \right\}^{-2} \quad . \quad \text{.....(3.1)}$$

Eq. 3.1 can be obtained by substituting $PV_{bt} = v_i/v_{wh}$ into Eq. 2.9 and solving for PV_{bt}. In these simulations, the wellbore is not segmented and no damage is assumed.

TABLE 3.1—ACID DATA (FROM BAZIN 2001).

HCl Conc., wt%	$PV_{bt,opt}$	$v_{i,opt}$, cm/min
0.70	14.267	0.244
3.50	5.733	0.308
7.0	3.684	0.491
17.50	0.449	0.925

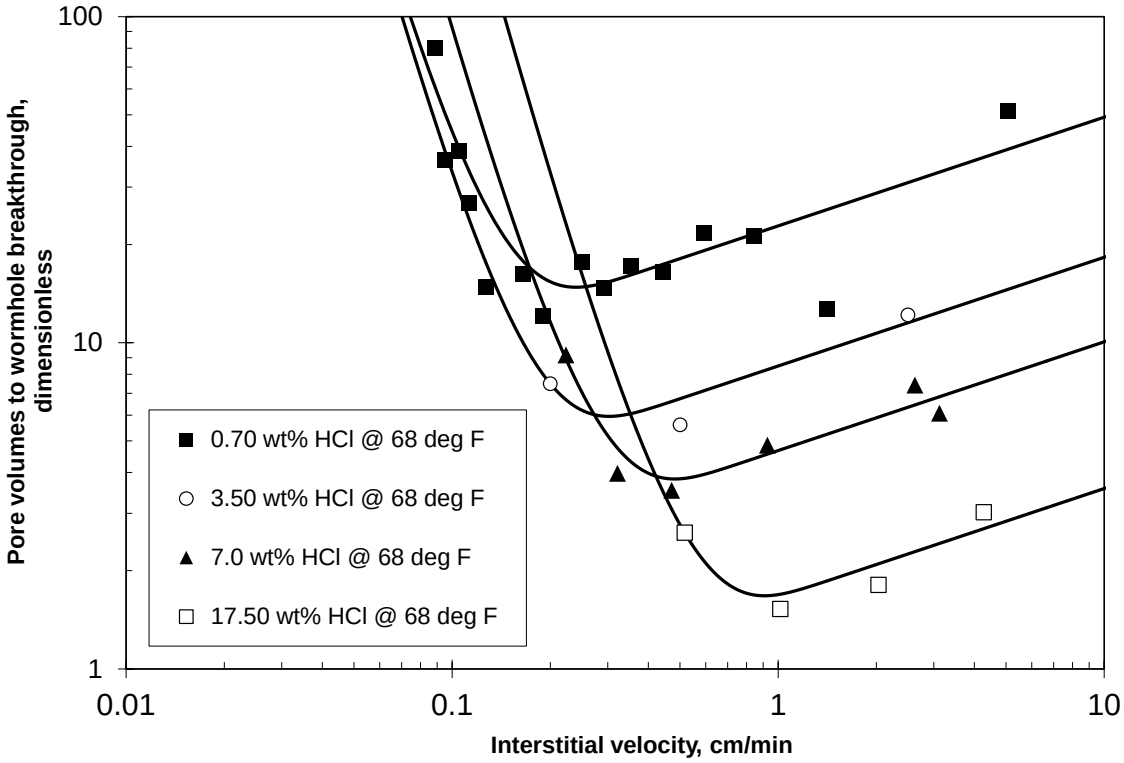

Fig. 3.1—Pore volumes to breakthrough versus interstitial velocity (from Bazin 2001).

TABLE 3.2—INPUT DATA FOR A HOMOGENEOUS THIN FORMATION.	
Wellbore radius, ft	0.25
Thickness, ft	30
Porosity, fraction	0.2
Rock density, g/cm^3	2.71
Injection rate, bbl/min	0.5-40
Total amount of acid, gal/ft	100
Core diameter, in. (*)	1.97
Core length, in. (*)	7.87
HCl concentration, wt%	0.7, 3.5, 7.0, and 17.5
Acid density, g/cm^3	1.07
Number of dominant wormholes per 2D plane (*)	6
Wormhole axial spacing coefficient (*)	0.25 and 0.5
Parameter for fluid-loss limited wormholing (*)	1/3

* The parameters required for Furui et al. model

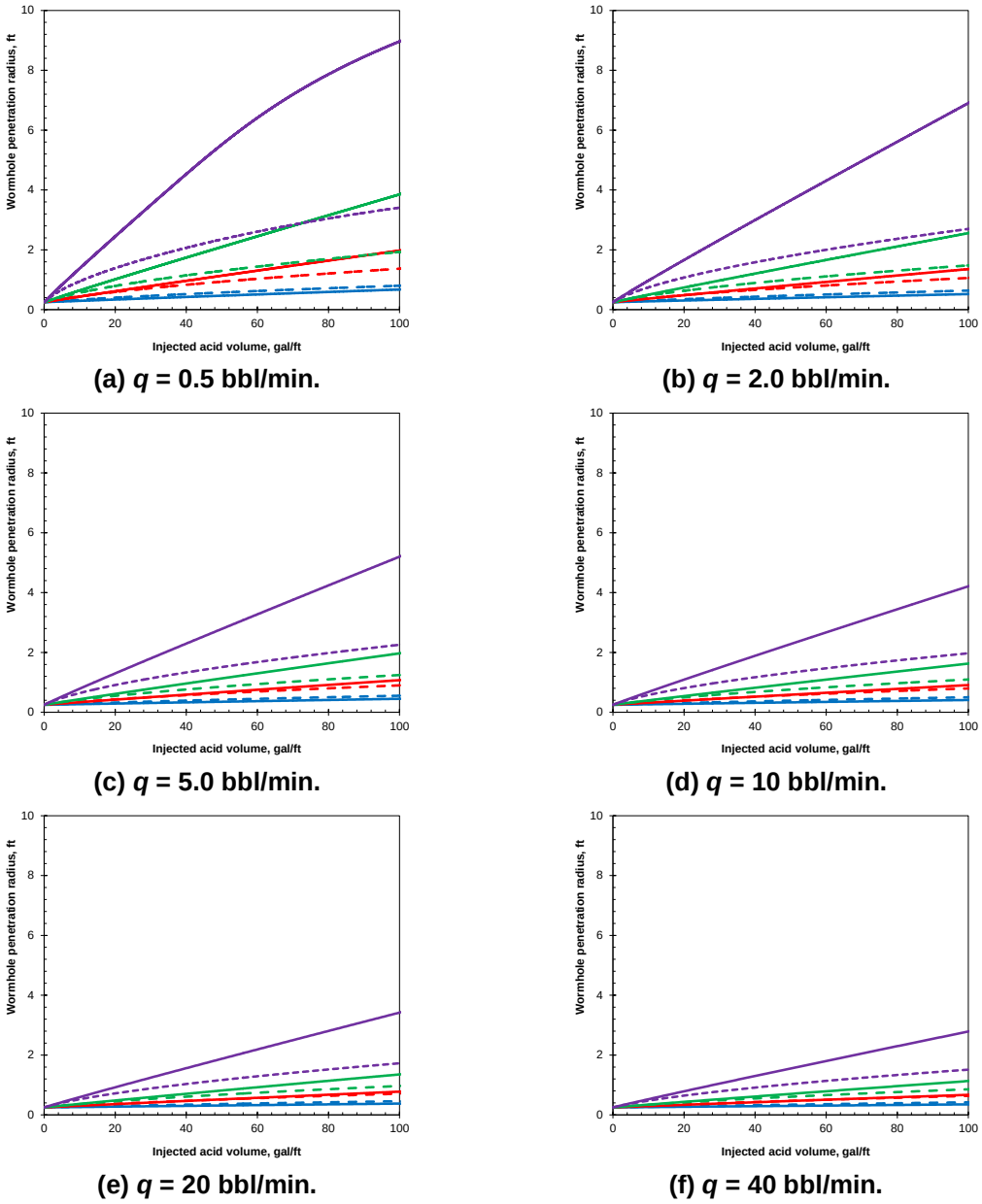

Fig. 3.2—Wormhole penetrations with different injection rates for α_z =0.25.

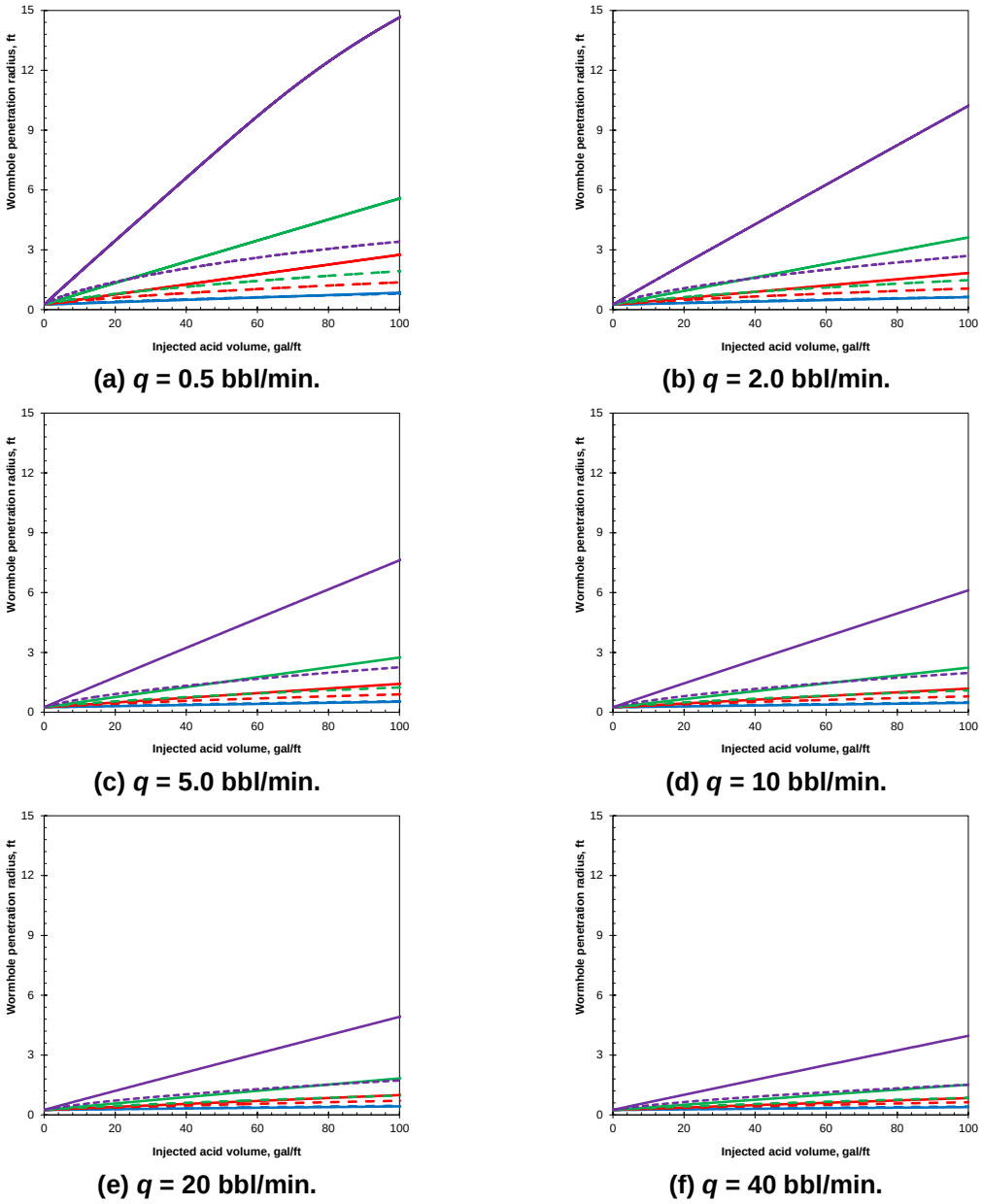

Fig. 3.3—Wormhole penetrations with different injection rates for α_z =0.50.

Figs. 3.2 and 3.3 show the results for α_z of 0.25 and 0.50, respectively. As seen in both Figs. 3.2 and 3.3, in most of the cases, the Furui et al. model (dashed line) predicts longer wormholes penetration than the Buijse and Glasbergen model as expected. Only for 0.7 wt% HCl injection, there is no significant difference. Actually, this concentration is not recommended because this does not create wormholes.

Now we see the effect of α_z. Higher α_z gives longer wormhole penetration (Figs. 3.2 and 3.3). This is because as α_z increases the number of dominant wormholes decreases. As we showed in Sec. 2.5.2, α_z is the wormhole axial spacing coefficient. This is defined by (Furui et al. 2010)

$$\alpha_z = \left(\frac{h_{wh}}{r_{wh}} \right)^{0.7}, \quad \text{.....(3.2)}$$

where h_{wh} is the wormhole axial spacing in ft. α_z is set to be 0 for wormholes closely spaced in the axial direction while α_z is set to be 1 for wormholes sparsely distributed in the axial direction. Hence, for a fixed thickness, as α_z increases, the number of dominant wormholes decreases. Accordingly, the interstitial velocity at the tip of wormholes becomes higher.

What is the impact of the flow rates? Usually constant injection rate is used in carbonate matrix acidizing. Hence, it is meaningful to see the effect of injection rate on wormhole propagation. As in linear coreflooding conditions, it is possible to have optimum injection rate in radial flow system. According to Figs. 3.2 and 3.3, for 17.5 wt% HCl treatments, 0.5 bbl/min of injection rate gives the longest wormhole penetration at 100 gal/ft of acid injection. We additionally calculate wormhole penetrations at 200 gal/ft of acid injection using different flow rates. **Table 3.3** shows wormhole penetration radius at different amounts of acid. At 200 gal/ft, 2 bbl/min of injection rate gives the longest wormhole penetration. Therefore, there is optimum injection rate. However, the optimum injection rate at 200 gal/ft is different from the result for 100 gal/ft.

TABLE 3.3—WORMHOLE PENETRATIONS WITH DIFFERENT FLOW RATES.		
	Wormhole penetration radius, ft	
Flow rate, bbl/min	100 gal/ft	200 gal/ft
0.5	8.96	12.13
2.0	6.91	13.31
5.0	5.21	9.95
10.0	4.21	8.00
20.0	3.42	6.45
40.0	2.79	5.21

3.3 Homogeneous Thick Single Layer Case

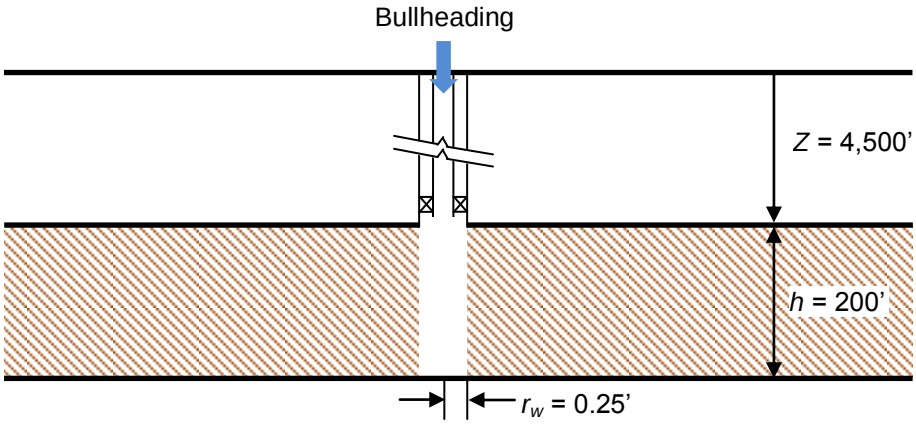

Fig. 3.4—Homogenous single layer with openhole completion.

TABLE 3.4—INPUT DATA FOR A HOMOGENEOUS THICK FORMATION.	
Porosity, fraction	0.2
Permeability, md	100
Initial reservoir pressure @ TVD = 4,515 ft, psia	1,500
Oil viscosity, cp	0.58
Deviation angle, degrees	0 (vertical)
Injection rate, bbl/min	5.0
Acid type	15 wt% HCl
Acid viscosity, cp	1.0
Optimum pore volume to breakthrough	0.7
Optimum interstitial velocity, cm/min	3.2
Core size, in. (*)	1 x 6
Number of dominant wormholes per 2D plane (*)	4
Wormhole axial spacing coefficient (*)	0.25 and 0.50
Parameter for fluid-loss limited wormholing (*)	1/3

* The parameters required for Furui et al. model

We study a matrix acidizing treatment in a homogenous thick layer (**Fig. 3.4**). **Table 3.4** shows the input data for this simulation. We compare the Buijse and Glasbergen model and the Furui et al. model in the same way as the previous case study. We assume no damage for this case study. To evaluate the overall skin factor, we use the following equation:

$$s_{overall} = \frac{\sum_i k_i \Delta z_i}{\sum_i \frac{k_i \Delta z_i}{\ln(r_e / r_w) + s_i}} - \ln \frac{r_e}{r_w} \quad \text{.....(3.3)}$$

where Δz is the thickness of the discretized zone and r_e is the external reservoir radius. To calculate the overall skin factor, the external reservoir radius is set as 500 ft for this case study.

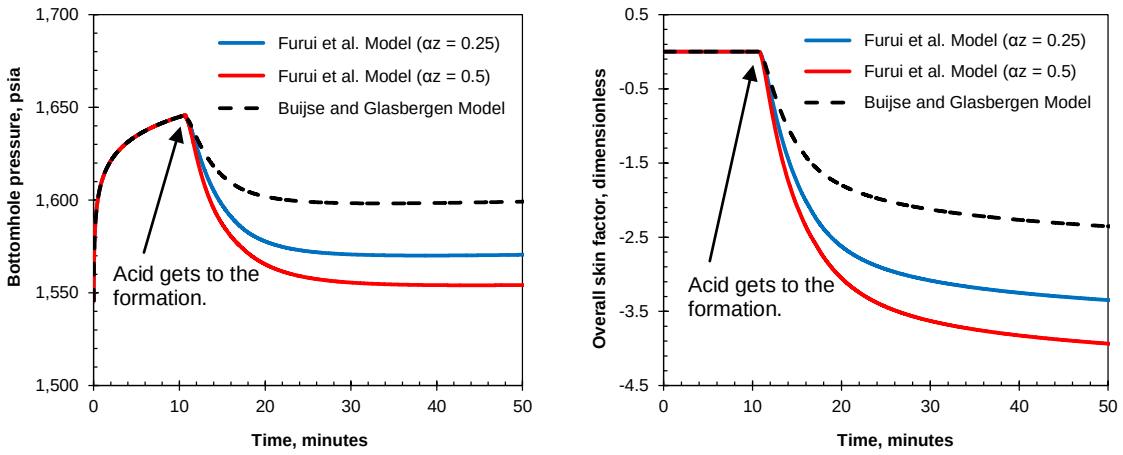

(a) Bottomhole pressure. **(b) Overall skin factor.**

Fig. 3.5—Results for a homogenous thick layer with openhole completion.

Fig. 3.5 shows the simulation results. As we discussed, larger α_z gives longer wormhole penetrations, resulting in lower skin factor. This result is consistent with the previous case study. As expected, the Furui et al. model gives better stimulation performance than the Buijse and Glasbergen model. After t = 20 minutes, the pressure almost stop changing for the Buijse and Glasbergen model while the pressure keeps changing for the Furui et al. model. If we use the Buijse and Glasbergen model to match

with the results of the Furui et al. model, we may change original permeability, porosity, optimum pore volume to breakthrough, or optimum interstitial velocity.

Fig. 3.6 shows the wormhole profiles along the wellbore. Correspondingly to Fig. 3.5, the Furui et al. model with α_z = 0.5 predicts the deepest wormhole penetration among the three. Although this layer is relatively thick (200 ft), good wormhole distribution is obtained for every model after 39.91 gal/ft of injection. Noticeably, the Buijse and Glasbergen model predicts relatively even wormhole distribution along the well while the Furui et al. predicts a relatively uneven wormhole distribution. For this case, this uneven distribution is not a problem, however, for a thicker formation, we may need a diversion.

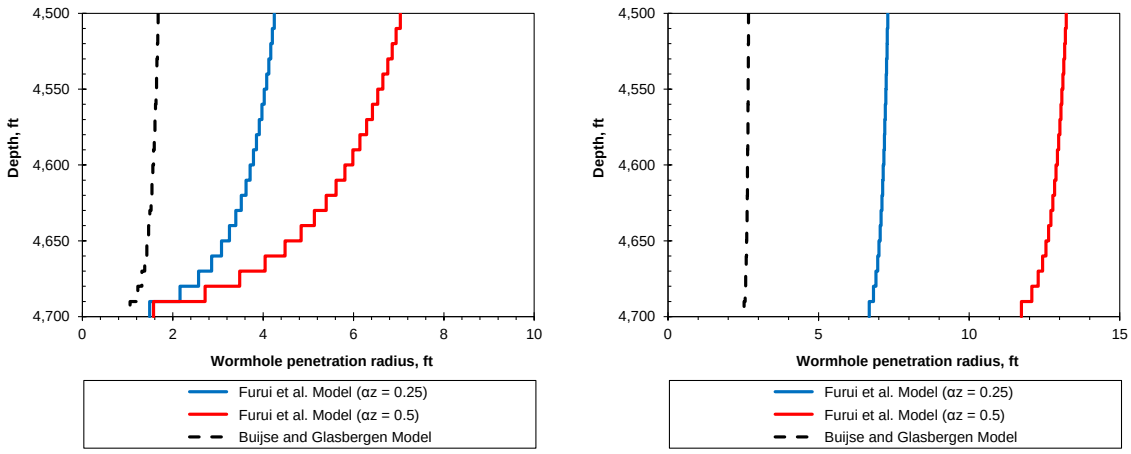

(a) *t* = 20 minutes (8.41 gal/ft). **(b) *t* = 50 minutes (39.91 gal/ft).**

Fig. 3.6— Wormhole profile along the wellbore for a homogeneous thick formation.

TABLE 3.5—PERFORATION DATA.	
Perforation length, in.	12
Perforation radius, in.	0.3
Perforation density, spf	5
Perforation phasing, degrees	60
Discharge coefficient	0.80

Next, we simulate a matrix acidizing treatment in a cased and perforated well. The perforation data used in this study is shown in **Table 3.5**. No crushed zone around the perforations is assumed. The other data is the same as in Table 3.4.

Fig. 3.7 shows the results. There is no significant difference from the openhole completion case. The overall skin factor at t = 60 minutes for the cased and perforated well is -4.21 while the one for the openhole completion is -4.01 when using the Furui et al. model with α_z = 0.50. Hence, the wormhole penetrations are longer in the cased and perforated well.

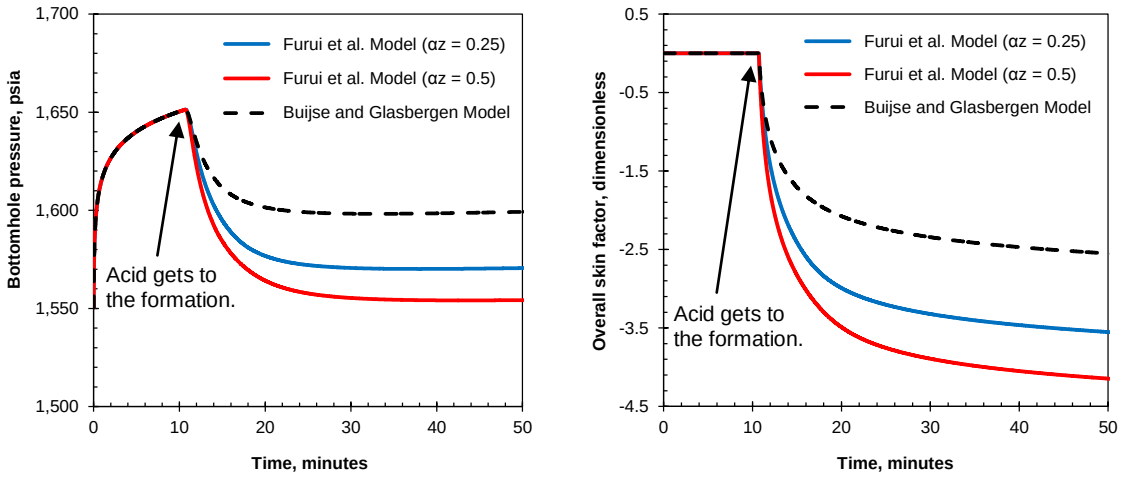

(a) Bottomhole pressure. **(b) Overall skin factor.**

Fig. 3.7—Results for a homogenous thick single layer with cased and perforated completion.

Fig. 3.8 shows the wormhole profiles. In the same way as the openhole completion case, the Buijse and Glasbergen model predicts relatively even wormhole distribution along the well while the Furui et al. predicts an uneven wormhole distribution.

One of the main differences between these two different completions in calculation is the pressure drop through perforations. However, for matrix acidizing treatments, injection rate is not high enough to see the effect of the pressure drop through perforations.

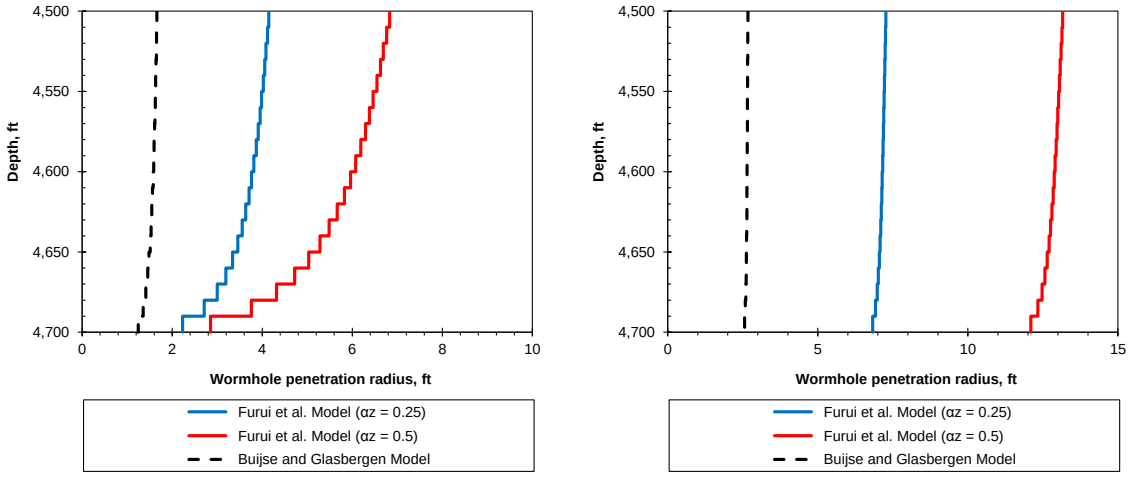

(a) *t* = 20 minutes (8.41 gal/ft). **(b) *t* = 50 minutes (39.91 gal/ft).**

Fig. 3.8— Wormhole profile along the wellbore for a homogeneous thick formation with cased and perforated completion.

3.4 Multi-Layer Case

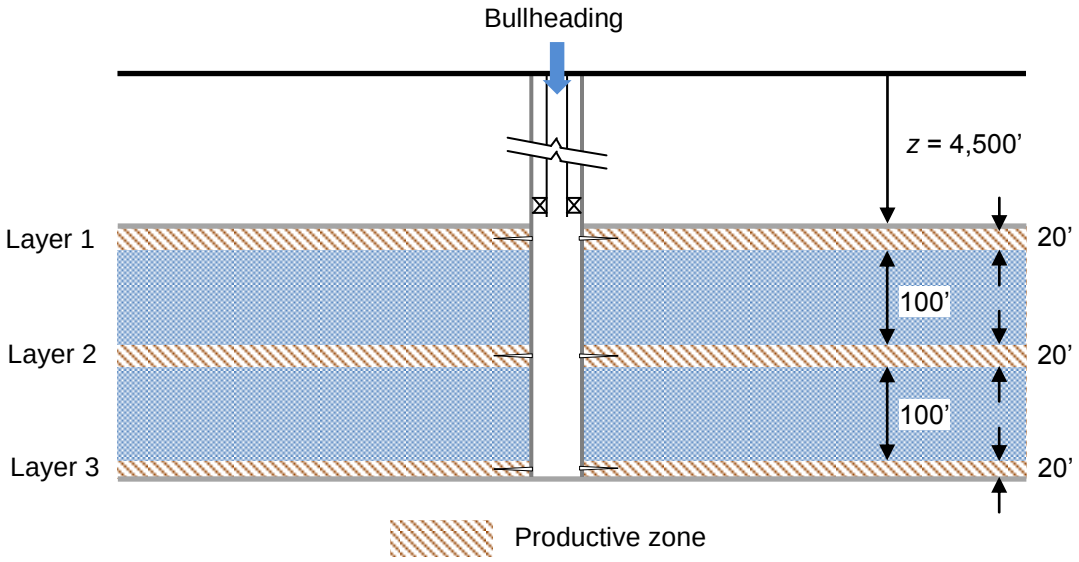

Fig. 3.9—Multi-layer formation with cased and perforated completion.

In this section, we study a matrix acidizing treatment in a three-layer formation (**Fig. 3.9**). **Table 3.6** shows the input data. Each layer has the same properties (thickness, porosity, and permeability). The well is cased and perforated. As described in Fig. 3.9,

the distance between layer 1 and 2 is 100 ft, and the distance between layer 2 and 3 is also 100 ft. The same perforation data as the previous case (Table 3.5) are used. As a wormhole propagation model, the Furui et al. model is used. For horizontal wells, 0.75 of α_z is recommended (Furui et al. 2010). To convert this value for vertical wells, we use the following equation:

$$\alpha_{z,vetical} = \alpha_{z,horizontal}\left(\frac{1}{I_{ani}}\right)^{0.7} . \quad \text{.....(3.4)}$$

where I_{ani} is the anisotropy ratio in dimensionless defined as $I_{ani} = (k_H/k_V)^{0.5}$. For this case study, we assume $k_H = 10\ k_V$. Hence, $\alpha_z \approx 0.335$ (Table 3.6).

TABLE 3.6—INPUT DATA FOR A MULTI-LAYER FORMATION.

Wellbore radius, ft	0.25
Pay Thickness, ft	60
Porosity, fraction	0.2
Original permeability, md	100
Damage permeability, md	10
Damage penetration radius, ft	2
Initial skin factor, dimensionless	20
Initial reservoir pressure @ TVD = 4,515 ft, psia	1,500
Oil viscosity, cp	0.58
Deviation angle, degrees	0 (vertical)
Injection rate, bbl/min	2.0
Acid type	15 wt% HCl
Acid viscosity, cp	1.0
Optimum pore volume to breakthrough	0.7
Optimum interstitial velocity, cm/min	3.2
Core diameter, in.	1
Core length, in.	6
Number of dominant wormholes per 2D plane	6
Wormhole axial spacing coefficient	0.335
Parameter for fluid-loss limited wormholing	1/3

Fig. 3.10 shows plots of the bottomhole pressure versus time and the overall skin factor versus time. The blue dash line in Fig. 3.10 represents the time when the acid reaches layer 1. The stimulation in layer 1 delays the start of the stimulation in layer 2 because the injectivity of layer 1 keeps increasing during the stimulation. The pressure

decline rate gets slower when the acid gets to layer 2. After the wormholes go beyond the damage zone in layer 2, both the pressure change and the skin change become insignificant. From these insignificant changes, we easily estimate the stimulation finished.

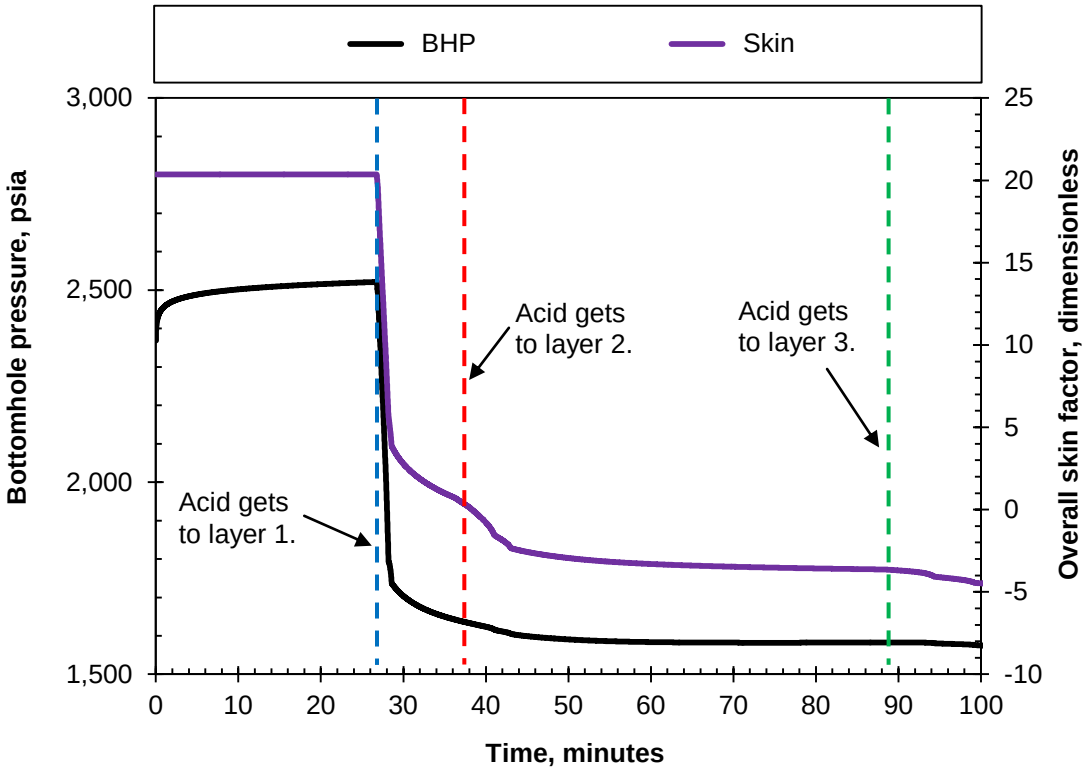

Fig. 3.10—Bottomhole pressure and overall skin factor.

As we discussed in Sec. 3.2, the Furui et al. model predicts fast wormholes' propagation. This is one of the reasons why the overall skin factor change shapely. There are additionally two possible reasons which explain this sharp change. Firstly, we simulate a cased and perforated well, and the perforations terminate inside the damage region. This causes a relatively large initial skin. For this type of completion, spherical flow exists in the vicinity of the perforations, resulting in a high wormhole propagation rate. Quickly, the wormholes in layer 1 penetrate the damage region. Secondly, one different skin factor has a significant effect on overall skin factor in Eq. 3.3. For instance,

$$s_{overall} = \frac{(3)(100\text{ md})(20\text{ ft})}{\frac{(100\text{ md})(20\text{ ft})}{\ln\frac{500\text{ ft}}{0.25\text{ ft}}+10} + \frac{(100\text{ md})(20\text{ ft})}{\ln\frac{500\text{ ft}}{0.25\text{ ft}}+20} + \frac{(100\text{ md})(20\text{ ft})}{\ln\frac{500\text{ ft}}{0.25\text{ ft}}+20}} - \ln\frac{500\text{ ft}}{0.25\text{ ft}} \cong 15.6,$$

$$s_{overall} = \frac{(3)(100\text{ md})(20\text{ ft})}{\frac{(100\text{ md})(20\text{ ft})}{\ln\frac{500\text{ ft}}{0.25\text{ ft}}+0} + \frac{(100\text{ md})(20\text{ ft})}{\ln\frac{500\text{ ft}}{0.25\text{ ft}}+20} + \frac{(100\text{ md})(20\text{ ft})}{\ln\frac{500\text{ ft}}{0.25\text{ ft}}+20}} - \ln\frac{500\text{ ft}}{0.25\text{ ft}} \cong 7.1, \text{ and}$$

$$s_{overall} = \frac{(3)(100\text{ md})(20\text{ ft})}{\frac{(100\text{ md})(20\text{ ft})}{\ln\frac{500\text{ ft}}{0.25\text{ ft}}-4} + \frac{(100\text{ md})(20\text{ ft})}{\ln\frac{500\text{ ft}}{0.25\text{ ft}}+20} + \frac{(100\text{ md})(20\text{ ft})}{\ln\frac{500\text{ ft}}{0.25\text{ ft}}+20}} - \ln\frac{500\text{ ft}}{0.25\text{ ft}} \cong 1.0.$$

Since that sharp pressure change is rare in the field, these calculation methods including the wormhole propagation should be improved.

Fig. 3.11 shows the wormhole propagation in each layer. As discussed, the stimulation in layer 1 starts first. Once the wormholes in layer 2 break through the damage region, the wormhole propagation rate in layer 1 slows down. Then, the wormholes in layer 2 keep propagating. At t = 89 minutes, the stimulation in layer 3 starts. Although about 6 minutes are spent, the wormholes in layer 3 also break through the damage region.

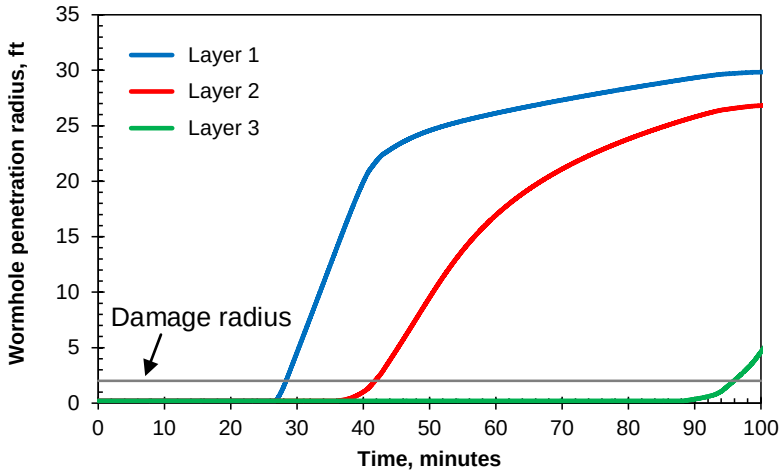

Fig. 3.11—Wormhole propagation in each layer.

3.5 Heterogeneous Thick Single Layer Case

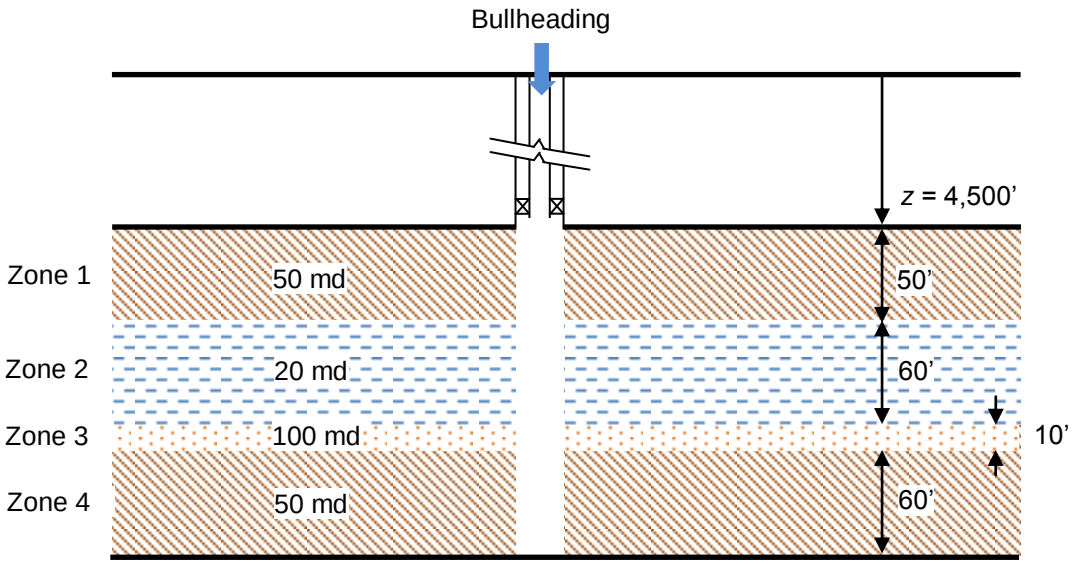

Fig. 3.12—Heterogeneous thick single layer with openhole completion.

TABLE 3.7—INPUT DATA FOR A HETEROGENEOUS THICK FORMATION.	
Wellbore radius, ft	0.25
Pay Thickness, ft	180
Porosity, fraction	0.2
Damage ratio (k_d/k)	0.1
Damage penetration radius, ft	3
Initial reservoir pressure @ TVD = 4,515 ft, psia	1,500
Oil viscosity, cp	0.58
Deviation angle, degrees	0 (vertical)
Injection rate, bbl/min	1.0-4.0
Acid type	15 wt% HCl
Acid viscosity, cp	1.0
Core diameter, in.	1
Core length, in.	6
Number of dominant wormholes per 2D plane	6
Wormhole axial spacing coefficient	0.335
Parameter for fluid-loss limited wormholing	1/3

Finally, we study a matrix acidizing treatment in a heterogeneous thick single layer described in **Fig. 3.12**. We simulate an openhole well with the Furui et al. wormhole propagation model. There is a high-permeability zone (100 md) in the middle of the

layer. As shown in **Table 3.7**, the damage ratio (the ratio of damage permeability to original permeability) and the damage penetration are constant along the well. The injection rate is set constant, and we simulate the treatment with different flow rates (1.0, 2.0, 3.0, and, 4.0 bbl/min). **Table 3.8** shows the properties of each zone.

TABLE 3.8—ZONES' DATA.

Zone #	k, md	$PV_{bt,opt}$	$v_{i,opt}$
1	50	0.7	3.2
2	20	0.7	3.2
3	100	0.3	2.0
4	50	0.7	3.2

Fig. 3.13 shows the plots of overall skin factor versus injected acid volume. The higher injection rate gives the better overall skin factor. This conclusion is a similar conclusion to Paccaloni (1996). The difference is that we don't maximize the injection pressure although we try a high injection rate with which we don't fracture the well at the initial condition.

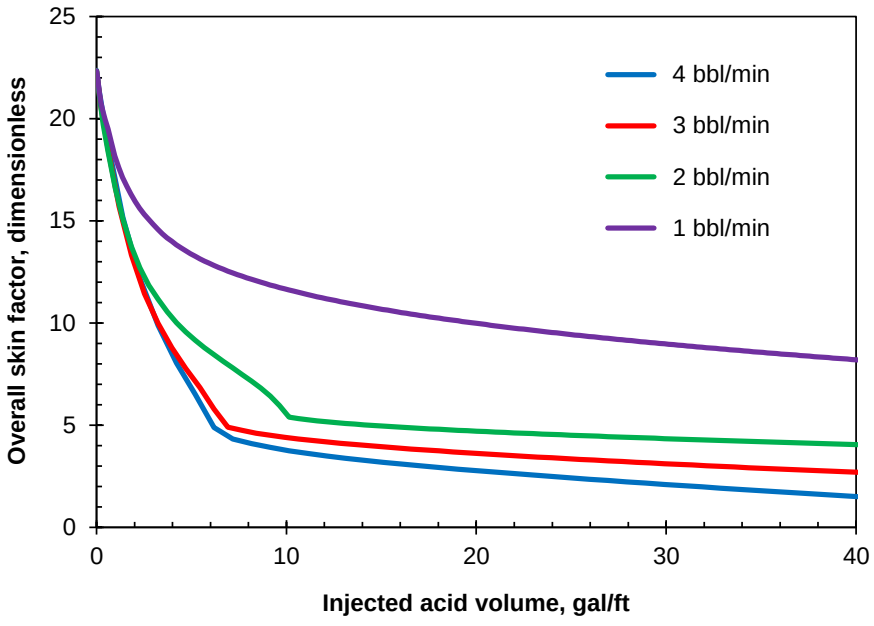

Fig. 3.13—Overall skin factor versus injected acid volume.

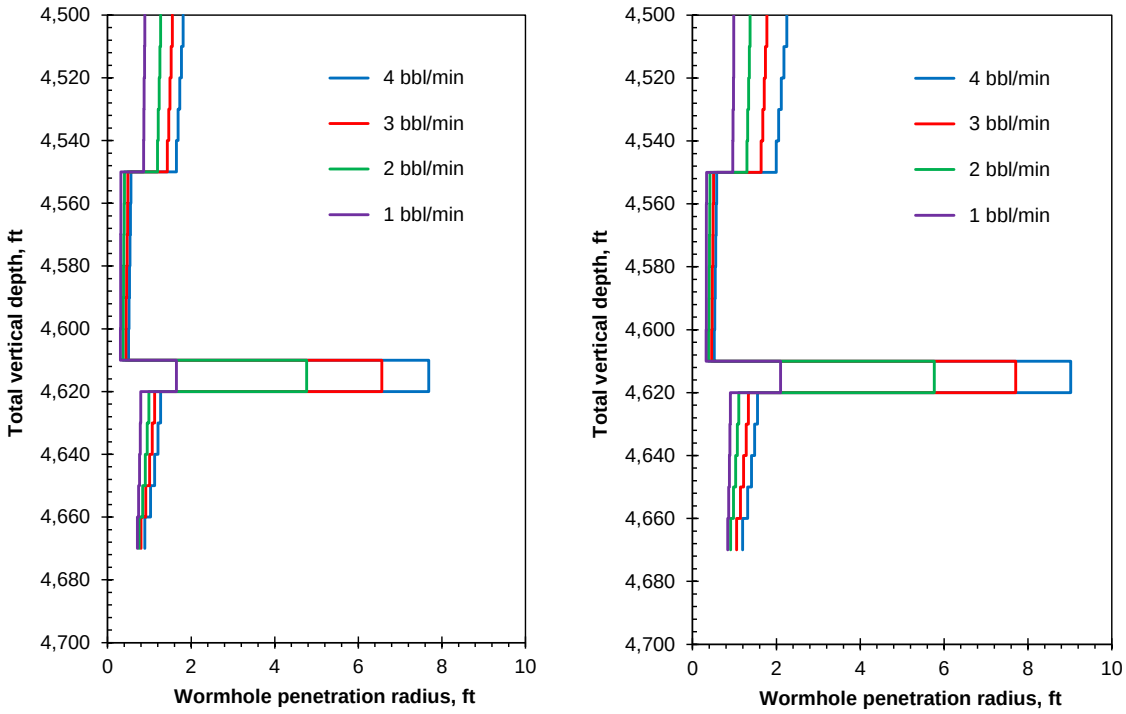

Fig. 3.14—Wormhole profile along the well for a heterogeneous thick formation.

Fig. 3.14 shows the wormhole profile along the well after 20 and 40 gal/ft of acid injection. Most of the acid goes to the high-permeability zones (zones 1 and 3). Zones 2 and 4 are not sufficiently treated (damage radius is 2 ft). For this kind of formation, we need to divert acid to lower permeability zones using some diversion method. If the permeability is >1,000 md (usually called a thief zone), the wormhole profile is expected to be much worse.

3.6 Section Summary

In this section, we firstly compared the Furui et al. model and the Buijse and Glasbergen model. Basically, the Furui et al. model was developed to fill the gap between the Buijse and Glasbergen model's results and field results. Furui et al. (2010) changed the way to calculate interstitial velocity at the tip of wormholes. Hence, we observed that the Furui et al. model gives longer wormhole penetrations than the Buijse and Glasbergen model.

Secondly, we studied matrix acidizing treatments in a multi-layer formation and a heterogeneous thick formation. For both cases, some diversion method is needed to stimulate the entire formation or improve the stimulation. In the next section, we develop a ball sealer diversion model to tackle this problem.

4. BALL SEALER DIVERSION MODEL*

4.1 Introduction

In this section, we develop a ball sealer diversion model. The model consists of:

- ball sealer tracking model,
- empirical correlation which determines ball seating efficiency, and
- a model which account for ball sealers' blockage.

4.2 Ball Sealer Tracking

As Dukowicz summarized (1980), regarding fluid flow containing particles, it may be placed in two categories. In the first category, the particles do not perturb the flow field. The solution then reduces to tracing particle trajectories in a known velocity field. In the second category, the particle carries sufficient momentum to entrain and set into motion the surrounding fluid. For ball sealer tracking, it is common to assume the first problem (Gabriel and Erbstoesser 1984; Li et al. 2005). In this study, we also assume ball sealers do not affect the flow field.

4.2.1 Single Ball Sealer

The following equation describes the ball velocity in the axial direction:

$$v_{ball} = \frac{q}{A_{pipe}} + v_{slip} \quad \text{.....(4.1)}$$

where v_{ball} is the ball velocity in ft/min, q is the injection rate in ft^3/min, A_{pipe} is the cross-sectional area of the pipe in ft^2, and v_{slip} is the slip velocity in ft/min.

---

*Part of this section is reprinted with permission from "Experimental and Field Data Analyses of Ball Sealer Diversion" by Nozaki, M., Zhu, D., and Hill, A.D., 2011. Paper SPE147632 presented at the SPE Annual Technical Conference and Exhibition, Denver, Colorado, USA, 30 October-2 November.

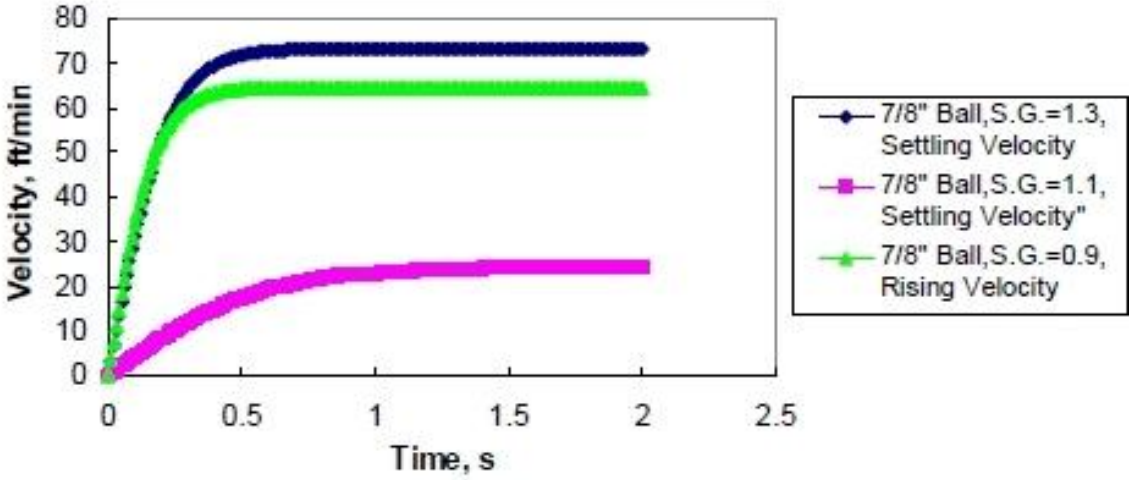

Fig. 4.1—Slip velocity versus time (from Li et al. 2005).

Li et al. (2005) showed that the time for a ball sealer to achieve terminal settling or rising velocity is short. In their examples, it is a few seconds (**Fig. 4.1**). Thus, we neglect the effect of the unsteady period on the ball sealer transport and use terminal settling or rising velocity as a slip velocity between the fluid and the ball sealer. Then Eq. 4.1 becomes:

$$v_{ball} \approx \frac{q}{A_{pipe}} + v_{t,0} \quad \text{.....(4.2)}$$

where $v_{t,0}$ is the terminal settling or rising velocity for a single spherical particle in ft/min. The terminal velocity is expressed as (Tilton 1997)

$$v_{t,0} = 20 \times \frac{\rho_{ball} - \rho_{fluid}}{\left|\rho_{ball} - \rho_{fluid}\right|} f_{wall} \sqrt{\frac{g d_{ball} \left|\rho_{ball} - \rho_{fluid}\right| \cos\theta}{\rho_{fluid} K_D}}, \quad \text{.....(4.3)}$$

where ρ_{ball} is the density of the ball sealer in g/cm^3, ρ_{fluid} is the density of the carrier fluid in g/cm^3, f_{wall} is the wall factor, dimensionless, g is acceleration of gravitation in ft/s^2, d_{ball} is the diameter of the ball sealer in inch, θ is the deviation angle in degrees, and K_D is the drag coefficient, dimensionless. 20 in Eq. 4.3 is a conversion factor to use units presented in the nomenclature.

The drag coefficient and the wall factor is a function of Reynolds number, N_{Re}. For Newtonian fluids,

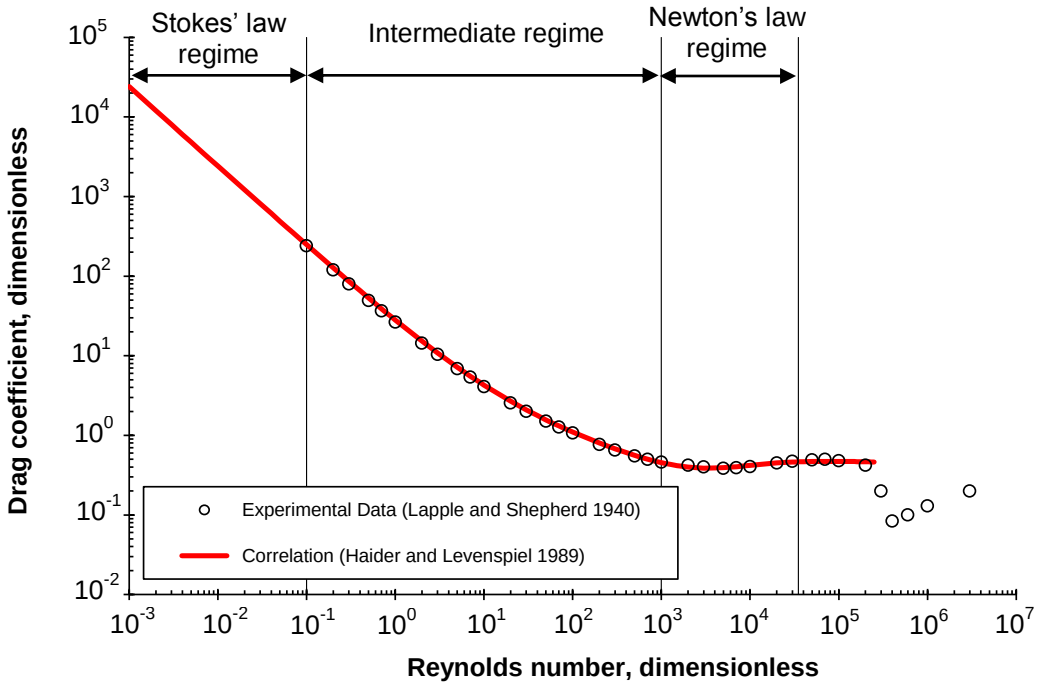

Fig. 4.2—Drag coefficient as a function of Reynolds number.

$$N_{\mathrm{Re}} = \frac{129\left|v_{slip}\right|d_{ball}\rho_{fluid}}{\mu}, \quad \text{.....(4.4)}$$

where μ is the viscosity of the carrier fluid in cp. **Fig. 4.2** shows some experimental data by Lapple and Shepherd (1940). Many researchers (e.g., Gabriel and Erbstoesser 1984) use the following correlations. At low Reynolds number ($N_{\mathrm{Re}} < 0.1$), Stokes' law gives

$$K_D = \frac{24}{N_{\mathrm{Re}}}. \quad \text{.....(4.5)}$$

In the intermediate regime ($0.1 < N_{\mathrm{Re}} < 1{,}000$), the drag coefficient may be estimated within 6 percent by

$$K_D = \left(\frac{24}{N_{\mathrm{Re}}}\right)(1+0.14N_{\mathrm{Re}}^{0.70}). \quad \text{.....(4.6)}$$

In the Newton's law regime ($1{,}000 < N_{\mathrm{Re}} < 35{,}000$), $K_D = 0.445$, within 13 percent. The slip velocity calculation needs iterations for the determination of the drag coefficient. To extend the range of Reynolds number and reduce both the number of equations and error, we use the following correlation (Haider and Levenspiel 1989) for $N_{\mathrm{Re}} < 2.6 \times 10^5$:

$$K_D = \left(\frac{24}{N_{\mathrm{Re}}}\right)(1+0.1806N_{\mathrm{Re}}^{0.6459}) + \frac{0.4251}{1+6{,}880.95N_{\mathrm{Re}}^{-1}} \quad \text{.....(4.7)}$$

with the root-mean square deviation of 0.024.

The settling/floating velocity of a ball is reduced by the presence of confining boundaries. According to the analysis by Chhabra et al. (2003), the following empirical correlations give the best prediction, for each Reynolds number regime:

(i) $N_{\mathrm{Re}} < 1$

$$f_{wall} = \frac{1-2.105\left(\frac{d_{ball}}{d_{pipe}}\right)+2.0865\left(\frac{d_{ball}}{d_{pipe}}\right)^3-1.7065\left(\frac{d_{ball}}{d_{pipe}}\right)^5+0.72603\left(\frac{d_{ball}}{d_{pipe}}\right)^6}{1-0.75857\left(\frac{d_{ball}}{d_{pipe}}\right)^5},$$

.....(4.8)

(ii) $1 < N_{\mathrm{Re}} < 200$

$$f_{wall} = \left(\frac{1-\frac{d_{ball}}{d_{pipe}}}{1-0.33\frac{d_{ball}}{d_{pipe}}}\right)^{\frac{3.3+0.0085N_{\mathrm{Re}}}{1+0.1N_{\mathrm{Re}}}}, \text{ and} \quad \text{.....(4.9)}$$

(iii) $N_{\mathrm{Re}} > 200$

$$f_{wall} = \left[1-\left(\frac{d_{ball}}{d_{pipe}}\right)^2\right]\left[1-\frac{1}{2}\left(\frac{d_{ball}}{d_{pipe}}\right)^2\right]^{0.5}. \quad \text{.....(4.10)}$$

For a neutrally buoyant ball sealer, $v_{t,0}$ is zero. Hence, Eq. 1 reduces to

$$v_{ball} = \frac{q}{A_{pipe}}. \quad \text{.....(4.11)}$$

One of the key factors for ball sealer tracking is whether a ball sealer bounces on the pipe wall or not. In a vertical well, it is reasonable to assume any type of ball sealer does not contact the wall (Eq. 4.1). In a deviated/horizontal well, both buoyant and non-buoyant balls may bounce at the wall. On the other hand, a neutrally buoyant ball may not bounce on the wall even in a deviated/horizontal well (Eq. 4.11). According to

Govier and Aziz (2008), in a horizontal pipe balls with densities close to the carrier fluid will be transported at or above the fluid velocity. This was confirmed by conducting a few visual studies using a 2-inch diameter horizontal Perspex pipe (Bern 1993). **Fig. 4.3** shows the results. The results show that above 100 ft/min (0.39 bbl/min) the balls are transported at or above the mean axial velocity. At 50 ft/min (0.19 bbl/min), the ball transport is less efficient. Indeed this fluid velocity is insufficient to transport the highest density ball tested (1.2 SG). Hence, below the critical velocity, Eq. 4.3 is no longer valid.

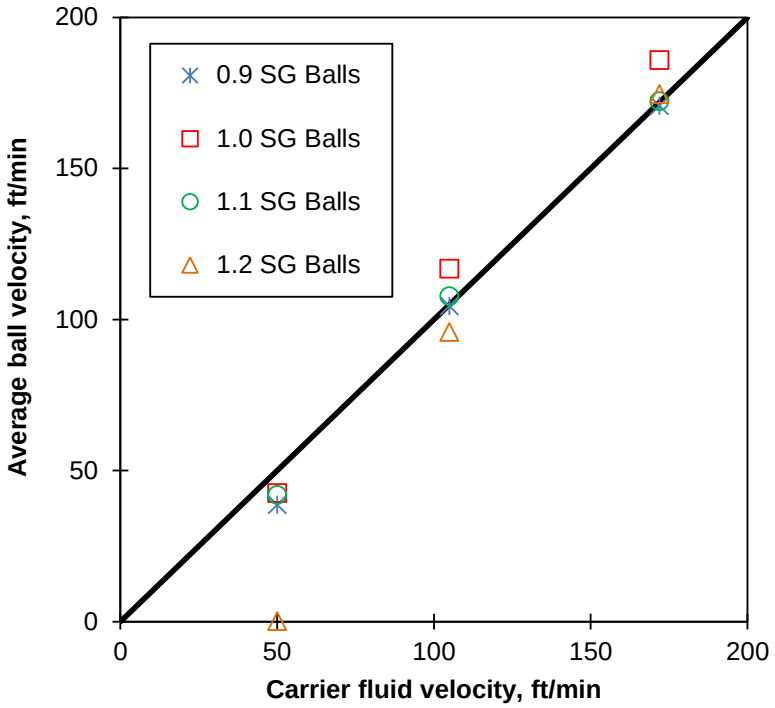

Fig. 4.3—Measured ball velocities in a horizontal pipe (from Bern 1993).

4.2.2 Multi-Ball Sealers

It is common to inject ball sealers in a batch. For this type of injection, Eq. 4.3 is not appropriate. In batch injection, the average ball velocity of ball sealers is slower than the velocity obtained by Eq. 4.3. This may be due to hydrostatic effect, the momentum transfer hindrance and the wall effect (Barnea and Mizrahi 1973). To account for these

effects on the balls' velocities, one variable is commonly introduced: the volumetric fraction occupied by the ball sealers, ϕ_{ball}, often called the hold-up (Barnea and Mizrahi 1973). On the basis of the experimental data in the literature, Barnea and Mizrahi (1973) developed the following semi-empirical correlation for the average terminal velocity of multi-ball sealers, $v_{t,\phi}$:

$$v_{t,\phi} = \frac{1-\phi_{ball}}{(1+\phi_{ball}^{1/3})\exp[5\phi_{ball}/3(1-\phi_{ball})]} v_{t,0} \quad \text{.....(4.12)}$$

where $v_{t,0}$ can be calculated by using Eq. 4.3. Note that f_{wall} in Eq. 4.3 has to be set as one because the wall effect is accounted for in Eq. 4.12 as mentioned. The average velocity of multi-ball sealers is defined as the relative average velocity between the ball sealers and the fluid. Mathematically,

$$v_{t,\phi} = \frac{v_{ball}}{\phi_{ball}} - \frac{q/A_{pipe}}{1-\phi_{ball}}. \quad \text{.....(4.13)}$$

Solving for v_{ball}, we obtain

$$v_{ball} = \frac{\phi_{ball}}{1-\phi_{ball}} \frac{q}{A_{pipe}} + \phi_{ball} v_{t,\phi}. \quad \text{.....(4.14)}$$

Hence, Eqs. 4.3, 4.12, and 4.14 are used to calculate the average ball velocity when ball sealers are injected as a batch.

For neutrally buoyant ball sealers, we use Eq. 4.11.

4.3 BP Experimental Study

4.3.1 Description of BP Experiments

BP laboratory study conducted an extensive series of full-scale flow experiments (Bern and Lewis 1992a; Bern and Lewis 1992b). Their experiments were similar to Erbstoesser's experiments (1980). The formation flow resistance was simulated by a series of parallel pipes which were joined in return manifolds (**Fig. 4.4**). The green pipe (larger diameter) in Fig. 4.4 is the main pipe which simulates a wellbore and the small diameter pipes which are connected to the green pipe are a series of parallel pipes which simulate perforations. In total, there were 120 perforations in BP experiments. Each bank

of ten perforations was connected to one of the return manifolds. There were 10 return manifolds. The flow change on the rotary flow meters on the outlet manifold was monitored to detect how many balls seated on the perforations. Table 4.1 shows both Erbstoesser's and Bern and Lewis' experiment specifications and parameters. Bern and Lewis conducted experiments not only with the vertical pipe but also with deviated/horizontal pipes.

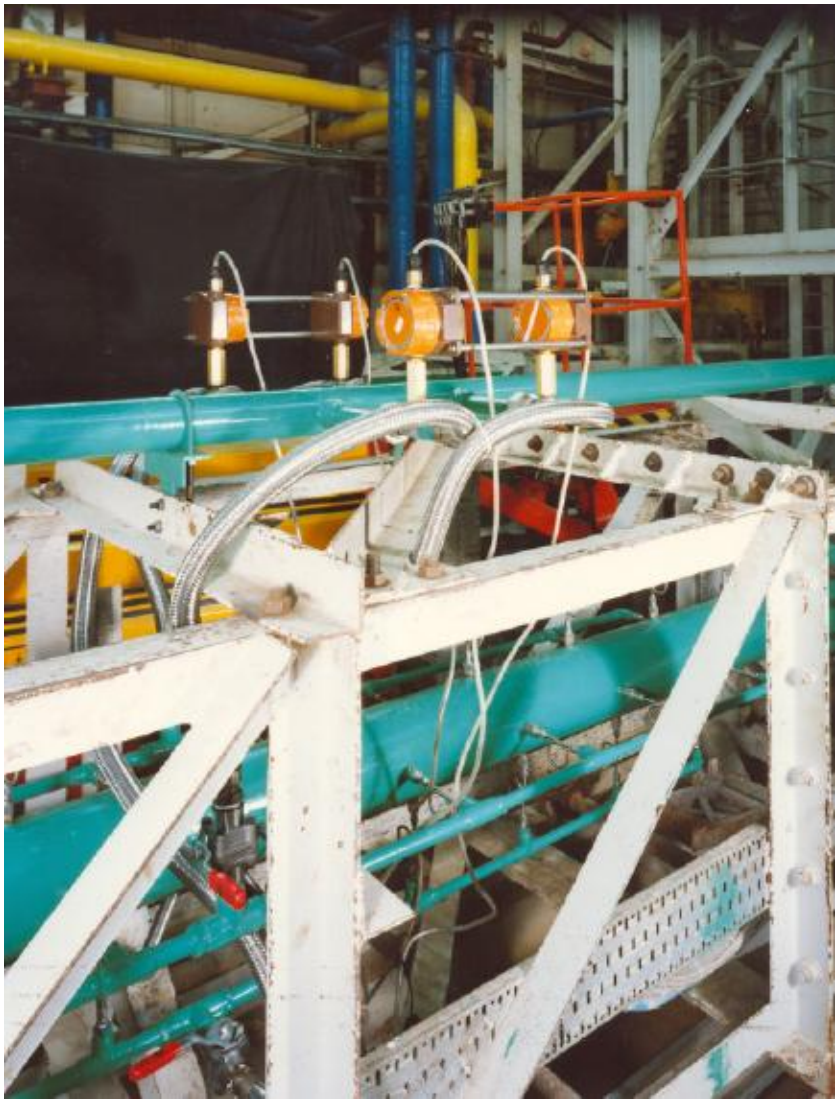

Fig. 4.4—BP experimental setup (from Bern and Lewis 1992a).

TABLE 4.1—EXPERIMENTS' SPECIFICATIONS AND PARAMETERS.

	Bern and Lewis (1992a; 1992b)	Erbstoesser (1980)	
		Setup 1 (5 perfs.)	Setup 2 (10 perfs.)
Well length, ft	30	8	35
Well ID, in.	6.094 (OD = 7")	3	3
Well deviation angle, ^{o}	0, 60, 75, and 90	0	0
Perforation pipe ID, in.	0.1, 0.12, and 0.5	0.38	0.38
Perforation phasing, ^{o}	45	0	0
Number of perforations	120	5	10
Perforation density, shots/ft	4	0.625	0.286
Carrier fluid	Water and polymer solution	Water and brine	Water and brine
Total flow rate, bbl/min	2, 4, and 6	0.202-2.12	0.36
Ball diameter, in.	0.875	0.875	0.875
Ball density, g/cm^3	0.93, 1.00, 1.10, and 1.19	0.98, 1.11, 1.39, and 2.17	0.98, 1.11, 1.39, and 2.17
Ball injection method	2 balls per bbl; batch injection	Batch injection	Batch injection
Number of balls	100 and 180	10	10

Fig. 4.5 shows one of BP experimental results. The number of balls seated in each of the three sections (top, middle, and bottom in the right schematic of Fig. 4.5) was recorded every minute. The top, middle, and bottom sections are the first four return manifolds, the middle four return manifolds, and last four return manifolds, respectively. Hence, each section has 40 perforations. A carrier fluid was circulated for the first five minutes. Then ball sealers were injected at the injection rate of 2 balls per bbl or in a batch. For instance, if the fluid injection rate is 2 bbl/min, then the ball injection rate is 4 balls per minute. After all the balls were injected, the carrier fluid was circulated for another ten minutes.

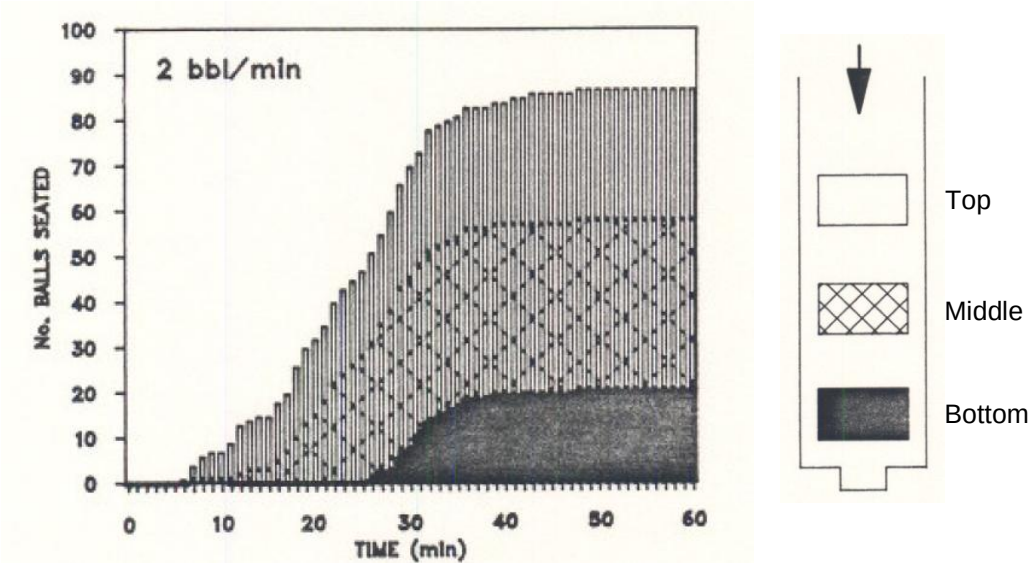

Fig. 4.5—Example of data obtained from BP experiments (from Bern and Lewis 1992a).

BP experiments were designed to simulate ball sealer diversion for matrix acidizing jobs. Under these conditions, balls which are attracted to the perforations will always be held in place by the relatively high differential pressure generated by flow through the formation. This contrasts with Erbstoesser's experiments which were carried out in the absence of a simulated formation. In Erbstoesser's experiments, the perforation friction pressure drop holds the balls. This more closely simulates an acid fracturing job above formation break-down pressure (Bern 1993).

4.3.2 Comparison to Experimental Data in the Literature

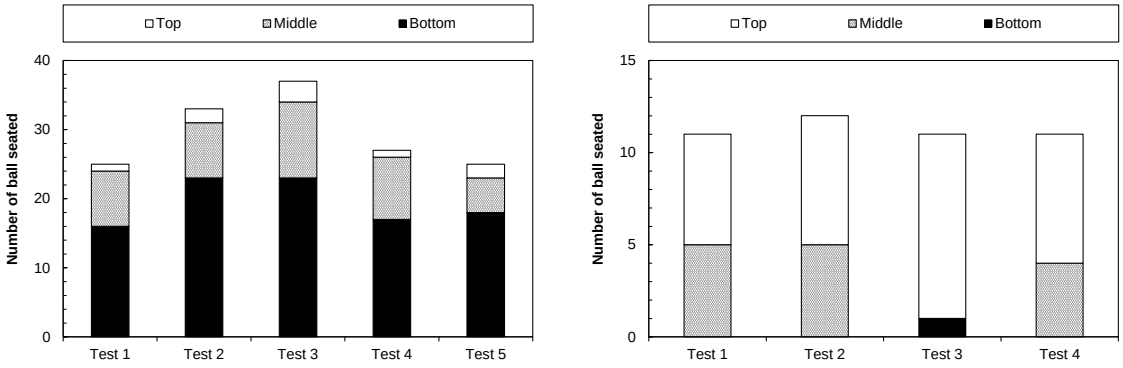

(a) Vertical tests (q = 6 bpm; ρ_{ball} = 1.00 g/cm^3).

(b) 60-degree tests (q = 2 bpm; ρ_{ball} = 0.93 g/cm^3).

Fig. 4.6—Repeatability tests (from Bern and Lewis 1992a)

Erbstoesser's original experimental study (1980) demonstrated that the seating process was statistical which led to considerable scatter in the measured data. BP conducted repeatability tests. **Fig. 4.6** shows the results. The data scatter observed in these tests was ± 20% of the averaged value. Even with this BP experimental setup (Table 4.1), the statistical nature in ball sealer's seating was observed.

Among BP experimental results shown in Table 4.1, we analyzed the experimental results for the cases with one type of perforation pipe (ID = ½"). **Fig. 4.7** shows the plots of seating efficiency versus normalized density contrast ($(\rho_{ball} - \rho_{fluid})/\rho_{fluid}$) for three flow rates, 2, 4, and 6 bbl/min. For comparison, Erbstoesser's results are plotted in Fig. 4.7 (a). In Erbstoesser's experiments, 100% seating efficiency was obtained for every buoyant ball test (Fig. 4.7 (a)). However, seating efficiency was less than 100% in cases of BP experiments. For deviated/horizontal wells (Figs. 4.7 (b) to (d)), buoyant ball sealers tended to seat on upward (high-side) perforations while non-buoyant ball sealers had a tendency to seat on downward (low-side) perforations.

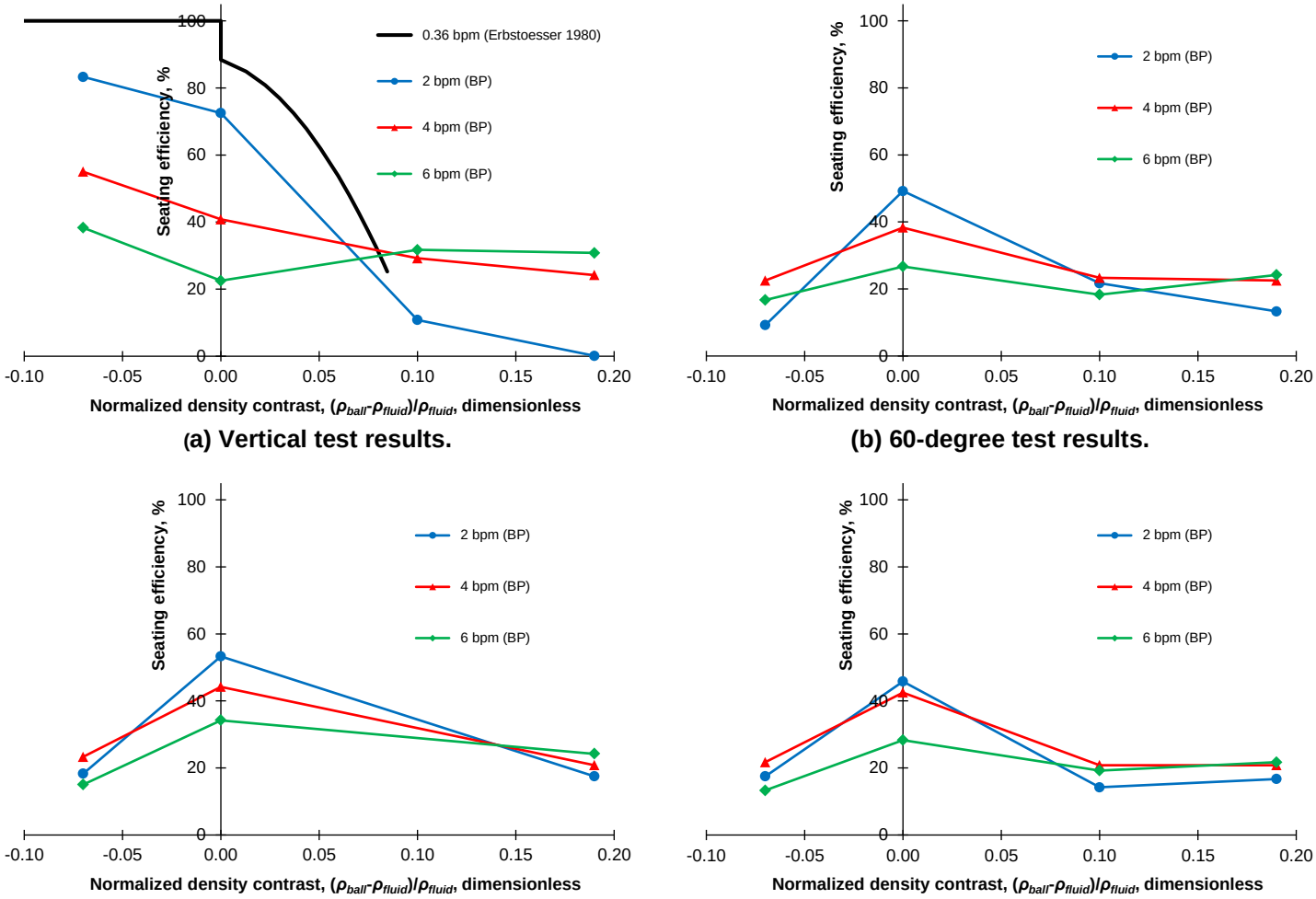

Fig. 4.7—Seating efficiency versus normalized density contrast (Erbstoesser 1980; Bern and Lewis 1992a).

On the other hand, neutrally buoyant ball sealers were prone to seat on the horizontally oriented perforations although some of them seated on either downward or upward perforations due to their density deviation from 1.0 specific gravity. Therefore, neutrally buoyant ball sealers gave the best seating efficiency in Figs. 4.7 (b) through (d) since the number of horizontally oriented perforations (40 perforations) is larger than the number of upward perforations (20 perforations) or the number of downward perforations (20 perforations). In vertical well tests, there are no tendencies such as in deviated/horizontal well tests. As a result, seating efficiencies were shown to be generally higher with vertical wells (Bern 1993). Additionally, seating behavior seemed to be essentially similar for the deviations between 60 and 90 degrees.

4.3.3 Seating Tendency

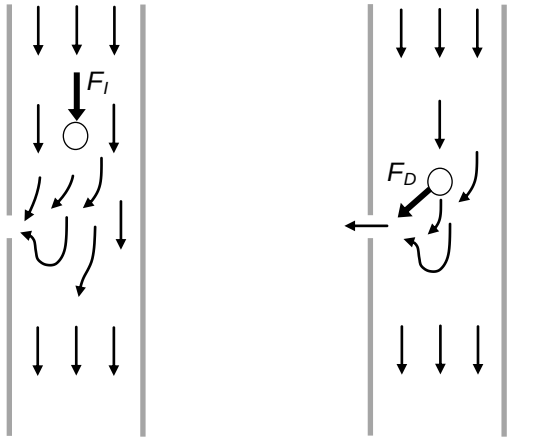

(a) Inertial force. **(b) Drag force.**

Fig. 4.8—Simplified sketch of the basic forces governing ball sealer efficiency (from Brown et al. 1963).

Brown et al. (1963) mentioned that when the drag force tending to divert a ball to a perforation, F_D, is greater than the inertial force on the ball sealer, F_I, the ball sealer will divert from the central flow channel to contact the perforation (**Fig. 4.8**). By following their assumptions, F_D and F_I are expressed as follows:

$$F_D = 1.18\times10^{-5} K_D \rho_{fluid} d_{ball}^2 v_{perf}^2, \quad \text{.....(4.15)}$$

and

$$F_I = 3.78\times10^{-4} \frac{\rho_{ball} d_{ball}^3 v_{perf}^2}{d_{pipe}} \quad \text{.....(4.16)}$$

where v_{perf} is the velocity through the perforation in ft/min. Here, we define a ratio of the drag force to the inertial force, R_{ball}, as follows:

$$R_{ball} = \frac{F_D}{F_I} = 0.0312 \frac{K_D \rho_{fluid} d_{pipe} v_{perf}^2}{\rho_{ball} d_{ball} v_{ball}^2}. \quad \text{.....(4.17)}$$

Here, we examine the relationship between R_{ball} and ball sealer seating tendency. **Fig. 4.9** shows R_{ball} at each perforation depth with different fluid injection rates when all the perforations are open and ball density is 1.10 g/cm^3. BP experimental results showed that the ball which seated on the perforation first seated on a perforation in the bottom part of the pipe at q = 2 bbl/min (blue circle). It is considered that larger R_{ball} gives higher seating tendency. Therefore, for higher injection rate, 4 and 6 bbl/min, it is expected that the first ball seats on a perforation in the top or middle part as Fig. 4.9 shows. However, for q = 4 (red circle) and 6 bbl/min (green circle), the first ball seated on a perforation in the bottom part according to BP experimental results. This may indicate that R_{ball} is not a sufficient condition for ball sealer seating tendency. As discussed previously, we assume that balls do not disturb the fluid flow. This assumption may not be valid. The calculated ball velocity is considered not to be accurate enough to evaluate R_{ball}. Also, it is possible that slight differences in perforation velocity among the perforations causes different ball sealer trajectories. As a result, the drag force tending to divert a ball to a perforation is not constant along the pipe.

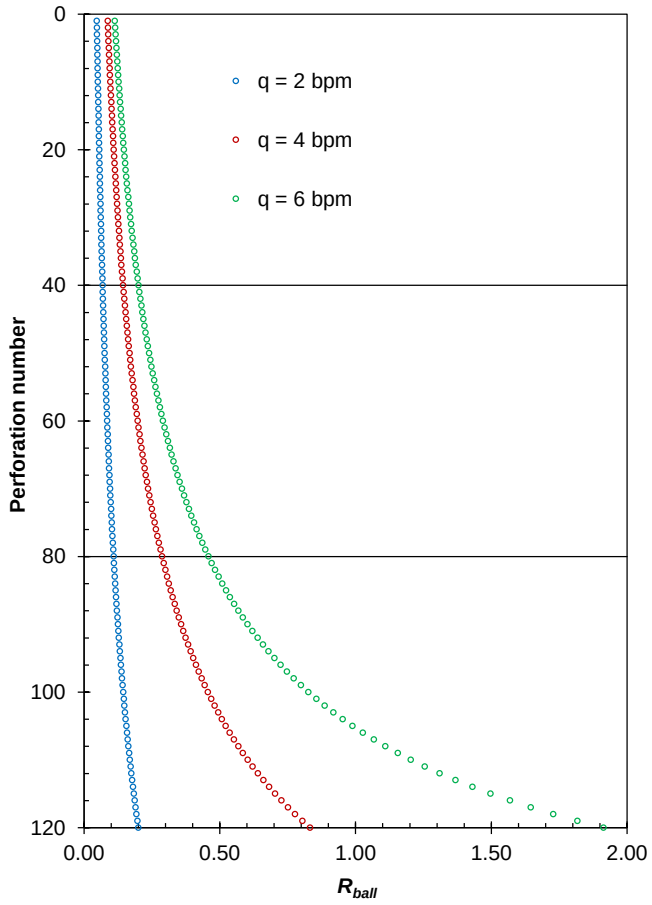

Fig. 4.9—R_{ball} at each perforation depth.

4.3.4 Ball Injection Method

We investigate the relationship between ball injection rate and seating tendency. In BP experiments, ball injection rate was set as one of the experimental parameters (Table 4.1). **Table 4.2** shows the results. For the horizontal tests, the results are similar. On the other hand, the results for the 60-degree tests are different. However, if we take into consideration the statistical nature of the balls' seating, that difference is considered to be insignificant. Then we can conclude that the ball injection rate is relatively unimportant to the seating tendency.

TABLE 4.2—EFFECT OF BALL INJECTION RATE.		
	Seating efficiency	
	2 balls per bbl	Batch injection
Horizontal tests		
• q = 2 bpm	14.2	14.2
• q = 4 bpm	16.7	19.2
60-degree tests		
• q = 2 bpm	18.3	12.5
• q = 4 bpm	16.6	13.3

4.3.5 Comparison to Field Result

Pressure change due to ball sealer blockage, Δp_{ball}, can be calculated by

$$\Delta p_{ball} \cong \Delta p_{perf,after} - \Delta p_{perf,before}. \quad \text{.....(4.18)}$$

Substitution of Eq. 2.26 into Eq. 4.18 gives

$$\Delta p_{ball} = \frac{1.98244 q^2 \gamma}{(K_d d_{perf}^2)^2}(n_{perf,after}^{-2} - n_{perf,before}^{-2}). \quad \text{.....(4.19)}$$

Solving for $n_{perf,after}$ gives

$$n_{perf,after} = n_{perf,before} - \left[\frac{\Delta p_{ball}(K_d d_{perf}^2)^2}{1.982444 q^2 \gamma} + \frac{1}{n_{perf,before}^2}\right]^{-0.5}. \quad \text{.....(4.20)}$$

Hence, the increment of the number of ball sealers seated on the perforations during the pressure change, $\Delta n_{perf,ball}$, is

$$\Delta n_{perf,ball} = n_{perf,before} - \left[\frac{\Delta p_{ball}(K_d d_{perf}^2)^2}{1.982444 q^2 \gamma} + \frac{1}{n_{perf,before}^2}\right]^{-0.5}. \quad \text{.....(4.21)}$$

For low rate treatments such as matrix acidizing, the pressure drop through the perforations is usually small. **Fig. 4.10** shows plots of pressure drop through perforations versus volumetric flow rate. In this example, K_d = 0.8, γ = 1.0, and d_{perf} = 0.29 inch. For high flow rate, pressure drop through perforation is significantly different among different numbers of open perforations (n_{perf}). On the other hand, for low rates, the pressure difference is quite small. Hence, a small change of number of open perforations does not make a significant change in the pressure drop through the perforations for low rate treatments as shown in **Fig. 4.10**. However, if we inject ball sealers as a batch and a

number of perforations are sealed at a time, Eq. 4.21 should be able to tell how many balls seat on the perforations in the batch injection.

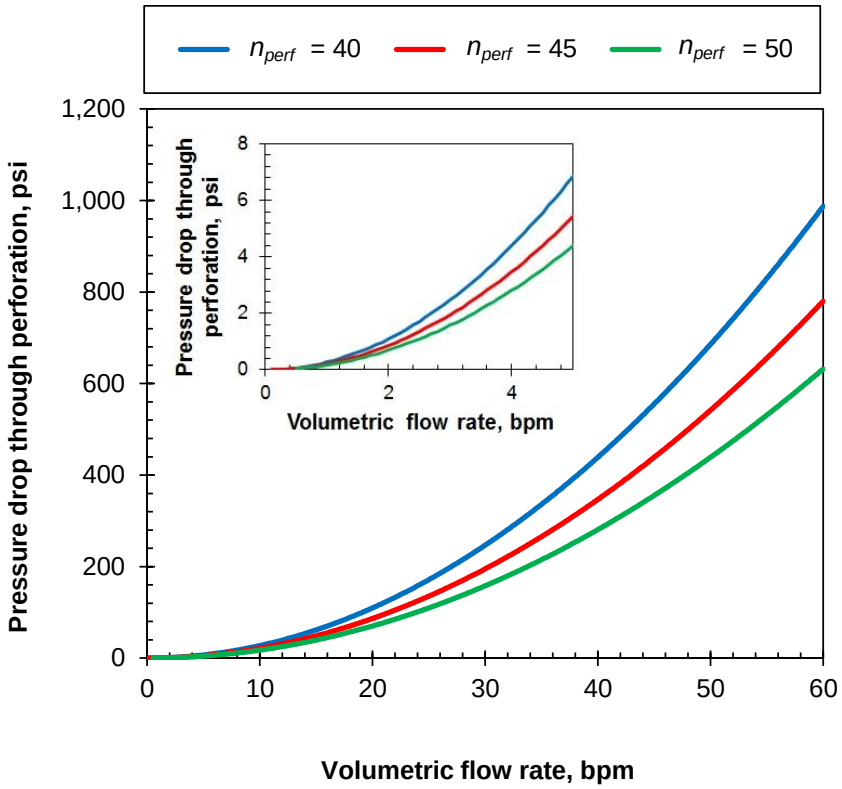

Fig. 4.10—Pressure drop through perforation versus volumetric flow rate.

Now we apply Eq. 4.21 to a high-rate acid treatment in a deviated well ($\theta = 11^{o}$).). In the treatment, a limited-entry technique (60 bbl/min; 30 perforations) and ball sealer diversion (14 ball sealers) were used to divert stimulation fluids to lower-injectivity zones. The treatment program consisted of a step-rate test and main acid stimulation (**Fig. 4.11**). The main acid stimulation consisted of five repeated stages consisting of gel pad, acid, and overflush. Fig. 4.11 shows the slurry rates, surface pressure (WHP) and bottomhole pressure (BHP). The first gel pad was injected from the surface at t = 23 minutes and reached the formation at t = 30 minutes. Ball sealers were injected as a batch. Non-buoyant ball sealers (specific gravity = 1.3) were used because the

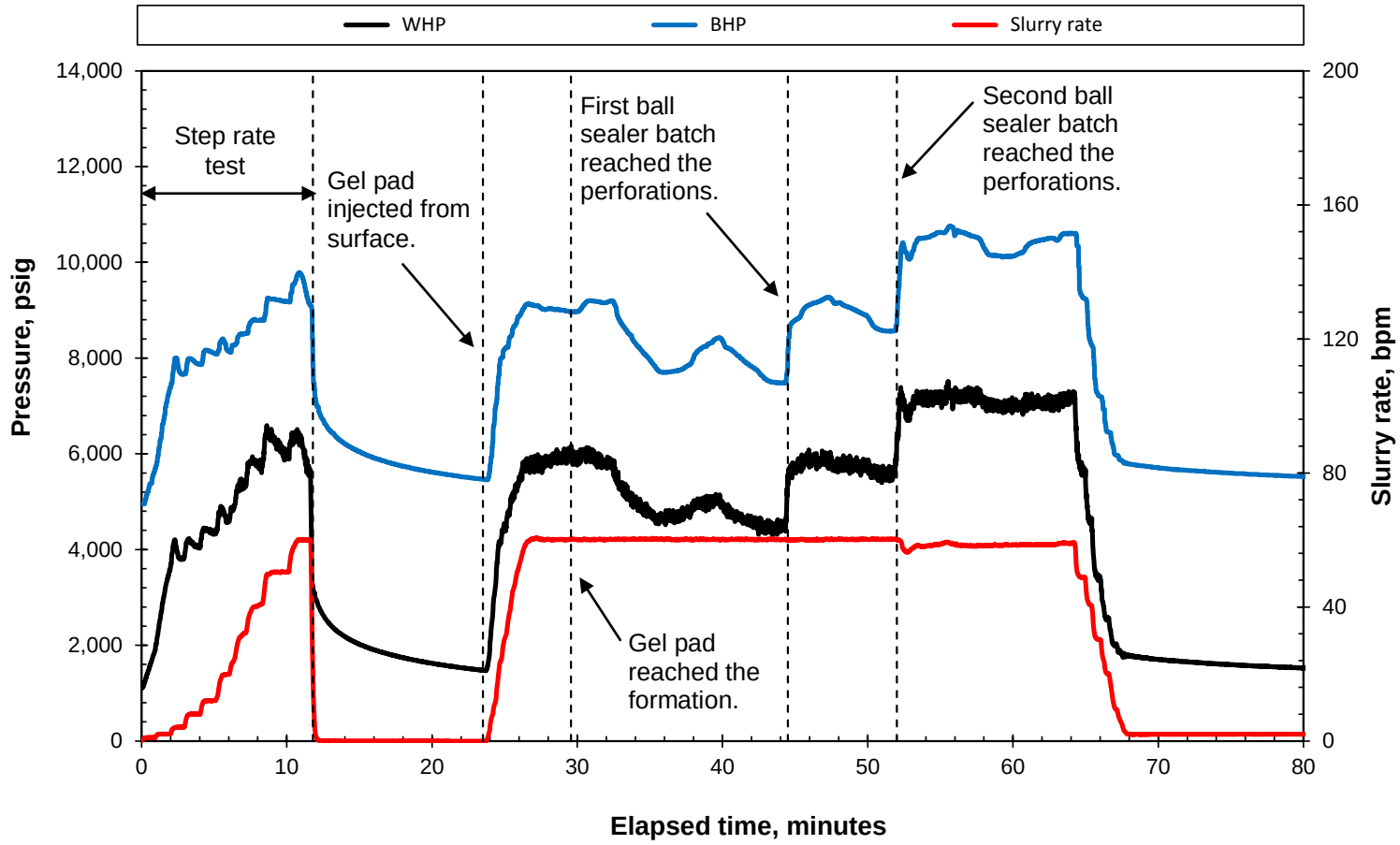

Fig. 4.11—Pressure and rate record.

perforations were downward (0^o phasing). 11 balls were injected first, and then 8 balls were injected next. The sudden pressure changes due to ball sealer blockages were observed in both WHP and BHP (t = 44 and 52 minutes).

First, it is necessary to identify how many perforations were open and connected to the fractures before the well stimulation. The instantaneous shut-in pressure and the bottomhole pressure just before shut-in were 7,475 psig and 8,992 psig, respectively. The pipe friction loss between the downhole gauge and the reservoir face is calculated to be 80 psi. Hence, the perforation pressure drop is 1,437 psi. Using Eq. 2.26, n_{perf} is calculated to be 30 (d_{perf} = 0.29 inch; K_d = 0.8; γ = 1.002). Therefore, all the perforations were open and connected to the fractures before the well stimulation.

Next, we use Eq. 4.21 to calculate the number of ball sealers seated on the perforations. At the first pressure change (Δp_{ball} = 1,154.4 psi),

$$\Delta n_{perf,after} = 30 - \left\{ \frac{(1{,}154.4\ \text{psi})[(0.8)(0.29\ \text{inch})^2]^2}{(1.982444)(60\ \text{bbl/min})^2(1.002)} + \frac{1}{(30)^2} \right\} \cong 8.$$

Hence, 5 balls out of 8 balls are found to be seated on the perforations. 63% of balls were successfully seated on the perforations. At the second pressure change (Δp_{ball} = 1,518.0 psi),

$$\Delta n_{perf,after} = 22 - \left\{ \frac{(1{,}518.0\ \text{psi})[(0.8)(0.29\ \text{inch})^2]^2}{(1.982444)(60\ \text{bbl/min})^2(1.002)} + \frac{1}{(25)^2} \right\} \cong 2.$$

4 balls out of 6 balls are found to be seated on the perforations. 67% of balls were seated. Cumulatively, 64% of injected balls blocked the perforations.

We plot the seating efficiency ($n_{perf}(t)/n_{perf,total}$) versus the ratio of number of injected ball sealers to number of perforations ($n_{ball}(t)/n_{perf,total}$) in **Fig. 4.12**. For comparison, we plot some of BP experimental results (60-degree tests). The highest ball density cases are selected since the specific gravity of the ball used in the field was 1.3. As discussed previously, non-buoyant ball sealers tend to seat on the downward perforations. BP experiments show that almost all of the buoyant ball sealers seated on the downward perforations. Hence, the total number of perforations was changed from 120 to 40 to calculate the effective seating efficiency. Interestingly, the results from the field analysis

are quite similar to the results for the cases with q = 4 and 6 bbl/min. This indicates the usefulness of BP experimental results. Bern (1993) observed in BP experimental results that seating behavior for the deviations between 60 and 90 degrees seems to be essentially similar. This may be the reason why the field result (11-degree deviation) is quite similar to the results in 60-degree tests.

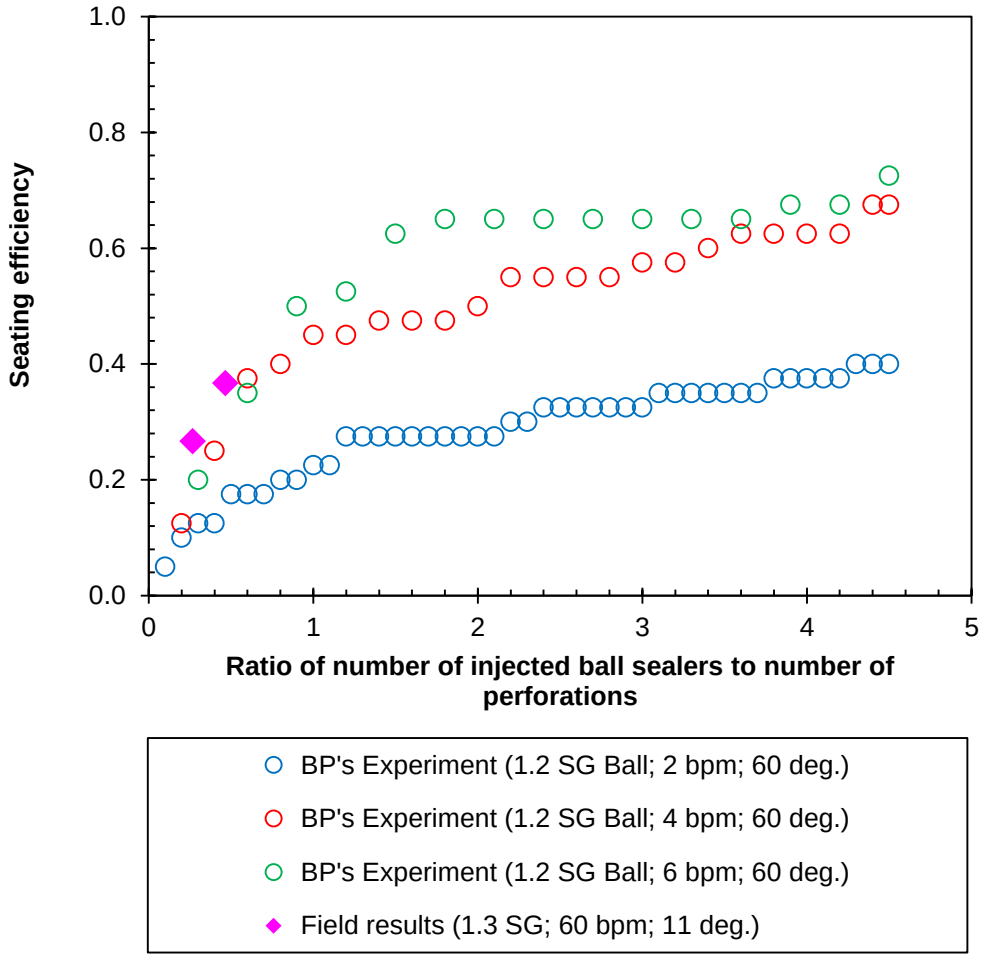

Fig. 4.12—Comparison between field results and BP laboratory results.

4.3.6 Development of Empirical Correlation

On the basis of the analysis we showed, we develop an empirical correlation which determines ball sealer seating efficiency. To the best of our knowledge, neutrally buoyant ball sealers are rarely used in field treatments. Therefore, we develop empirical correlations for buoyant and non-buoyant ball sealers respectively. Also, since the characteristics of seating efficiency in deviated/horizontal wells are different from the ones in vertical wells, we develop an empirical correlation for each.

In order to simulate acid distribution, we simulate wormhole propagation with time. In the same way, it is necessary to simulate ball seating with time. In the literature, only final seating efficiency was focused on, however, for acidizing simulation, the final seating efficiency is not enough. Hence, the empirical correlation we develop needs to predict ball sealer seating efficiency with time. To predict the seating efficiency in this way, we see the seating efficiency with respect to the number of balls injected. Since the number of ball injected for the number of perforations is more appropriate to see the seating efficiency in different conditions, we use the ratio of the number of injected balls to the number of perforations as in Fig. 4.12.

As discussed, the behavior of ball sealers has a statistical nature. Some of the experimental data departs from some general trends such as that higher flow rates gives higher seating efficiencies for non-buoyant ball sealers. To develop empirical correlations, we neglect those data. However, even after deleting those data, there are still some data which empirical correlations cannot capture quite well.

We developed the following empirical correlation:

$$\frac{n_{perf,ball}}{n_{perf,total}} = \mathrm{erf}\left(K_1 q + K_2\right) \times \frac{\gamma\left(K_3, \dfrac{n_{ball}(t)/n_{perf,total}}{K_4}\right)}{\Gamma(K_3)} \quad \text{.....(4.22)}$$

where $n_{perf,ball}$ is the total number of ball sealers seated on the perforations, $n_{perf,total}$ is the total number of perforations, n_{ball}(t) is the number of balls injected, and K_1, K_2, K_3, and K_4 are the correlation constants. Γ is the upper incomplete gamma function and γ is the lower incomplete gamma function defined as follows:

$$\Gamma(s) = \int_0^{\infty} w^{s-1} e^{-w} dw \quad \text{.....(4.23)}$$

and

$$\gamma(s,x) = \int_0^{x} w^{k-1} e^{-w} dw. \quad \text{.....(4.24)}$$

$\gamma(k, x)/\Gamma(k)$ is the cumulative gamma distribution function. The range of $n_{perf,ball}/n_{perf,total}$ is between 0 and 1. For this reason, we use the error function. The correlation constants are shown in **Table 4.3**.

TABLE 4.3—CORRELATION CONSTANTS IN EQ. 4.22.

Non-buoyant/ buoyant	Well inclination	K_1	K_2	K_3	K_4
Non-buoyant	Horizontal/Deviated	0.0913	0.596	1.47	0.533
Buoyant	Horizontal/Deviated	0.114	0.552	2.37	0.260
Buoyant	Vertical	-0.180	1.40	2.04	0.254

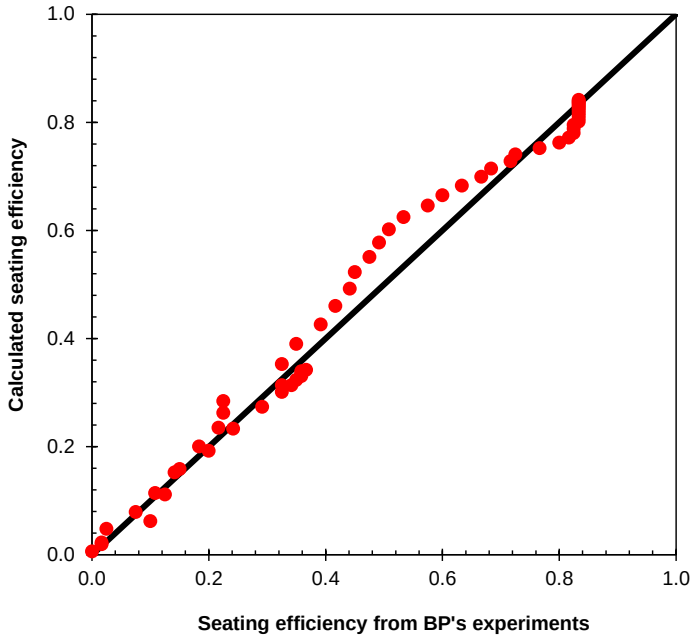

Fig. 4.13—Verification of empirical correlation for buoyant ball sealers in vertical wells.

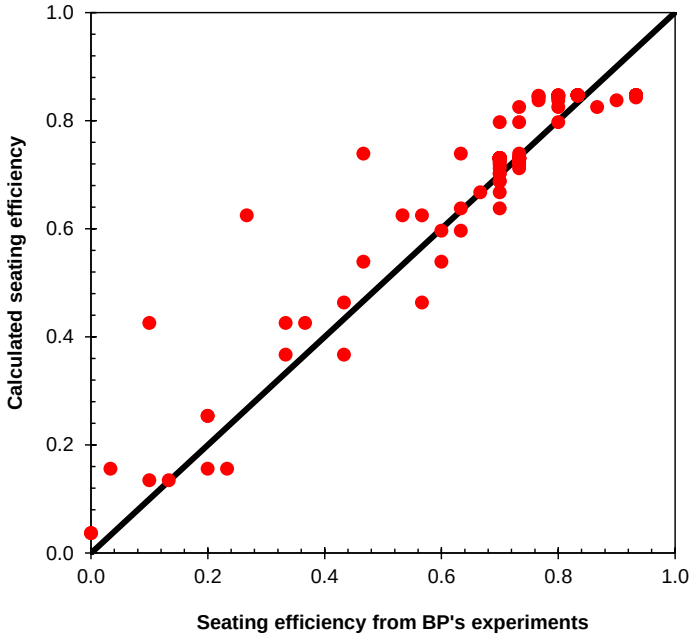

Fig. 4.14—Verification of empirical correlation for buoyant ball sealers in deviated/horizontal wells.

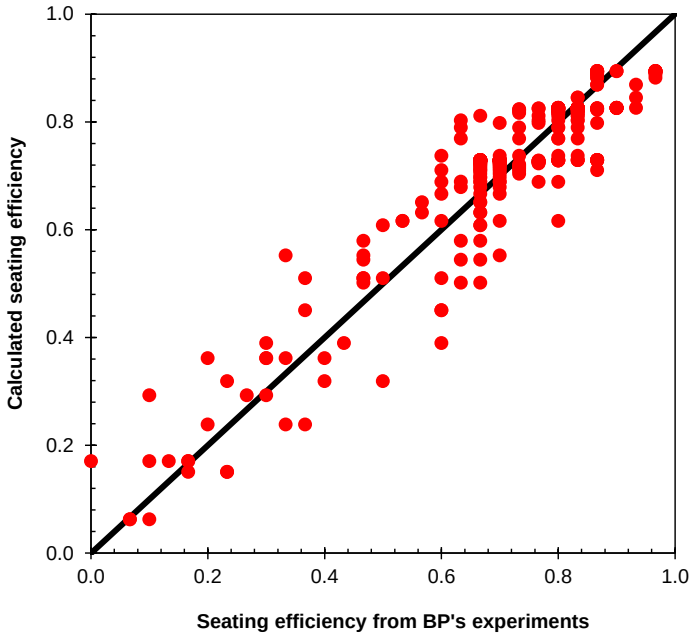

Fig. 4.15—Verification of the empirical correlation for non-buoyant ball sealers in deviated/horizontal wells.

Figs. 4.13 through 4.15 show the plots of seating efficiency from BP experiment data versus calculated seating efficiency using the empirical correlation Eq. 4.22. **Fig. 4.16** shows one example of the data fit.

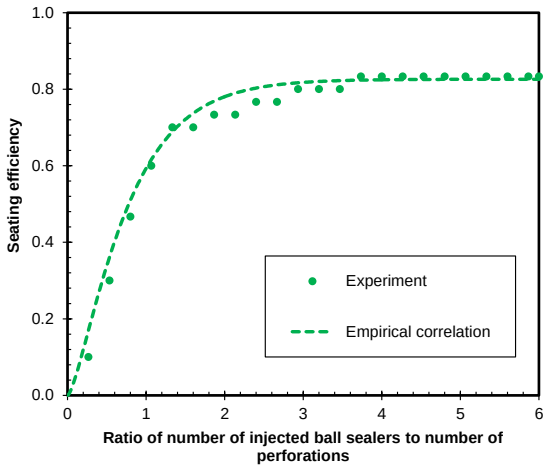

Fig. 4.16—Example of the data fit by Eq. 4.22 for non-buoyant ball sealers in a 60-deg. inclined well.

The empirical correlation can be used when there is a significant contrast in injectivity along the wellbore. Total injection rate has to be nearly equal to the reservoir out flow rate in the highest permeability zone (or layer) since that's the condition of BP experiments. Actually, this type of formation is the one which needs diversion for acid distribution.

4.4 Effect of Ball Sealers' Blockage

As we discussed in Sec. 4.3.5, the pressure drop through perforations changes after ball sealers seat on the perforations. Using Eq. 2.26, we take this into consideration in our simulation.

In addition, the thickness of the treated zone will be changed as shown in **Fig. 4.17**. However, there should be a partial penetration effect. If the partial penetration effect is dominant, we should use h instead of h_{eff}. Wormhole also can propagate above and below zones. If this happens, then the difference between spherical and radial flows no

longer causes additional pressure drop to the pressure drop calculated from the radial Darcy's flow equation. In our study, we use h_{eff} for an entire treatments after the ball sealer blockage although it is better to switch from h_{eff} to h in a certain duration. This duration is considered to be identified by history matching with field data. This can be a very short time and also a very long time. It strongly depends on the geometry of open perforations and thickness.

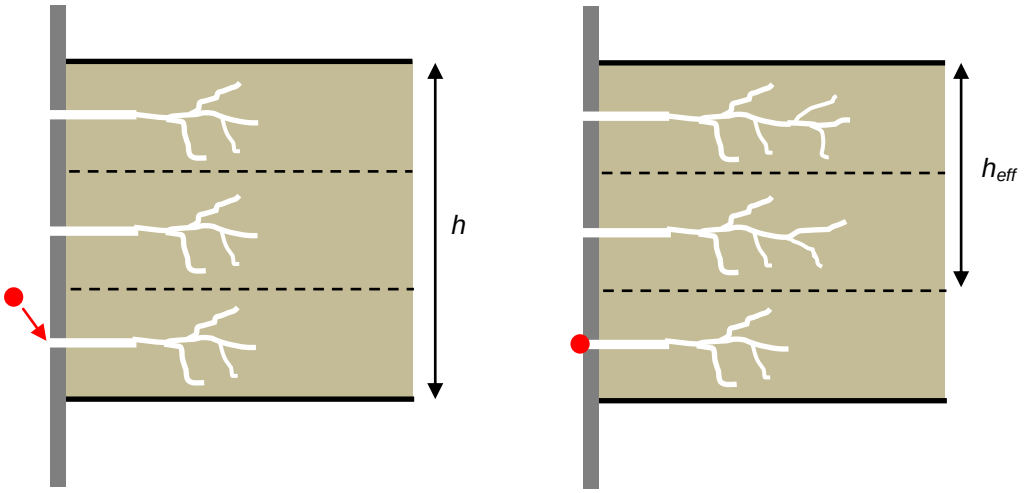

Fig. 4.17—Effective thickness.

4.5 Computer Program Structure

We use the acid placement model presented in Sec. 2. In addition to the model, we introduce ball sealers into the model. **Fig. 4.18** shows the flow chart. The steps of the ball sealer diversion model in Fig. 4.18 are as follows:

1. Calculate the ball velocity,
2. Calculate the seating efficiency,
3. Calculate the number of ball sealers seated on the perforations, and
4. Update the effective thickness of the treating zone.

All the calculations are implemented explicitly.

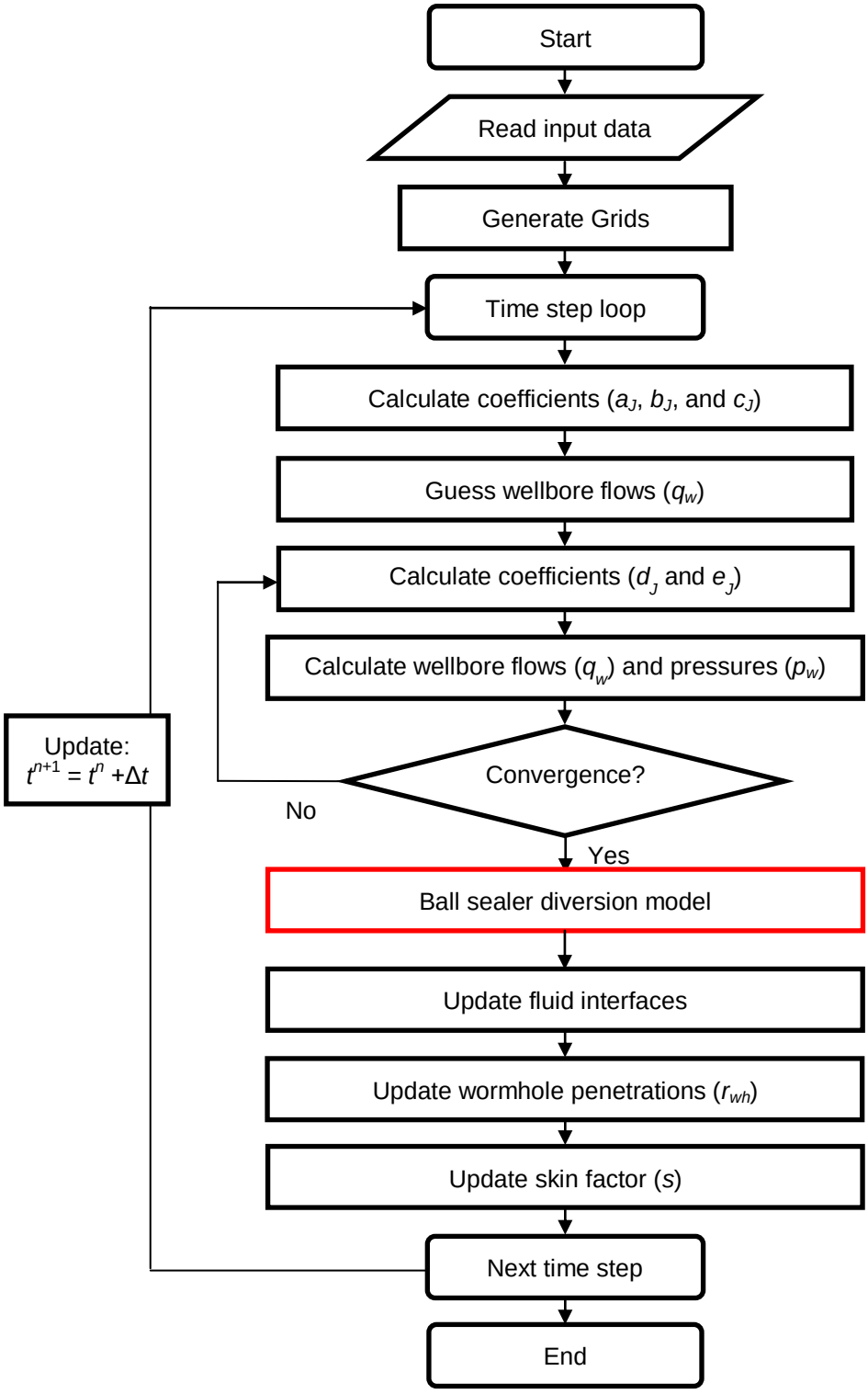

Fig. 4.18—Flow chart for the acid placement and ball sealer diversion model.

4.6 Section Summary

We develop a ball sealer diversion model which includes

- ball sealer tracking model
- ball sealer seating efficiency model (empirical correlation), and
- the model which accounts for ball sealer blockage.

In the next section, we simulate a hypothetical case using the ball sealer diversion model.

5. HYPOTHETICAL CASE STUDY II

5.1 Introduction

In this section, we study a hypothetical case using the ball sealer diversion presented in Sec. 4. We simulate a matrix acidizing treatment in a multi-layer formation.

5.2 Multi-layer Case

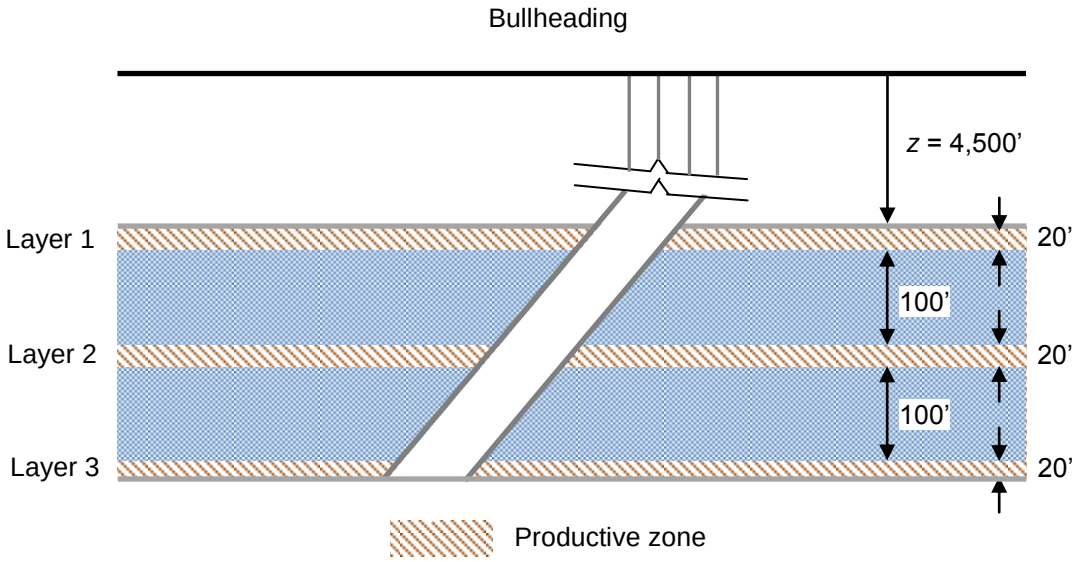

Fig. 5.1—Multi-layer formation with cased and perforated completion.

TABLE 5.1—LAYERS’ DATA.

Layer #	k, md	$PV_{bt,opt}$	$v_{i,opt}$
1	20	0.7	3.2
2	1,000	0.5	2.0
3	20	0.7	3.2

TABLE 5.2—INPUT DATA FOR A MULTI-LAYER FORMATION.	
Wellbore radius, inch	3.047
Pay Thickness, ft	60
Porosity, fraction	0.2
Damage ratio (k_d/k)	0.1
Damage penetration radius, ft	2
Initial reservoir pressure @ TVD = 4,515 ft, psia	1,500
Oil viscosity, cp	0.58
Deviation angle, degrees	60
Perforation length, inch	12
Perforation diameter, inch	0.25
Perforation density, spf	4
Perforation phasing, degree	0
Discharge coefficient	0.80
Injection rate, bbl/min	6.0
Acid type	15 wt% HCl
Acid viscosity, cp	1.0
Core diameter, in.	1
Core length, in.	6
Number of dominant wormholes per 2D plane	6
Wormhole axial spacing coefficient	0.50
Parameter for fluid-loss limited wormholing	1/3

We study matrix acidizing in a multi-layer formation. **Fig. 5.1** shows the assumed well. There are three productive layers, and the well is deviated. **Tables 5.1 and 5.2** show the layers' data and the other data used in this case study, respectively. Layer 2 has a very high permeability compared to the other two layers. This layer is supposed to take most of the stimulation fluids, and hence we need a diversion to stimulate layer 1 and 3. We use ball sealer as a diverter. **Table 5.3** shows the ball sealer data. Since we assume downward perforations with 0^o phasing, we use non-buoyant ball sealers.

TABLE 5.3—BALL SEALER DATA.	
Ball diameter, inch	0.875
Specific gravity	1.1
Start time, min	10
Number of ball sealers	240
Ball injection rate, balls/bbl	2

Fig. 5.2 shows plots of the bottomhole pressure versus time. We also simulate the matrix acidizing without the ball sealers to compare with the one with the ball sealers. As we expected, after treating layer 2, the ball sealers get to the layer and start sealing the perforations. As a result, at t = 20 minutes, the bottomhole pressure starts increasing. As engineers analyze, this pressure increase indicates the acid diversion.

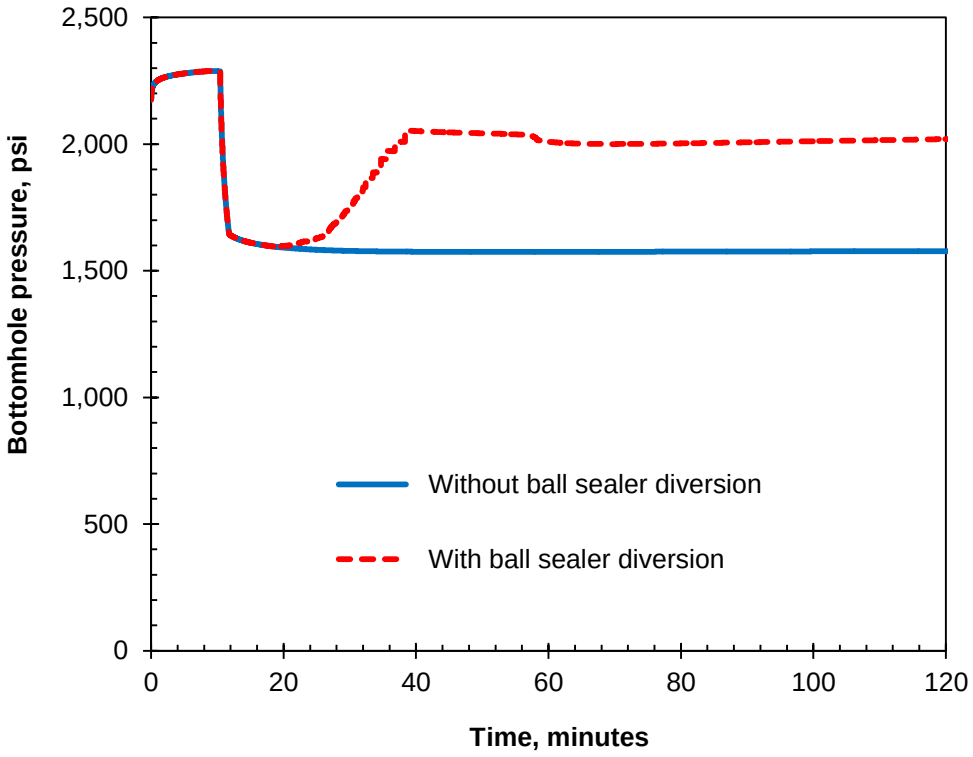

Fig. 5.2—Bottomhole pressure versus time for a multi-layer formation.

Fig. 5.3 shows the wormhole profile along the well (the wormhole penetration in layer 2 is longer than 5 ft). Successfully, the acid is diverted to layer 1. However, layer 3 is not treated at all. In order to treat layer 3, we need to inject more ball sealers to block the flow into layer 1.

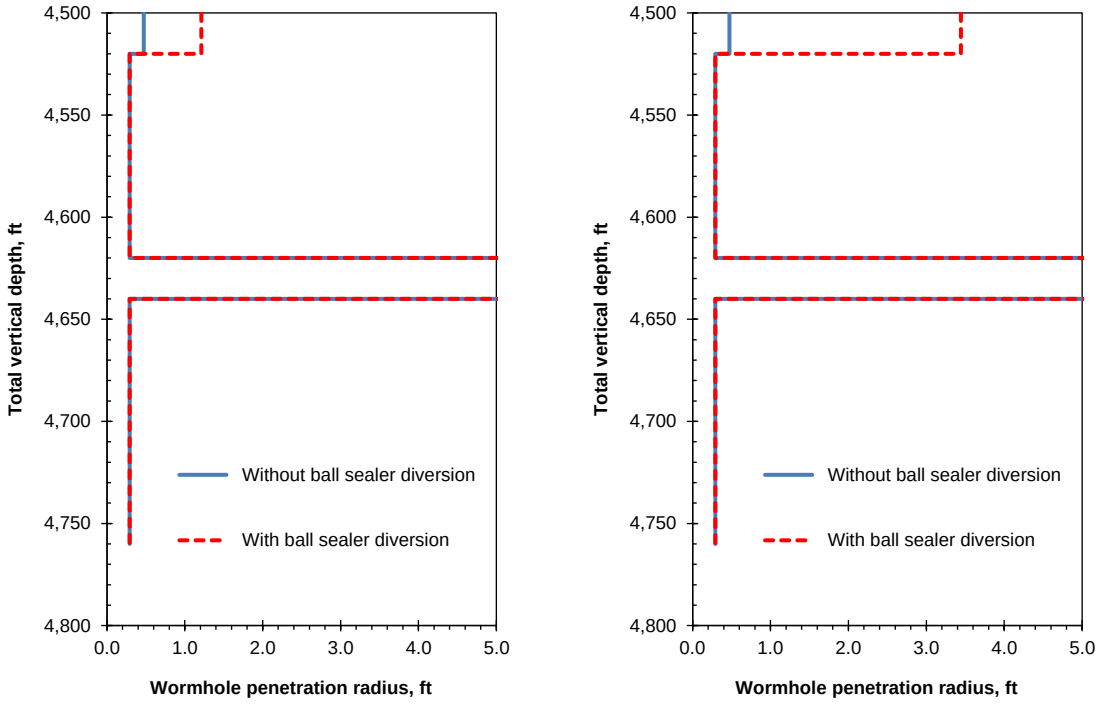

(a) after 40 gal/ft of injection. **(b) after 50 gal/ft of injection.**

Fig. 5.3—Wormhole penetration profile.

To design the next diversion, we need a simulator. Can we find a point in Fig. 5.2 when the wormholes in layer 1 break through the damage region? We can barely find the point (at t = 58 min, the pressure change is about 40 psi) when we look at the simulation result, but it may not be clear since the data we obtain in the field is not as smooth as Fig. 5.2.

5.3 Section Summary

In this section, we show the usefulness of the ball sealer diversion model. With the model, we can design and/or evaluate matrix acidizing treatments in carbonates.

6. SUMMARY AND CONCLUSIONS

6.1 Conclusions

We developed an acid placement and diversion model. The model can deal with ball sealer diversion. The ball sealer diversion model is based on the experiments which were carried out by BP in 1992. With the model, we can estimate acid distribution along the wellbore with time. Hence, we can design and/or evaluate matrix acidizing treatments. As a design example, we showed a hypothetical example in Sec. 5. In the section, we showed the usefulness of the simulator.

6.2 Recommendations

One of the most important things for acidizing simulation is to get reliable input data such as layer permeability, porosity, etc. Even if we have a matrix acidizing simulator, we may not be able to simulate an acidizing treatment reasonably if the input data does not represent the formation to be stimulated. It is recommended to conduct a fall-off test to get the information about formations with good accuracy.

Also, it is recommended to measure downhole pressure. As Furui et al. noticed (2010), once friction reducer is introduce into the acid recipe, it is difficult to simulate downhole pressures using surface pressures. If we history match the wrong downhole pressures which are calculated based on the surface pressures, then it is easy to evaluate the acidizing treatment in a wrong way. It is highly possible to misunderstand the acidizing treatments.

REFERENCES

Bale, G.E. 1984. Matrix Acidizing in Saudi Arabia Using Buoyant Ball Sealers. *J Pet Technol* **36** (10): 1748-1752. SPE-11500-PA. http://dx.doi.org/10.2118/11500-PA.

Barnea, E. and Mizrahi, J. 1973. A Generalized Approach to the Fluid Dynamics of Particulate Systems. *The Chemical Engineering Journal* **5** (2): 171-189. http://dx.doi.org/10.1016/0300-9467(73)80008-5.

Bartko, K.M., Montgomery, C.T., Boney, C.L., and Ward, V.L. 1996. Development of a Stimulation Treatment Integral Model. Paper SPE 35991 presented at the Petroleum Computer Conference, Dallas, Texas, USA, 2-5 June. http://dx.doi.org/10.2118/35991-MS.

Baylocq, P., Fery, J.J., Parra, L., and Derbez, E. 1999. Ball Sealer Diversion When Fracturing Long and Multiple Triassic Sand Intervals on Alwyn Field, North Sea. Paper SPE 54740 presented at the SPE European Formation Damage Conference, The Hague, The Netherlands, 31 May-1 June. http://dx.doi.org/10.2118/54740-MS.

Bazin, B. 2001. From Matrix Acidizing to Acid Fracturing: A Laboratory Evaluation of Acid/Rock Interactions. *SPE Prod & Fac* **16** (1): 22-29. SPE-66566-PA. http://dx.doi.org/10.2118/66566-PA.

Bern, P.A. and Lewis, R.C. 1992a. Ball Sealer Diversion in Deviated Wellbores. Interim report, BP, Sunbury-on-Thames, United Kingdom (unpublished).

Bern, P.A. and Lewis, R.C. 1992b. Ball Sealer Diversion in Deviated Wellbores. Final report, BP, Sunbury-on-Thames, United Kingdom (unpublished).

Bern, P.A. 1993. Modeling of Ball Sealer Diversion. Technical report, BP, Sunbury-on-Thames, United Kingdom (unpublished).

Besson, J. 1990. Performance of Slanted and Horizontal Wells on an Anisotropic Medium. Paper SPE 20965 presented at the European Petroleum Conference, The Hague, The Netherlands, 21-24 October. http://dx.doi.org/10.2118/20965-MS.

Bird, R.B., Stewart, W.E., and Lightfoot, E.N. 1960. *Transport Phenomena*. New York City, New York: John Wiley and Sons Inc.

Brown, R.W. and Loper, R.G. 1959. Stimulation Treatment Selectivity through Perforation Ball Sealer Technology. *The Petroleum Engineer*: B-82, 84, 86, 88, 96, 98, 102, and 108.

Brown, R.W., Neill, G.H., and Loper, R.G. 1963. Factors Influencing Optimum Ball Sealer Performance. *J Pet Tech* **15** (4): 450-454. SPE-553-PA. http://dx.doi.org/10.2118/553-PA.

Buijse, M.A. 2000. Understanding Wormholing Mechanisms Can Improve Acid Treatments in Carbonate Formations. *SPE Prod & Fac* **15** (3): 168-175. SPE-65068-PA. http://dx.doi.org/10.2118/65068-PA.

Buijse, M. and Glasbergen, G. 2005. A Semiempirical Model to Calculate Wormhole Growth in Carbonate Acidizing. Paper SPE 96892 presented at the Annual Technical Conference and Exhibition, Dallas, Texas, USA, 9-12 October. http://dx.doi.org/10.2118/96892-MS.

Chen, N. H. 1979. An Explicit Equation for Friction Factor in Pipe. *Ind. Eng. Chem. Fundamen.* **18** (3): 296-297. http://dx.doi.org/10.1021/i160071a019.

Chhabra, R.P., Agarwal, S., and Chaudhary, K. 2003. A Note on Wall Effect on the Terminal Falling Velocity of a Sphere in Quiescent Newtonian Media in Cylindrical Tubes. *Powder Technology* **129** (1-3): 53-58. http://dx.doi.org/10.1016/S0032-5910(02)00164-X.

Dake, L. P. 1983. *Fundamentals of Reservoir Engineering*. Amsterdam, The Netherlands: Elsevier Science.

Derrick, J. V. and Kaltenberger, L. H. 1956. Method of Temporarily Closing Perforations in the Casing. US Patent No. 2,754,910.

Dukowicz, J.K. 1980. A Particle-fluid Numerical Model for Liquid Sprays. *Journal of Computational Physics* **35**: 229-253. http://dx.doi.org/10.1016/0021-9991(80)990087-X.

Earlougher, R.C., Jr. 1977. *Advances in Well Test Analysis*, Vol. 5, 186-191. Richardson, Texas: Monograph Series, SPE.

Eckerfield, L.D., Zhu, D., Hill, A.D., and Robert, J.A. 2000. Fluid Placement Model for Horizontal-Well Stimulation. SPE *Drill & Compl* **15** (3): 185-190. SPE-65408-PA. http://dx.doi.org/10.2118/65408-PA.

Economides, M.J., Hill, A.D., and Ehlig-Economides, C. 1993. *Petroleum Production System*. Englewood Cliffs, New Jersey: Prentice Hall PTR.

Edwardson, M.J., Girner, H.M., Parkison, H.R., et al. 1962. Calculation of Formation Temperature Disturbances Cased by Mud Circulation. *J Pet Technol* **14** (4): 416-426. http://dx.doi.org/10.2118/10.2118/124-PA.

Erbstoesser, S.R. 1980. Improved Ball Sealer Diversion. *J Pet Technol* **32** (11): 1903-1910. SPE-8401-PA. http://dx.doi.org/10.2118/10.2118/8401-PA.

Furui, K. 2004. A Comprehensive Skin Factor Model for Well Completions Based on Finite Element Simulations. PhD dissertation, The University of Texas at Austin, Austin, Texas (May 2004).

Furui, K., Zhu, D., and Hill, A.D. 2008. A New Skin-factor Model for Perforated Horizontal Wells. *SPE Drill & Compl* **23** (3): 205-215. SPE-77363-PA. http://dx.doi.org/10.2118/77363-PA.

Furui, K., Burton, R.C., Burkhead, D.W., Abdelmalek, N.A., Hill, A.D., et al. 2010. A Comprehensive Model of High-Rate Matrix Acid Stimulation for Long Horizontal Wells in Carbonate Reservoirs. Paper SPE 134265 presented at the SPE Annual Technical Conference and Exhibition, Florence, Italy, 19-22 September. http://dx.doi.org/10.2118/134265-MS.

Gabriel, G.A. and Erbstoesser, S.R. 1984. The Design of Buoyant Ball Sealer Treatments. Paper SPE 13085 presented at the SPE Annual Technical Conference and Exhibition, Houston, Texas, USA, 16-19 September. http://dx.doi.org/10.2118/13085-MS.

Gilchrist, J.M., Stephen, A.D., and Lietard, O.M.N. 1994. Use of High-angle, Acid-fractured Wells on the Machar Field Development. Paper SPE 28917 presented at the European Petroleum Conference, London, UK, 25-27 October. http://dx.doi.org/10.2118/28917-MS.

Glasbergen, G. and Buijse, M. 2006. Improved Acid Diversion Design Using a Placement Simulator. Paper SPE 102412 presented at the SPE Russian Oil and Gas Technical Conference and Exhibition, Moscow, Russia, 3-6 October. http://dx.doi.org/10.2118/102412-MS.

Govier, G.W. and Aziz, K. 2008. *The Flow of Complex Mixtures in Pipes*. Richardson, Texas: SPE.

Gregory, G.A. and Fogarasi, M. 1985. Alternate to Standard Friction Factor Equation. *Oil and Gas J.* **127** (1 April) 120-127.

Greyvenstein, G.P. and Laurie, D.P. 1994. A Segregated CFD Approach to Pipe Network Analysis. *Int. J. Num. Meth. Eng.* **37** (21): 3685-3705. http://dx.doi.org/10.1002/nme.1620372107.

Haider, A. and Levensipiel, O. 1989. Drag Coefficient and Terminal Velocity of Spherical and Nonspherical Particles. *Powder Technology* **58** (1): 63-70. http://dx.doi.org/10.1016/0032-5910(89)80008-7.

Hill, A.D. and Galloway, P.J. 1984. Laboratory and Theoretical Modeling of Diverting Agent Behavior. *J Pet Technol* **36** (7): 1157-1163. SPE-11576-PA. http://dx.doi.org/10.2118/11576-PA.

Hill, A.D. and Rossen, W.R. 1994. Fluid Placement and Diversion in Matrix Acidizing. Paper SPE 27982 presented at the University of Tulsa Centennial Petroleum Engineering Symposium, Tulsa, Oklahoma, USA, 29-31 August. http://dx.doi.org/10.2118/27982-MS.

Hill A.D. and Schechter, R.S. 2000. Fundamentals of Acid Stimulation. In *Reservoir Stimulation*, ed. M. J. Economides and K. G. Nolte, Chap. 16. New York City, New York: John Wiley & Sons.

Howard, E. 1962. Ball Sealers in Fracturing and Acidizing. *Canadian Oil and Gas Industries*: 43-46.

Hung, K.M., Hill, A.D., and Sepehrnoori, K. 1989. A Mechanistic Model of Wormhole Growth in Carbonate Matrix Acidizing and Acid Fracturing. *J. Pet Tech* **41** (1): 59-66. SPE-16886-PA. http://dx.doi.org/10.2118/16886-PA.

Jones, A.T. and Davies, D.R. 1996. Quantifying Acid Placement: The Key to Understanding Damage Removal in Horizontal Wells. Paper SPE 31146 presented at the SPE Formation Damage Control Symposium, Lafayette, Louisiana, USA, 14-15 February. http://dx.doi.org/10.2118/31146-MS.

Karakas, M. and Tariq, S.M. 1991. Semianalytical Productivity Models for Perforated Completions. *SPE Prod Eng* **6** (1): 73-82. http://dx.doi.org/10.2118/18247-PA.

Kastrop, J.E. 1956. Newest Aid to Multi-stage Fracturing. *The Petroleum Engineer*: B40-47.

Lagrone, K.W. and Rasmussen, J.W. 1963. A New Development in Completion Methods – The Limited Entry Technique. *J Pet Technol* **15** (7): 695-702. SPE-530-PA. http://dx.doi.org/10.2118/530-PA.

Lapple, C.E. and Shepherd, C.B. 1940. Calculation of Particle Trajectories. *Ind. Eng. Chem*. **32** (5): 605-617. http://dx.doi.org/10.1021/ie503665a007.

Li, X., Chen, Z., Chaudhary, S., and Novotony, R.J. 2005. An Integrated Transport Model for Ball-Sealer Diversion in Vertical and Horizontal Wells. Paper SPE 96339 presented at the SPE Annual Technical Conference and Exhibition, Dallas, Texas, USA, 9-12 October. http://dx.doi.org/10.2118/96339-MS.

Lord, D.L., Shah, S.N., Rein, Jr., R.G., and Lawson, III, J.T. 1994. Study of Perforation Friction Pressure Employing a Large-Scale Fracturing Flow Simulator. Paper SPE 28508 presented at the SPE Annual Technical Conference and Exhibition, New Orleans, Louisiana, USA, 25-28 September. http://dx.doi.org/10.2118/28508-MS.

McDuff, D.R., Shuchart, C.E., Jackson, S.K., Postl, D., and Brown, J.S. 2010. Understanding Wormholes in Carbonates: Unprecedented Experimental Scale and 3-D Visualization. Paper SPE 134379 presented at the SPE Annual Technical Conference and Exhibition, Florence, Italy, 19-22 September. http://dx.doi.org/10.2118/134379-MS.

Mishra, V., Zhu, D., Hill, A.D., and Furui, K. 2007. An Acid-placement Model for Long Horizontal Wells in Vertical and Horizontal Wells in Carbonate Reservoirs. Paper SPE 107780 presented at the European Formation Damage Conference,

Scheveningen, The Netherlands, 30 May-1 June. http://dx.doi.org/10.2118/107780-MS.

Mogensen, K. and Hansen, J.H. 2007. A Dynamic Model for High-rate Acid Stimulation of Very Long Horizontal Wells. Paper SPE 110135 presented at the Annual Technical Conference and Exhibition, Anaheim, California, USA, 11-14 November. http://dx.doi.org/10.2118/110135-MS.

Neill, G.H., Brown, R.W., and Simmons, C.M. 1957. An Inexpensive Method of Multiple Fracturing. *Drilling and Production Practice*: 27-32.

Nozaki, M. and Hill, A.D. 2010. A Placement Model for Matrix Acidizing of Vertically Extensive, Heterogeneous Gas Reservoirs. *SPE Prod & Fac* **25** (3): 388-397. SPE-124881-PA. http://dx.doi.org/10.2118/124881-PA.

Nozaki, M., Zhu, D., and Hill, A.D. 2011. Experimental and Field Data Analyses of Ball Sealer Diversion. Paper SPE 147632 presented at the SPE Annual Technical Conference and Exhibition, Denver, Colorado, USA, 30 October-2 November. http://dx.doi.org/102118/147632-MS.

Paccaloni, G. 1996. A New, Effective Matrix Stimulation Diversion Technique. SPE *Prod & Fac* **10** (3): 151-156. http://dx.doi.org/10.2118/24781-PA.

Robert, J.A. and Rossen, W.R. 2000.Fluid Placement and Pumping Strategy. In *Reservoir Stimulation*, ed. M.J. Economides and K.G. Nolte, Chap. 19. New York City, New York: John Wiley & Sons.

Stipp, L.C. and Williford, R.A. 1968. Pseudolimited Entry: A Sand Fracturing Technique for Simultaneous Treatment of Multiple Pays. *J Pet Technol* **20** (5): 457-462. SPE-1903-PA. http://dx.doi.org/10.2118/1903-PA.

Tilton, J.N. 1997. Fluid and Particle Dynamics. In *Perry's Chemical Engineers' Handbook*, ed. R.H., Perry and D.W., Green, Sec. 6. New York City, New York: McGraw-Hill Professional.

van Everdingen, A.F. and Hurst, W. 1949. The Application of the Laplace Transformation to Flow Problems in Reservoirs. In Transactions of the Society of

Petroleum Engineers, Vol. 186, 305-324. Richardson, Texas: Society of Petroleum Engineers.

Virk, P.S. 1975. Drag Reduction Fundamentals. *AIChE Journal* **21** (4): 626-656. http://dx.doi.org/10.1002/aic.690210402.

Webster, K.R., Goins Jr., W.C., and Berry, S.C. 1964. A Continuous Multistage Tracing Technique. *J Pet Technol* **17** (6): 619-625. SPE-977-PA. http://dx.doi.org/10.2118/977-PA.

Williams, B.B., Gidley, J.L., and Schechter, R.S. 1979. *Acidizing Fundamentals*, Vol. 6, 10-14. Richardson, Texas: Monograph Series, SPE.

VITA

Name:	Manabu Nozaki
Address:	3116 TAMU, 507 Richardson Building, College Station, TX 77843, USA
Email Address:	manabu.nozaki@pe.tamu.edu
Education:	B.Eng., Resources and Environmental Engineering, Waseda University, Japan, 2006 M.S., Petroleum Engineering, Texas A&M University, USA, 2008 Ph.D., Petroleum Engineering, Texas A&M University, USA, 2012